NASA CR-165545
W - 81-9D6-NASAC-R3

EVALUATION OF PRESENT THERMAL BARRIER COATINGS FOR POTENTIAL SERVICE IN ELECTRIC UTILITY GAS TURBINES

by R. J. Bratton, S. K. Lau and S. Y. Lee

WESTINGHOUSE ELECTRIC CORPORATION
Research and Development Center
Pittsburgh, Pennsylvania 15235

prepared for

NASA-Lewis Research Center
Cleveland, OH 44135

and

Electric Power Research Institute
Palo Alto, CA 94303

Contract NAS3-21377

PREFACE

This work was performed for NASA-Lewis Research Center under the sponsorship of the Electric Power Research Institute. The NASA Technical Manager was Dr. Robert A. Miller. The EPRI Program Manager was Dr. A. Cohn.

TABLE OF CONTENTS

TABLE OF CONTENTS (Cont'd)

LIST OF TABLES

LIST OF TABLES (Cont'd)

LIST OF FIGURES

LIST OF FIGURES (Cont'd)

LIST OF FIGURES (Cont'd)

LIST OF FIGURES (Cont'd)

LIST OF FIGURES (Cont'd)

LIST OF FIGURES (Cont'd)

EXECUTIVE SUMMARY

The objective of this program was to evaluate the resistance of present-day thermal barrier coatings - all in the early stages of development - to combustion gases which are found in electric utility turbines fired on petroleum fuels of varying impurities. The program was conducted in three technical tasks: Task I - Thermal Barrier Sensitivity Tests, Task II - High Pressure Effects, Task III - Endurance Testing.

The substrate alloys used for testing in the form of air-cooled cylindrical specimens were Udimet 720 (blade alloy) and ECY 768 (vane alloy). Two basic plasma sprayed coating structures were evaluated. The first was a duplex coating which consisted of a thin NiCrAlY bond coat and a thick refractory oxide overcoat. The second was a graded coating which consisted of a graded NiCrAlY/oxide formulation.

The NiCrAlY composition selected for all coatings was Ni-19.93 Cr - 11.07 Al - 0.44Y. The refractory oxides were primarily zirconia-based compositions, although a calcium silicate coating was also evaluated. These coating systems were selected on the basis of powder availability and state-of-the-art plasma spray processing.

In Task I - Thermal Barrier Sensitivity Tests, ambient pressure burner rig tests were used to evaluate $ZrO_2 \cdot Y_2O_3$, $ZrO_2 \cdot MgO$ and Ca_2SiO_4 coating systems. Tests were conducted at a gas temperature of 1150°C and air-cooled metal temperatures of 800°C to 900°C using a GT No. 2 fuel as the reference and impurity doped versions to simulate heavy oils and sea salt contaminated fuel.

These burner rig tests showed that there are several present day thermal barrier coatings that show a high potential for service in gas turbines burning the relatively clean GT No. 2 fuel. The best candidates were the duplex $ZrO_2 \cdot 8Y_2O_3$, duplex Ca_2SiO_4 and graded $ZrO_2 \cdot 8Y_2O_3$. A major constraint for the graded coatings is the oxidation-temperature limitation of the NiCrAlY used for grading purposes.

In contrast to the clean fuel test results, the impurity-doped fuel tests showed that none of the present day thermal barrier coatings have acceptable durability. The vanadium impurity which is present in most heavy fuels was particularly detrimental to the coatings tested. The graded coatings proved superior to duplex coatings in contaminated fuel, at the lower metal temperatures, but further development work is required to optimize these coatings.

The degradation mechanisms of the oxide coatings in the presence of vanadium, sodium and sulfur impurities were determined. Vanadium impurity caused destabilization of $ZrO_2 \cdot Y_2O_3$ coatings which in turn caused cracking and spalling during thermal cycling. The destabilization reaction occurred between the oxide coating and solid vanadate condensates or gaseous vanadium oxides. Sodium sulfate impurity caused coating degradation through a mechanical mode rather than a chemical one. Molten Na_2SO_4 or Na_2SO_4-$MgSO_4$ condensates that deposited in the porous coatings caused cracking and spalling due to the large mismatch in thermal expansion coefficients between the oxide coating and solidified salts.

The Ca_2SiO_4 and $ZrO_2 \cdot MgO$ coatings were also found to be reactive towards fuel impurity condensates such as $MgSO_4$ and solid vanadates. In addition these coatings were highly reactive towards the SO_2/SO_3 gas produced from the sulfur impurity in the fuel. The reaction products with SO_2/SO_3 are $CaSO_4$ and $MgSO_4$ that are rather friable.

In Task II - High Pressure Effects, the test conditions closely simulated those of actual turbines operating at 135 psig. Both clean fuel and fuel sensitivity tests were run. In the relatively clean GT No. 2 fuel tests, the coatings performed very well even when the coatings were subjected to thermal transients more severe than would be expected in actual turbines. However, in the contaminated fuel tests, coating failures generally occurred in less than 20 one-hour cycles of start-up steady state, and cool down operation. Detailed analysis of tested specimens showed that the reactions between the coatings and fuel contaminants were qualitatively very similar to those found in the atmospheric burner rig tests. The effect of the greater gas pressure and hence contaminant levels, greater gas velocity and greater heat fluxes in the pressurized test was to accelerate the failures induced by the fuel contaminants.

A pressurized passage test was also conducted on three selected coatings using a coal derived liquid fuel - SRC-2, which was a 2.9 middle distillate/1 heavy distillate mix. This test was concluded after 20 cycles of testing due to the limited availability of fuel. All the coatings tested, viz., duplex $ZrO_2 \cdot 8Y_2O_3$, graded $ZrO_2 \cdot 8Y_2O_3$, and duplex Ca_2SiO_4, survived without any sign of degradation. Although this test was limited, it was a very encouraging result since previous experience has shown that if chemical induced failures occur, they usually begin in less than 20 cycles of testing in the pressurized passage.

In Task III - 4000 hr Endurance Test, three ceramic coatings; duplex $ZrO_2 \cdot 8Y_2O_3$, graded $ZrO_2 \cdot 8Y_2O_3$ and duplex Ca_2SiO_4, and a NiCrAlY coating; were tested in the atmospheric burner rig where the fuel was undoped GT No. 2 fuel. Except for the NiCrAlY specimen which was tested at a metal temperature of 857°C, the gas/metal temperatures were 1150°C and 800°C, respectively. This test served to confirm the strengths and

weaknesses of the coatings as determined from earlier tests. The duplex coatings performed best and successfully survived the test without failure. Even in the presence of an accidental temperature excursion which occurred for some specimens during the 2200th cycle, the duplex coatings showed excellent durability. The graded coatings showed susceptibility to oxidation of the NiCrAlY in the graded zone as observed in earlier tests. This demonstrated conclusively that a more oxidation resistant MCrAlY was needed for long term durability of the graded type coating. Although the duplex Ca_2SiO_4 coating survived the endurance test without failure, the coating showed surface microchipping which was traced to the formation of $CaSO_4$ due to reaction with SO_2/SO_3 gas. The NiCrAlY coated specimens showed oxidation and extensive void formation after the 4000 hr. test.

This program has provided a reliable engineering assessment of the resistance of present-day thermal barrier coatings - all in the early stages of development - to combustion gases as would be found in electric utility turbines. Clean fuel ambient pressure burner rig tests have demonstrated that some coatings can withstand long cyclic exposure at high temperatures while clean fuel pressurized passage rig tests have demonstrated that these same coatings can withstand cyclic thermal stresses far more severe than would be encountered in a utility turbine.

The partially stabilized duplex $ZrO_2 \cdot 8Y_2O_3$/MCrAlY coating is the most promising candidate for continued development efforts, followed by the duplex Ca_2SiO_4/MCrAlY and their graded versions. Field testing of these coatings in utility turbines burning GT No. 2 fuel is recommended for the near term. This will provide the operating experience needed to determine if any unusual problems exist and pave the way for taking full advantage of the potential benefits offered by the use of ceramic coatings. For more corrosive operating conditions, further coating development work is required. Progress has been made in this area in the DOE/NASA Contract DEN3-110, "Advanced Ceramic Coatings," also being conducted by Westinghouse.

I. INTRODUCTION

1.1 BACKGROUND

The concept of thermal barrier coatings is to provide insulation to critical air-cooled metal components. An important application is in gas turbine engines where there are several ways to take advantage of ceramic insulation at high temperatures (Refs. 1-4), e.g., increased engine reliability by reducing metal temperature by about 100°C increased engine efficiency and power by maintaining current metal temperature and increasing gas temperature, and reduced fabrication cost by eliminating elaborate cooling schemes. Durability and fuel flexibility may also be achieved if the ceramic coatings were resistant to inorganic salt contaminants (Ref. 5). It should be noted that plasma sprayed ceramic coatings have been used for over ten years to reduce metal temperatures in aircraft burners and afterburners. But because of the more stringent environmental requirements, turbine airfoils with ceramic coatings are not yet in use.

A contemporary two-layer (duplex) thermal barrier coating is shown schematically in Figure 1. Typically this consists of a thick plasma sprayed ceramic layer deposited over a thin metallic bond coat. Another version not shown is to introduce a graded intermediate region of ceramic/metal to minimize thermal expansion mismatch between the ceramics and metal.

The coating properties required for turbine engine application are achieved through the selection of material properties and coating process parameters. Desired ceramic properties include low thermal conductivity, a relatively high coefficient of thermal expansion, thermodynamic stability in the gas turbine environment and mechanical stability toward thermal cycling. The plasma spray process (Refs. 6, 7) helps achieve increased thermal protection and improved thermal stress resistance due to the coating porosity that is characteristic of this process. On the other hand, gas permeability and condensed salt penetration into the porous coating structure may induce coating degradation. Plasma sprayed zirconia compositions have been of most interest for thermal barrier coatings and have been under periodic development for about the past 30 years. Since the metal bond coats primary function is to provide a substrate for adherence of the ceramic coating, it is very important that the bond coat be oxidation and/or corrosion resistant at the metal (Refs. 8-10) operating temperature. In this respect MCrAlY alloys developed for coating turbine airfoils are proving very useful as the bond coat for the thermal barrier coating concept, and in part, are responsible for recent successes compared to earlier work.

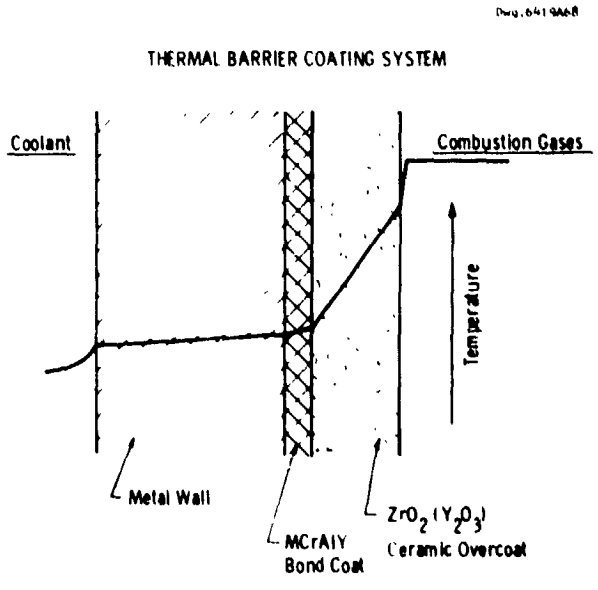

Figure 1 - Schematic representation of the duplex thermal barrier coating

Most of the early thermal barrier coating research which extended from the 1950's to early 1970's (Refs. 11-14) was conducted at NASA-Lewis Research Center. This work focused on surface protection of both aircraft engine and rocket engine components. By mid 1970's encouraging results were achieved with a zirconia-based two layer system as shown in Figure 1 (Refs. 15-18). From several stabilized zirconia compositions, which included CaO, MgO and Y_2O_3 stabilizers, the ZrO_2·12 w/o Y_2O_3/NiCrAlY system was chosen on the basis of adherence to the NiCrAlY bond coat, thermal stress resistance, erosion resistance and stability in the aircraft turbine environment. This work as well as that of others (Refs. 19-22) stimulated further development of ZrO_2-Y_2O_3 coating compositions and compatible MCrAlY bond coats. Figure 2 (Refs. 23, 24) shows the recent improvements made as judged by durability to cyclic testing using a very clean burning fuel. Yttria content in the ZrO_2-Y_2O_3 coating as well as yttrium content in the NiCrAlY bond coat are obviously important to coating life. However the reasons for the improved durability have not been established. Other factors such as bond coat roughness are also important to coating adherence and durability (Ref. 20).

It should be noted that the most durable zirconia coatings are those formed from the two-phase (partially stabilized) region of the zirconia-yttria phase system Figure 3 (Ref. 25). This equilibrium system would predict that the stable phases are cubic ZrO_2 (high Y_2O_3) and monoclinic ZrO_2 (low Y_2O_3) at room temperature where the latter transforms from the tetragonal ZrO_2 (low Y_2O_3) that is stable above about 600°C. However, this equilibrium case does not exist during the rapid cooling of plasma sprayed ZrO_2·8 w/o Y_2O_3 and other compositions (Ref. 5). The room temperature phases consist primarily of a non-equilibrium high yttria tetragonal phase and minor amounts of cubic phase and monoclinic phase similar to that obtained with rapidly quenched bulk material. A more detailed study of the stability of these phases has been reported recently (Ref. 26).

Although the durability of zirconia coatings have been exceptional in tests conducted in relatively clean high temperature gases such as natural gas and jet aircraft fuel, preliminary studies conducted at Westinghouse (Ref. 5) and NASA (Ref. 4) suggested potential adherence problems when the coatings are subjected to combustion environments that contain impurities. Impurities are often found in turbine systems that enter the engine either through injested run-way dust or sea salt aerosals (Ref. 27). This may lead to the deposition of the highly corrosive sodium sulfate salt onto turbine blades and vanes. In non-aircraft application a similar result may occur. In addition imputities are introduced through the use of lower grade fuels such as crude and residual oils. Major impurities found in these fuels include sodium, potassium, vanadium, iron, lead, phosphorous and sulfur. Also, minimally processed coal-derived fuels may be burned in turbines in the future. Although trace metal impurity levels in these fuels are uncertain, the durability of thermal barrier coatings will need to be established as they become available.

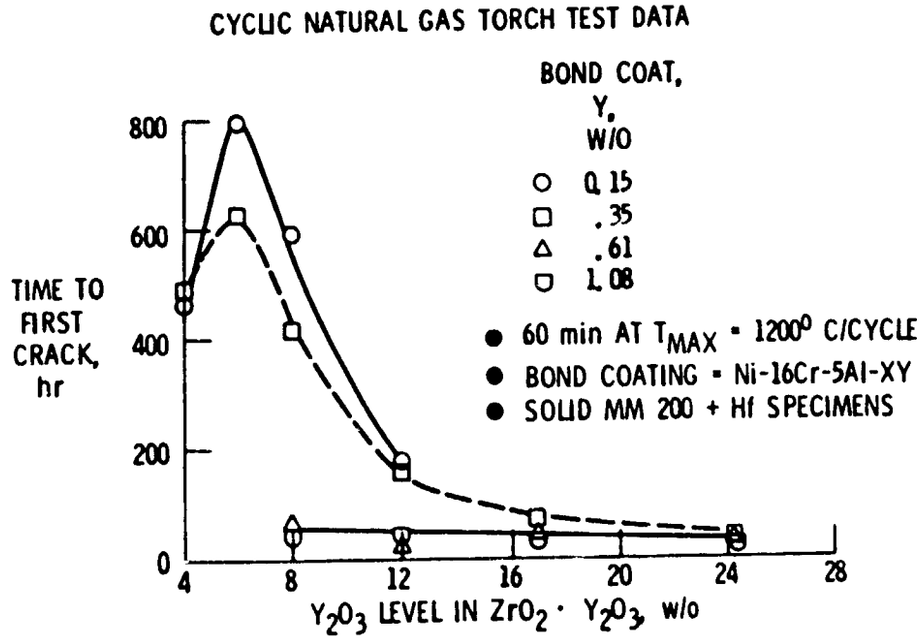

Figure 2 - TBC cracking in natural gas torch tests varies with oxide and bond coat composition (NASA REF.23,24)

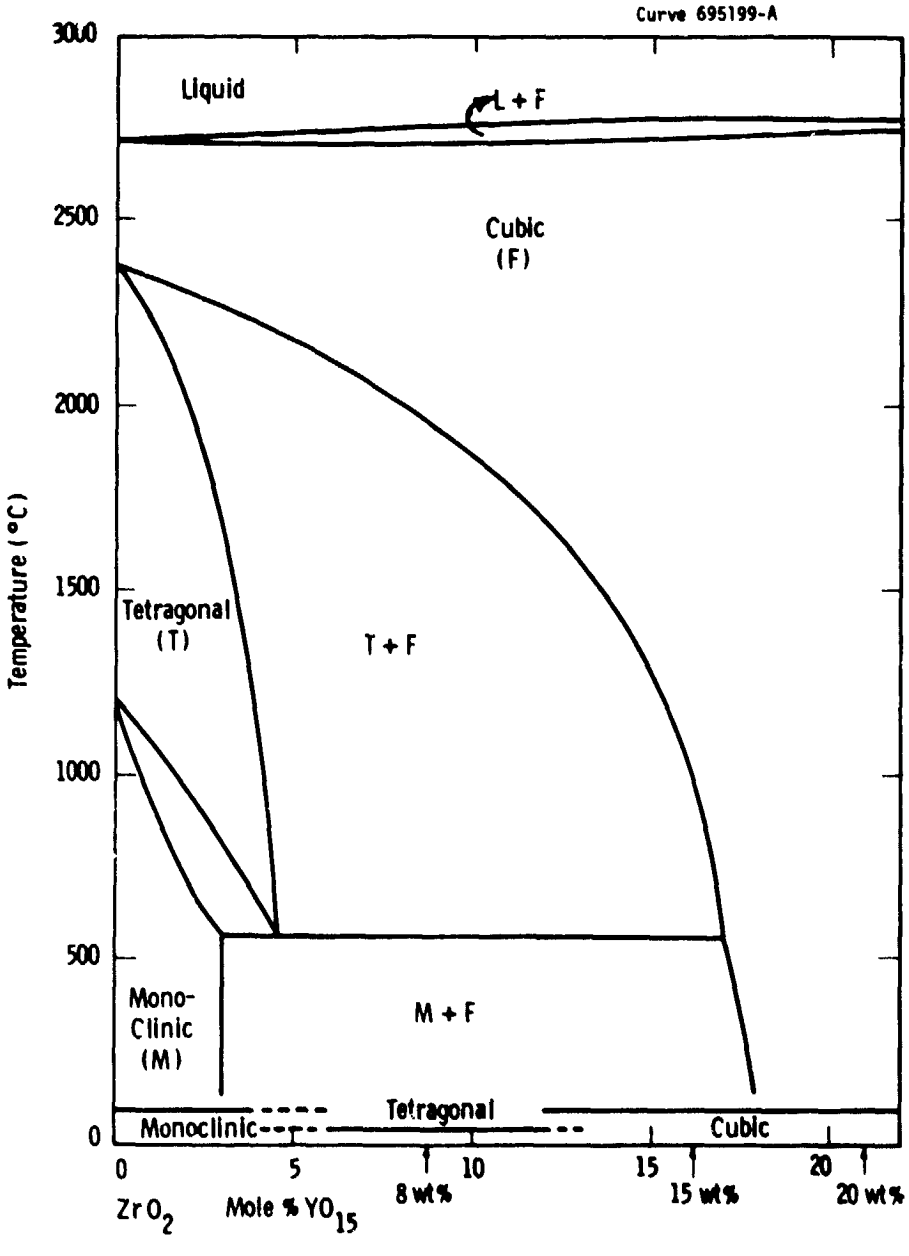

Figure 3 - Phase diagram for the Zirconia-rich region of the ZrO_2-Y_2O_3 system after H. G. Scott (Ref. 25)

In this program, emphasis was placed on the evaluation of the resistance of thermal barrier coatings to combustion gases that contain corrosive metal impurities. While preliminary studies were undertaken earlier (Ref. 5), up to this program there had been no systematic study of fuel sensitivity effects that would allow an assessment of the coating limitations and potentials especially for electric utility turbine applications. (Refs. 28, 29).

1.2 PROGRAM OBJECTIVE AND PLAN

The objective of this program was to evaluate the resistance of present-day thermal barrier coatings -- all in the early stages of development -- to combustion gases which are found in electric utility turbines fired on petroleum fuels of varying impurities. In this program, thermal barrier coated air-cooled specimens were evaluated to establish temperature, fuel impurity, pressure effects, and water-washing sensitivity as well as coating lifetimes. The program was carried out in four tasks as follows:

Task I Thermal Barrier Sensitivity Tests

Task II High Pressure Effects

Task III Endurance Testing

Task IV Reporting

The substrate alloys used for testing in the form of air-cooled cylindrical specimens were Udimet 720 (blade alloy) and ECY 768 (vane alloy), which represent present-day turbine alloys.

The coating systems were selected on the basis of powder availability and state-of-the-art plasma spray processing. These were primarily zirconia-based coatings. Both duplex (two-layer) coatings consisting of NiCrAlY bond coat and an oxide overcoat, and graded NiCrAlY/oxide coatings were evaluated. The NiCrAlY composition selected for all coatings was Ni-19.93 Cr - 11.07 Al - 0.44Y.

In Task I, Thermal Barrier Sensitivity Tests, ambient pressure burner rig tests were conducted. Task IA, Clean Fuel Tests, consisted of testing the coating systems in clean No. 2 GT fuel wherein the gas or metal substrate temperatures were variables. Task IB, Fuel Impurity Sensitivity Tests, consisted of testing the coating systems under dirty-fired fuel conditions. The approach was to dope No. 2 GT fuel with impurities to simulate heavy petroleum fuels used by utilities. Task IC, Water Washing Sensitivity, consisted of evaluating the coating sensitivity to turbine clean up (washing procedures).

In Task II, High Pressure Effects, three selected coatings were exposed to high-pressure combustion gases and then evaluated as in Task I to establish the comparative influence of exposure pressure.

In Task III, Endurance Testing, a long-time (to 4,000 hours) endurance test was conducted in an atmospheric burner rig using the most promising coating systems with life potential beyond 500 hours. The selection was based on previous 500 hour burner rig tests.

Evaluation and comparison of specimens of the as-deposited and exposed specimens included visual, microscopic, X-ray diffraction (XRD), electron microprobe (EMP), chemical analysis as appropriate, and non-destructive measurements such as weights, dimensions, etc.

The expected result from this program was a reliable engineering assessment of the resistance of present-day thermal barrier coatings to combustion gases as would be found in electric utility turbines.

II. EXPERIMENTAL

2.1 MATERIALS

2.1.1 Test Specimen Geometry

The specific geometry of the test specimen used throughout the program was a base alloy cylinder 7.6 cm long and 1.27 cm in diameter with a 6.35 mm diameter cooling hole located in the center of the cylinder. Four thermocouple wells of 1.1 mm diameter and 6.35 cm deep were bored from one end of the cylinder at midway between the cooling hole and outer surface to accommodate thermocouples at different locations. The surface of the test specimens was centerless ground to about 0.38 μm surface finish. A 0.127 mm thick NiCrAlY bond coating was applied to the specimen from end to end, whereas the thermal barrier oxide coating, which was 0.38 mm in thickness, covered the middle 5.8 cm of the specimen and only that portion of the specimen was exposed to the high temperature gaseous environments. The ends of the oxide coating were tapered to reduce the possibility of premature spalling due to end effects. The design of the specimen is shown in Figure 4.

The alloy substrate materials were Udimet 720 (blade alloy) and ECY 768 (vane alloy). The Udimet 720 alloy was obtained from Special Metals in the form of rolled bars, while the ECY 768 alloy was obtained from Misco Hampton Division as cast bars.

Some of the machined U720 specimens were given a solution heat treatment at 1168°C for 4 hours and a stabilizing heat treatment at 1080°C for 4 hours under a vacuum of 10^{-6} torr and furnace cooled. Specimens sent to Linde Division of Union Carbide for coating were subjected only to the solution heat treatment because their post-plasma sprayed diffusion heat treatment overlapped that of the stabilizing heat treatment. The cast ECY 768 specimens were not heat treated prior to coating by vendors.

2.1.2 Coating Systems

Nine oxide coating systems were evaluated in this study (Table 1). They included both duplex and graded coatings, and with the exception of Ca_2SiO_4, all the overcoats were based on zirconia compositions. Both the bond coat and oxide overcoat of each of the coating systems were deposited by plasma spraying. Most of the zirconia coated specimens

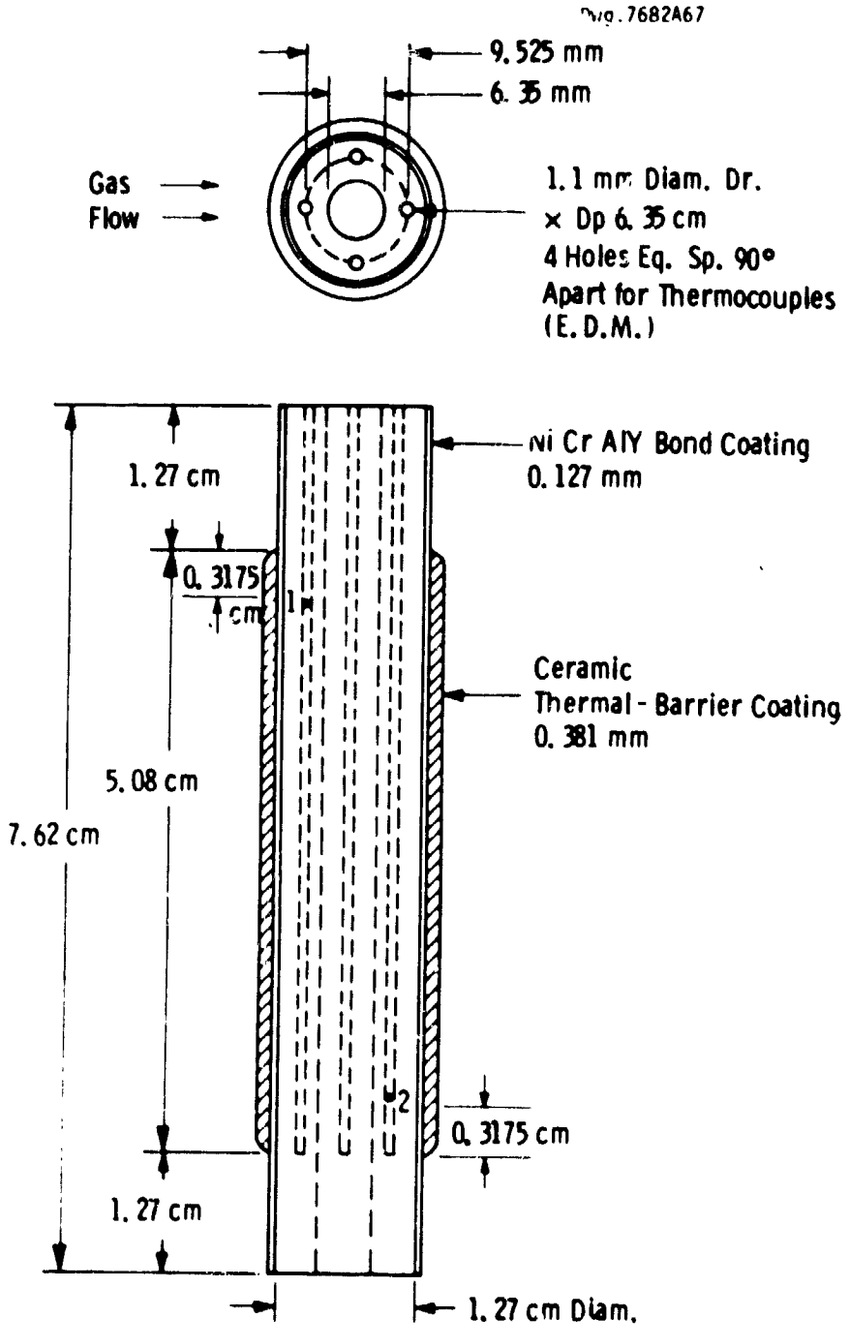

Fig. 4 – Thermal-barrier coating test specimen showing location of thermocouples

Table 1

Thermal Barrier Coating Systems

Oxide* Thermal Barrier	Coating** Description	Oxide Phase
1. $ZrO_2 \cdot 8Y_2O_3$	Duplex- Two Layers: 0.127 mm NiCrAlY Bond Coat 0.38 mm Oxide Overcoat	95 Tetragonal/cubic 5 monoclinic
2. $ZrO_2 \cdot 15Y_2O_3$		Tetragonal/cubic
3. $ZrO_2 \cdot 20Y_2O_3$		Tetragonal/cubic
4. $ZrO_2 \cdot 24.65MgO$		82 Tetragonal/cubic 18 monoclinic and Free MgO
5. Ca_2SiO_4		Ca_2SiO_4
	* * * * * * * * *	
1. $ZrO_2 \cdot 8Y_2O_3$	Graded - Three Layers: 0.1 mm NiCrAlY 0.2 mm Graded Zone 0.2 mm Oxide Overcoat	Tetragonal/cubic monoclinc
2. $ZrO_2 \cdot 15Y_2O_3$		Tetragonal/cubic
3. $ZrO_2 \cdot 20Y_2O_3$		Tetragonal/cubic
4. $ZrO_2 \cdot 24.65MgO$		82 Tetragonal/cubic 18 Monoclinic and Free MgO

*Nominal oxide compositions in wt%

**Nominal NiCrAlY compositions (wt%): Ni-20Cr-11Al-0.4Y

were plasma sprayed from -200 + 300 mesh powders by the Linde Division of Union Carbide, the exceptions were that some of the duplex $ZrO_2 \cdot 8Y_2O_3$/NiCrAlY specimens were prepared by Plasmadyne and NASA Lewis Research Center. The Ca_2SiO_4 specimens were supplied exclusively by NASA Lewis Research Center.

2.1.3 Pre-test Analysis

The as-deposited phases present in the oxides as determined by X-ray diffraction analysis are also shown in Table 1. It should be noted that due to the rapid cooling from the melt during plasma spraying, the as-sprayed zirconia phases do not reach equilibrium. Both the partially stabilized and fully stabilized $ZrO_2(Y_2O_3)$ compositions consisted primarily of tetragonal $ZrO_2(Y_2O_3)$ phases. They possibly also contained cubic $ZrO_2(Y_2O_3)$ phase. However, its determination was uncertain because the diffraction peaks obtained were rather broad and the lattice parameters of the yttria-doped cubic and tetragonal zirconia phases differed only very slightly. The partially stabilized $ZrO_2 \cdot 8$ w/o Y_2O_3 also contained a minor amount of monoclinic $ZrO_2(Y_2O_3)$ phase. The $ZrO_2 \cdot 24.65$ w/o MgO composition, in addition to tetragonal/cubic and monoclinic $ZrO_2(MgO)$, also contained some free MgO. For reference, the location of the $ZrO_2(Y_2O_3)$ compositions are shown in the ZrO_2-rich regions of the $ZrO_2 \cdot Y_{1.5}$ system (see arrows in Fig. 3).

Detailed chemical analysis was performed on the NiCrAlY as well as the $ZrO_2 \cdot 8Y_2O_3$, $ZrO_2 \cdot 15Y_2O_3$ and $ZrO_2 \cdot 24.65$ MgO powders used for plasma spraying. The NiCrAlY powder was found to consist of 11.07 wt % aluminum, 19.93 wt % Cr and 0.44 wt % yttrium. This is listed in Table 2 along with the compositions of the base alloys. The chemical analysis results of the oxides are shown in Table 3.

Typical metallographic cross sections of the duplex (2 layer) and graded coatings are shown in Figs. 5 and 7, respectively. The elemental characterization of the coatings was determined by electron microprobe mapping. Typical electron microprobe scans obtained on cross sections of the duplex and graded coatings are shown in Figs. 6 and 8, respectively. Although the elements analyzed were Zr, Y, Mg, Al, Ni, Co, Si, Fe, Na, S, Cu, only the major elements are shown to illustrate the as-coated U720 substrate/NiCrAlY bond coat/oxide structure of the duplex and graded coatings.

The thickness of the bond coats and oxide overcoats was statistically measured at a central cross-section with an optical microscope using a calibrated Filar eye piece. It was found that all the coatings examined were rather uniform in thickness around the circumference of the specimens. The standard deviations in the coating thickness obtained for each of the coatings were less than 20%. The target thickness of the graded coating compositions, which represent current practice, was 0.1 mm bond coat, 0.2 mm graded zone and 0.2 mm of oxide.

Table 2

CHEMICAL ANALYSIS OF NiCrAlY BOND COAT AND BASE ALLOYS

Material	Composition	Manufacturer
NiCrAlY	Ni - 19.93 Cr - 11.07 Al - 0.44 Y	Alloy Metals, Inc.
Udimet 720	Ni - 15 Co - 18 Cr - 2.5 Al - 5 Ti - 3 Mo - 1.5 W - 0.04 B - 0.04 Zr - 0.04 C	Special Metals Corp.
ECY 768	Co - 10 Ni - 24 Cr - 7 W - 3.5 Ta - 0.2 Ti - 0.05 Zr	MISCO Hampton Div.

Table 3

Chemical Analyses of Oxide Overcoats

Element (Oxide)	Concentration Wt.%		
	$ZrO_2 \cdot 8Y_2O_3$	$ZrO_2 \cdot 15Y_2O_3$	$ZrO_2 \cdot 24.65MgO$
ZrO_2	Balance	Balance	Balance
Y_2O_3	7.98	15.75	-
MgO	-	-	25.5
Si	1	0.3	1
Ca	0.3	0.1	0.1
Fe	0.15	0.1	0.15
Al	0.1	0.1	0.1
Mg	<0.1	<0.1	-
Ni	0.1	0.05	0.1
Sb	0.1	0.1	0.1
Ti	0.2	0.05	0.2
Co	0.05	<0.05	0.05
Cr	0.05	<0.05	<0.05
Cu	<0.05	<0.05	<0.05
Mo	0.05	<0.05	<0.05
V	<0.05	<0.05	<0.05

ORIGINAL PAGE
BLACK AND WHITE PHOTOGRAPH

(50X)

Fig. 5 - Typical metallographic cross-section of a duplex $ZrO_2 \cdot Y_2O_3$ coating

ORIGINAL PAGE
BLACK AND WHITE PHOTOGRAPH

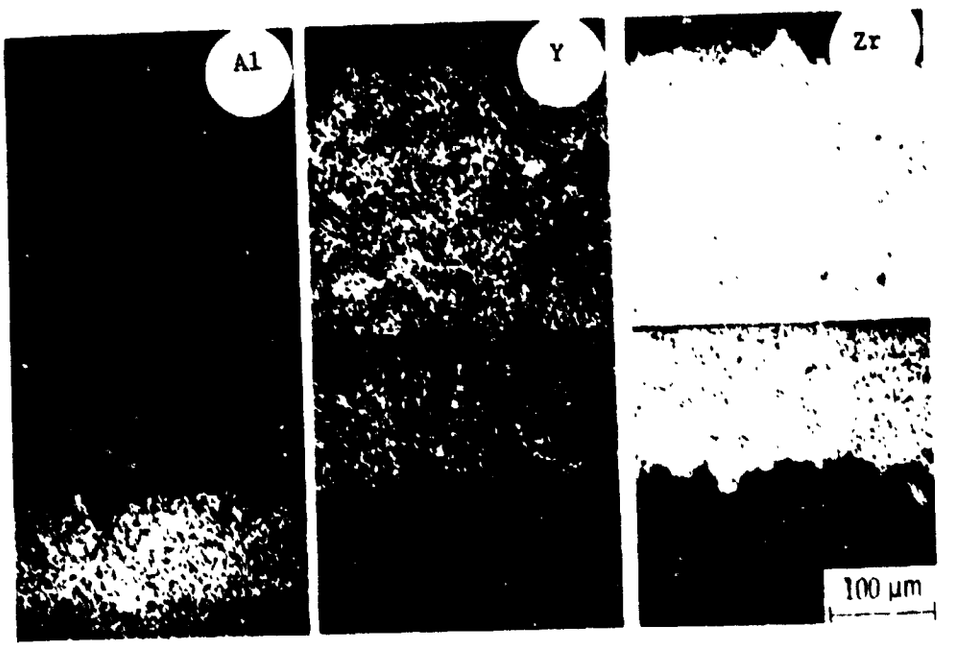

Fig. 6 - Electron microprobe scans from a pretest duplex ZrO_2-Y_2O_3 coating

ORIGINAL PAGE
BLACK AND WHITE PHOTOGRAPH

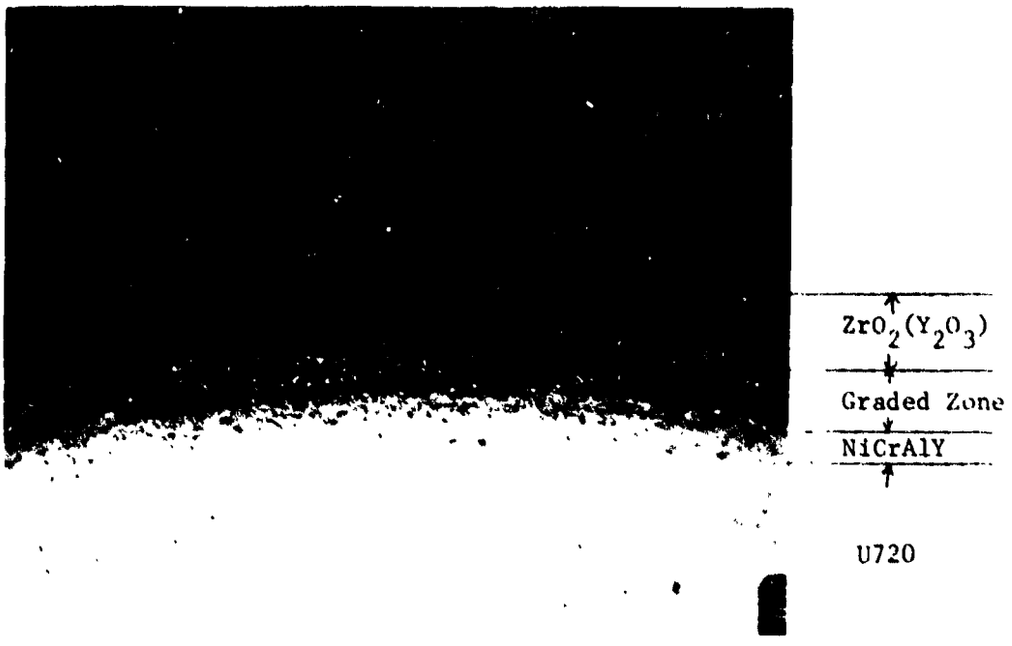

(50X)

Fig. 7 - Typical metallographic cross-section of a graded $ZrO_2 \cdot Y_2O_3$ coating

ORIGINAL PAGE
BLACK AND WHITE PHOTOGRAPH

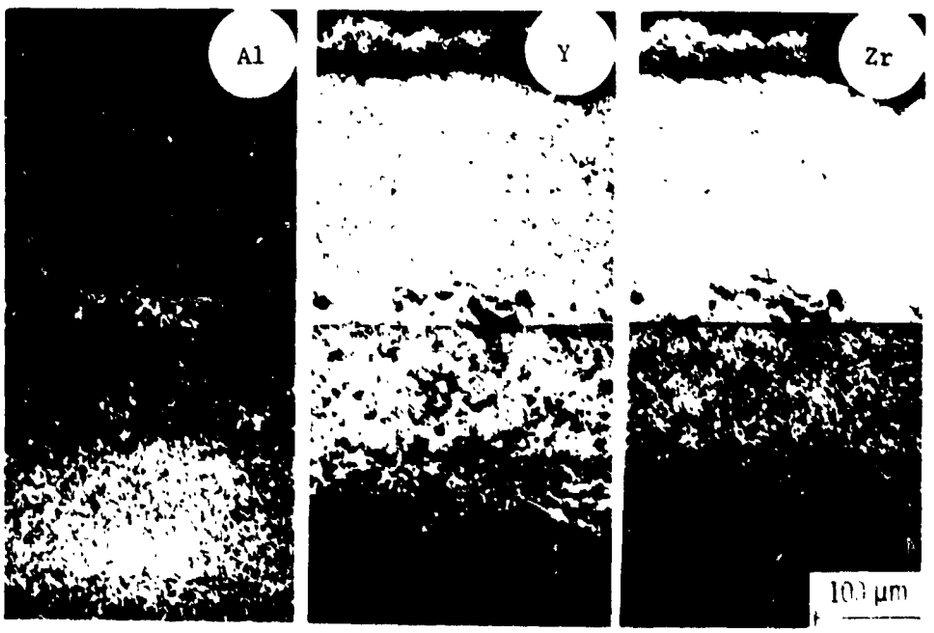

Fig. 8 - Electron microprobe scans from a pretest graded ZrO_2-Y_2O_3 coating

All the incoming specimens were subjected to pretest nondestructive evaluation (NDE) that consisted of weighing, dimensioning, visual and optical screening for defects. Special attention was given to the optical examination of the coating terminals because they were possibly sites of premature failure. Most of the specimens examined showed excellent structural integrity.

2.2 TASK I - THERMAL BARRIER SENSITIVITY TESTS

2.2.1 Test Equipment and Procedure

All the tests in Task I were carried out in two burner rigs operating at ambient pressure. The atmospheric burner rig was essentially a small furnace with a fuel-burning combustor attached at one end (Fig. 9a). The burner was operated at various fuel:air ratios and secondary diluent air was injected to the post combustion zone to facilitate further variation of combustion gas temperature. Eight air-cooled specimens mounted on a platform were inserted from the bottom so that hot combustion gas from the burner impinged at a right angle to the specimens. The platform was mounted on a pneumatic cylinder so that the specimen could be inserted or retracted from the furnace to achieve thermal cycling (Fig. 9b). During actual testing, the test specimens were thermally cycled once an hour (five minute heating cycle, 50 minute steady state hold at test temperature and five minute cooling cycle).

To simulate an emergency shutdown of an industrial gas turbine, the specimens were subjected to hot gas and room temperature air instantaneously during a heating and cooling cycle, respectively, in order to achieve approximately 11 to 22°C per second of cooling rate. A front view of the specimen holding platform with mounted specimens as well as the specimen heating and cooling cycles are shown in Fig. 10.

Due to the inherent characteristics of the combustor used in the burner rigs, the gas temperature spread across the specimen pack was generally one to two hundred degrees, especially in a straight-through duct. In order to reduce the temperature spread, the burner rigs were modified by mounting a 15.2 cm wide rectangular refractory baffle (duct was 20.3 cm wide) directly behind the specimen pack. The effect of the baffle was to change the hot core of gas flow from through the specimen pack to around the pack, thus spreading it wider. Temperature profiles after the modification were found to be improved significantly. Maximum gas temperature difference between center and edge of the specimen pack was reduced to 80°C.

The variation of the metal temperatures due to specimen location as well as that due to the presence of various thermal barrier coatings was adjusted by using individual metering valves to externally adjust the

ORIGINAL PAGE
BLACK AND WHITE PHOTOGRAPH

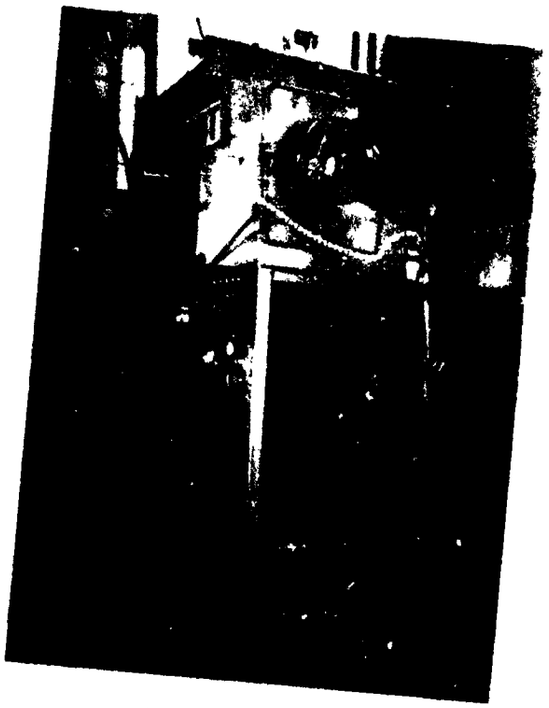

(a) Burner rig

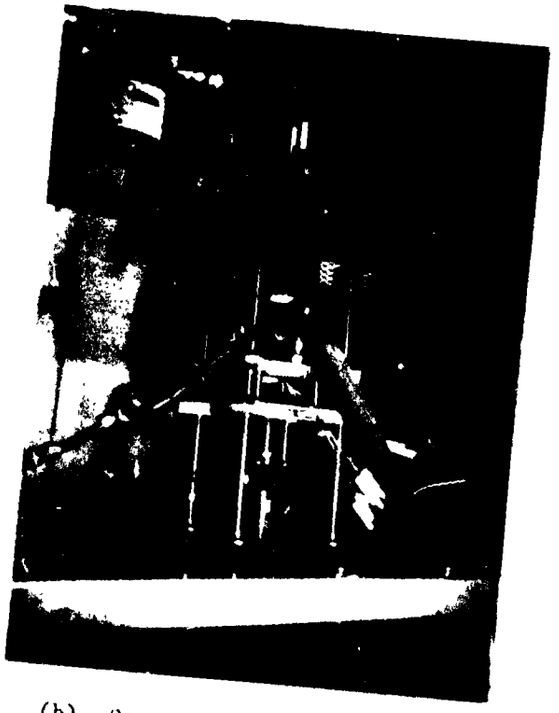

(b) Specimen holder mounted on retracting mechanism

Fig. 9 - Atmospheric burner rig

ORIGINAL PAGE
BLACK AND WHITE PHOTOGRAPH

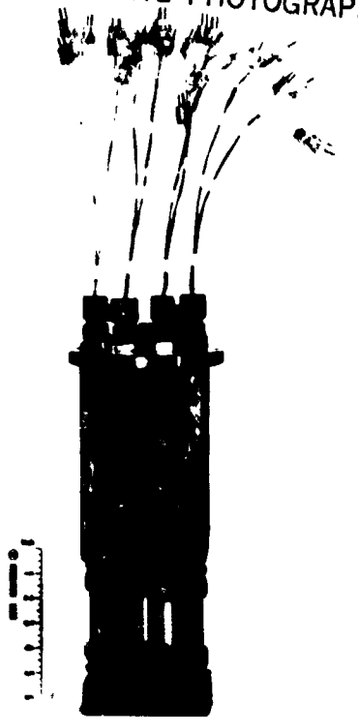

(a)

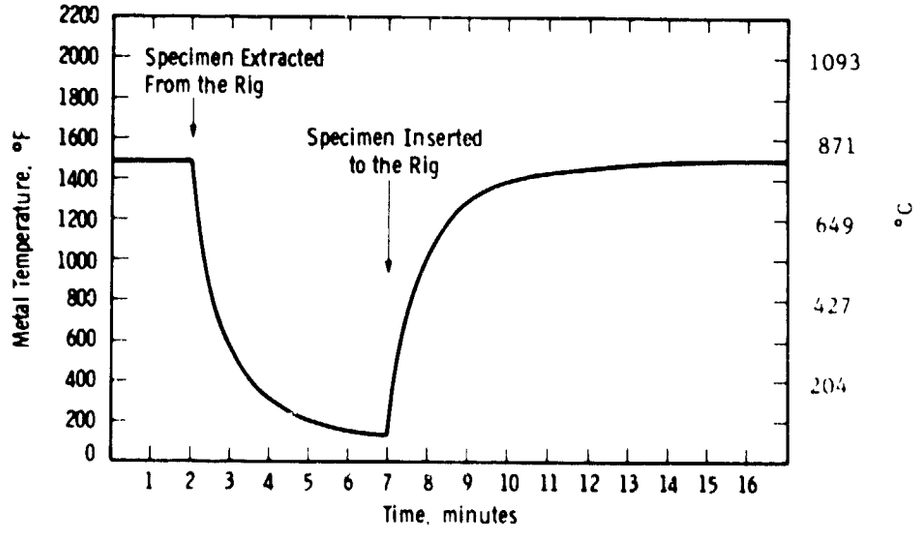

(b)

Fig. 10 - (a) air-cooled specimen assembly
(b) specimen cooling and heating cycle

cooling air flow rate without dismantling the specimen holder. Two thermocouples for each specimen were used to monitor the high and the low temperature of a test specimen. The variation of maximum metal temperature in all eight test specimens were within ± 8°C.

Surface temperatures of thermal barrier coatings, when the test specimens were exposed to 1150°C gas while substrate alloys were air-cooled to 800°C, were determined by several methods. Since a steady state value could not be obtained due to lack of a suitable view port in the burner rig, transient values were recorded during the cooling down cycle and extrapolated back to the steady state value. An infrared radiation pyrometer (IRCON Model 300) with emissivity adjustment was used for the measurement after calibrating for emissivity at 800°C. The surface temperature of a graded $ZrO_2 \cdot 20Y_2O_3$ specimen was measured to be 900°C. The measured value was checked with an optical pyrometer and Tempil stick method. The optical pyrometer agreed with the IR Pyrometer reading within 10°C and Tempil stick indicated that the surface temperature was between 870°C and 927°C. The surface temperature determined on a duplex $ZrO_2 \cdot 8Y_2O_3$ specimen was also about 900°C. The fact that there was insignificant difference between the surface temperatures of duplex and graded specimens indicated that radiation probably played an important part in determining the heat transfer condition inside the burner rig. This may not be the case in actual gas turbines.

Both clean-fuel and impurity-doped fuel sensitivity tests were conducted in the atmospheric burner rigs. Detailed tests are described in the following sections.

2.2.2 Task 1A - Clean Fuel Test

2.2.2.1 Test Results

Clean fuel tests were conducted using GT No. 2 fuel (ASTM 2880-76). A typical chemical analysis of this fuel is shown in Table 4. Four different tests were run in which the gas temperature was maintained at 1150°C but the metal substrate temperature was varied from 800°C to 845°C to 900°C (Table 5). All tests were terminated after 500 one-hour cycles.

Generally, four types of coating systems with duplicate specimens were evaluated in each test. The uncoated alloy specimens were also included for references purposes. Fig. 11 is a schematic diagram showing the location of the eight test specimens in the burner rig. The list of coating systems tested in these positions together with the summary of the detailed visual observations made during each test are given in Tables 6-9.

Table 4

TYPICAL CHEMICAL ANALYSIS OF NO. GT-2 FUEL OIL

Element	Concentration (ppm)
Fe	2.0
Cu	0.8
Si	0.8
Mn	0.6
Pb	0.5
Al	0.3
Mg	0.3
Na and K	0.3
P	0.3
Ca	0.2
Cr	0.2
V	0.07
S	0.242 (wt %)

Table 5

SUMMARY OF CLEAN FUEL TEST CONDITIONS

Test No.	Gas/Metal Temp. (°C)	Fuel
1A2	1150/800	GT No. 2
1A2R	1150/800	GT No. 2
1AX	1150/845	GT No. 2
1A1	1150/900	GT No. 2

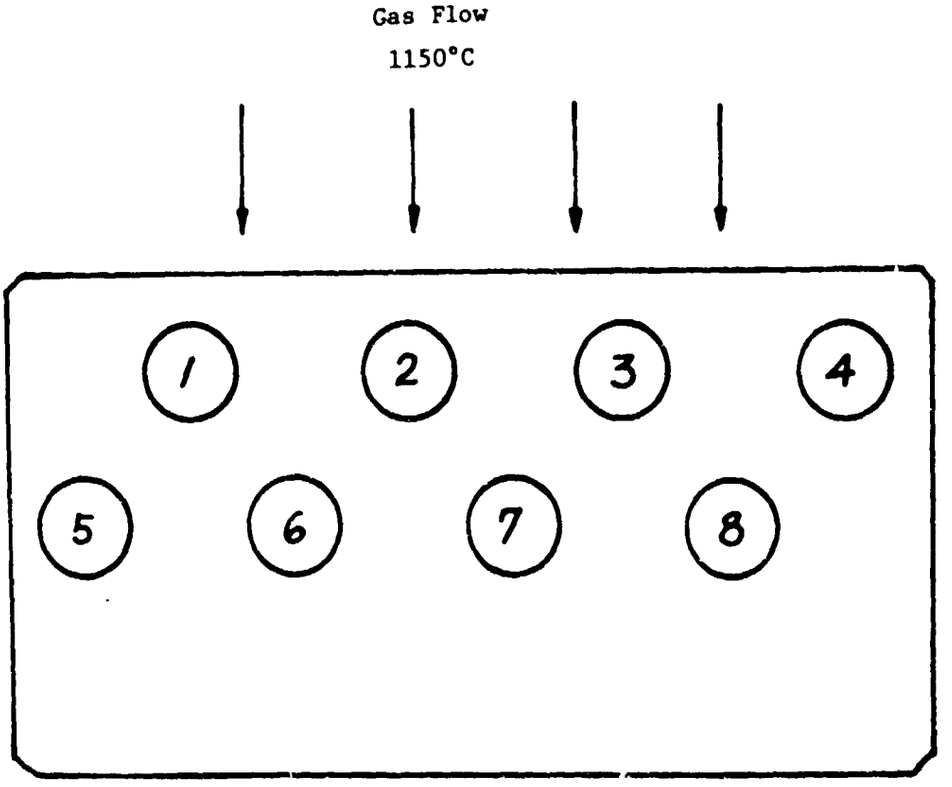

Figure 11 - Schematic diagram of specimen holder showing specimen location

The plan for each test was to extract a specimen after 150 hours (or after failure*) and replace that specimen with a new one to accumulate a total of 500 one-hour cycles and thereby have specimens for analysis that were exposed for 150, 350 and 500 one-hour cycles. The original plan was modified in some cases to accumulate hours even though a coating spalled in order to assess corrosion/oxidation protection even in the event of spalling.

Figure 12 shows the results of the clean fuel tests in terms of the minumum number of one-hour cycles to cause a spalling failure. The detailed test specimen locations and visual observations made during the tests are listed in Tables 6-9.

It can be seen from Fig. 12a that only one coating, a duplex $ZrO_2 \cdot 15Y_2O_3$/NiCrAlY did not survive the 1150°C gas/800°C metal test condition. The failure has been attributed to thermal stress since insignificant impurity condensate could be found in post-test analysis. It is interesting to note that the graded $ZrO_2 \cdot 15Y_2O_3$/NiCrAlY coating survived the test without failure indicating that at these lower test temperature conditions, graded coatings are more durable than their duplex counterparts. This is attributed to the reduction of thermal expansion mismatch between the ceramic overcoat and the NiCrAlY bond coat and the prevention of crack propagation.

Figures 12b and 12c show that the duplex $ZrO_2 \cdot 8Y_2O_3$ coatings survived the higher metal temperature test conditions while the graded $ZrO_2 \cdot 8Y_2O_3$/NiCrAlY and $ZrO_2 \cdot 24.65$ MgO/NiCrAlY did not. The latter cracked and spalled after exposures as short as 50 one-hour cycles at the 1150°C gas/900°C metal test conditions. The residual layer beneath the spalled-off regions showed a greenish color, suggesting the likelihood of oxidation of NiCrAlY particles contained in the graded zone.

The post-test conditions of some representative specimens from the clean fuel tests are shown in Figs. 13 and 14.

2.2.2.2 Post-Test Analysis

Detailed post-test analysis, which included X-ray diffraction, metallographic as well as electron microprobe analysis, were conducted on representative specimens from the four clean fuel tests.

Metallographic cross-section of a failed D-$ZrO_2 \cdot 15Y_2O_3$/NiCrAlY specimen after 350 hours of exposure in test 1A2 (1150°C gas, 800°C metal) is shown in Fig. 15. It was observed that spalling generally occurred within the oxide layer close to the bond coat and that there was always a thin oxide layer (0.01 to 0.1 mm) remaining.

*For the purpose of this program failure is defined as severe and hence noticeable cracking and/or spallation of any part of the coating.

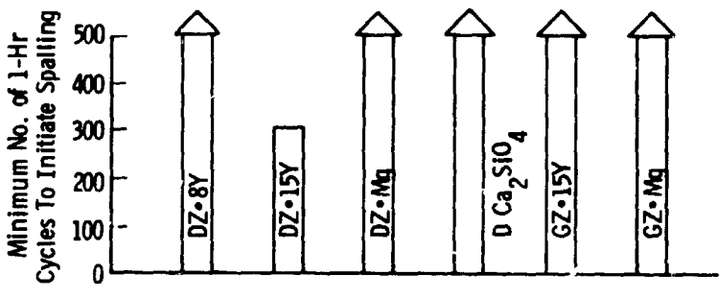

(a) Tests 1A2 and 1A2R (1150°C gas/800°C metal)

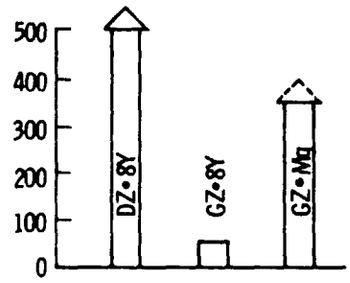

(b) Test 1A1
(1150°C gas/
900°C metal)

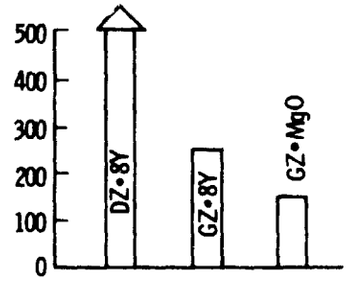

(c) Test 1AX
(1150°C gas/845°C metal)

Figure 12 - Cycles to failure in 500-hour cycle burner rig tests using clean fuel (GT No. 2)

Table 6

Test IA2 Summary*

Specimen No.	Position	Time (1-hr cycles) In	Time (1-hr cycles) Out	Net Cycles Completed	Failure Description
A-2	5	0	150	150	Chip on upper rear corner before test, did not change after 150 1-hr cycles - No Failure
A-3	3	0	500	500	No failure
B-1	6	0	500	500	At 182 hrs, cracked at lower side; at 269 hrs, cracked at upper side; at 292 hrs, a piece spalled from upper side.
B-2	4	0	150	150	No failure
C-1	7	0	500	500	"
C-2	1	0	150	150	"
U-1	2	0	500	500	"
U-2	8	0	150	150	"
A-7	5	151	500	350	"
B-3	4	151	500	350	At 350 hr, cracked at bottom front and back
C-3	1	151	500	350	No failure
U-3	1	151	500	350	"

A - $ZrO_2 \cdot 8Y_2O_3$ (duplex)

B - $ZrO_2 \cdot 15Y_2O_3$ (duplex)

C - $ZrO_2 \cdot 24.65$ MgO (duplex)

U - Uncoated U-720 alloy

*Fuel: GT No. 2
Temperatures: 1150°C gas/800°C metal

Table 7

Test IA2R Summary*

Specimen No.	Position	Time (1-hr cycles) In	Time (1-hr cycles) Out	Net Cycles Completed	Failure Description
D-2	2	0	500	500	No failure
D-3	8	0	353	353	No failure
E-1	3	0	500	500	No failure
E-2	5	0	353	353	No failure
F-1	6	0	500	500	No failure
F-2	4	0	353	353	No failure
G-1	7	0	500	500	No failure
G-2	1	0	353	353	No failure
D-6	5	354	500	147	No failure
E-5	1	354	500	147	No failure
F-5	4	354	500	147	No failure
H-4	8	354	500	147	No failure

D - Graded $ZrO_2 \cdot 15Y_2O_3$

E - Graded $ZrO_2 \cdot 24.65$ MgO

F - Duplex $ZrO_2 \cdot 8Y_2O_3$ (NASA)

G - Duplex Ca_2SiO_4 (NASA)

*Temperatures: 1150°C gas/800°C metal
Fuel: GT No. 2

Table 8

Test IA1 Summary*

Specimen No.	Position	Time (1-hr Cycles) In	Time (1-hr Cycles) Out	Net Cycles Completed	Failure Description
AB1	6	0	500	500	No Failure
AB2	3	0	150	150	" "
AB3	8	0	150	150	" "
AV1	2	0	500	500	" "
AV2	1	0	150	150	" "
AV3	4	0	150	150	" "
UB1	5	0	500	500	" "
UV1	7	0	500	500	" "
BB2	8	151	283	133	Spalled at upper end at 50 net cycles
BV2	3	151	283	133	Spalled at upper end at 73 net cycles
CB2	4	151	500	350	No Failure
CV2	1	151	500	350	" "
BB3	8	284	500	217	Spalled at upper end at 78-93 net cycles
BV3	3	284	500	217	Spalled at upper end at 78-93 net cycles

AB - Duplex $ZrO_2 \cdot 8Y_2O_3$ on U-720 alloy substrate
AV - Duplex $ZrO_2 \cdot 8Y_2O_3$ on ECY-768 alloy substrate
BB - Graded $ZrO_2 \cdot 8Y_2O_3$ on U-720 alloy substrate
BV - Graded $ZrO_2 \cdot 8Y_2O_3$ on ECY-768 alloy substrate
CB - Graded $ZrO_2 \cdot 24.65$ MgO on U-720 alloy substrate
CV - Graded $ZrO_2 \cdot 24.65$ MgO on ECY-768 alloy substrate
UB - Uncoated U-720 alloy
UV - Uncoated ECY-768 alloy

*Fuel = GT No. 2
Temperature = 1150°C gas/900°C metal

Table 9

Test IAX Summary*

Specimen No.	Position	Time (1-hr Cycles) In	Out	Net Cycles Completed	Failure Description
AV1	3	0	500	500	No Failure
AV2	7	0	150	150	" "
BV1	4	0	150	150	" "
BV2	8	0	500	500	Spalled at top end at 264 cycles
OV1	1	0	150	150	No failure
CV2	6	0	214	214	Spalled at top end at 214 cycles
SV1	5	0	500	500	No Failure
UV1	2	0	500	500	" "
AV3	7	151	500	350	" "
BV3	4	151	500	350	Spalled at top end at 240 cycles
CV3	1	151	500	350	Spalled at top end at 142 cycles
CV4	6	215	500	286	Spalled at top end at 172 cycles

AV - Duplex $ZrO_2 \cdot 8Y_2O_3$ on ECY-768 alloy substrate
BV - Graded $ZrO_2 \cdot 8Y_2O_3$ on ECY-768 alloy substrate
CV - Graded $ZrO_2 \cdot 24.65MgO$ on ECY-768 alloy substrate
SV - Duplex Ca_2SiO_4 on ECY-768 alloy substrate
UV - Uncoated ECY-768 alloy

*Fuel = GT No. 2
Temperature = 1150°C gas/845°C metal

ORIGINAL PAGE
BLACK AND WHITE PHOTOGRAPH

D - $ZrO_2 \cdot 8Y_2O_3$ 500 Cycles

G - $ZrO_2 \cdot 8Y_2O_3$ 133 Cycles

G - $ZrO_2 \cdot MgO$ 350 Cycles

Uncoated 500 Cycles

Fig. 13 - Exposed specimens from burner rig test IA1
Fuel: GT No. 2
Temperature: 1150°C gas/900°C metal

ORIGINAL PAGE
BLACK AND WHITE PHOTOGRAPH

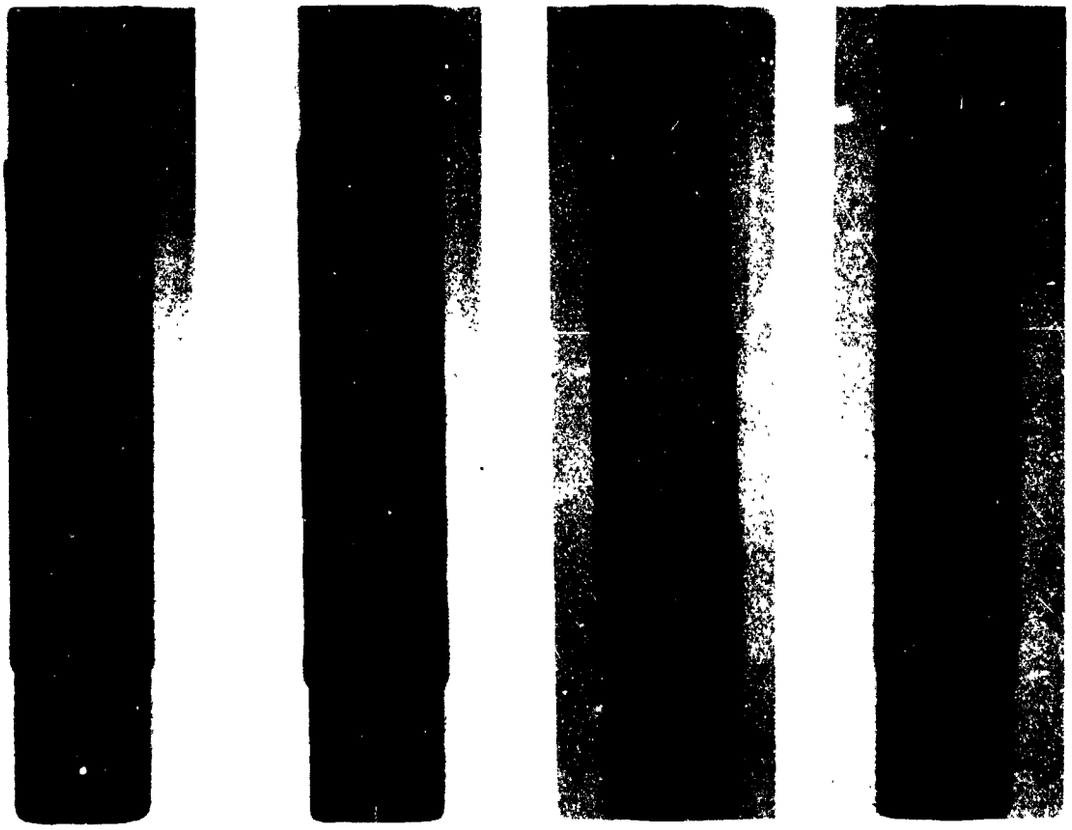

D - $ZrO_2 \cdot 8Y_2O_3$* 500 Cycles | G - $ZrO_2 \cdot 8Y_2O_3$ 500 Cycles | G - $ZrO_2 \cdot MgO$ 218 Cycles | D - Ca_2SiO_4 500 Cycles

Fig. 14 - Exposed specimens from burner rig test IAX
Fuel: GT No. 2
Temperature: 1150°C gas/ 845°C metal

*Mechanically chipped after 150 cycles.

ORIGINAL PAGE
BLACK AND WHITE PHOTOGRAPH

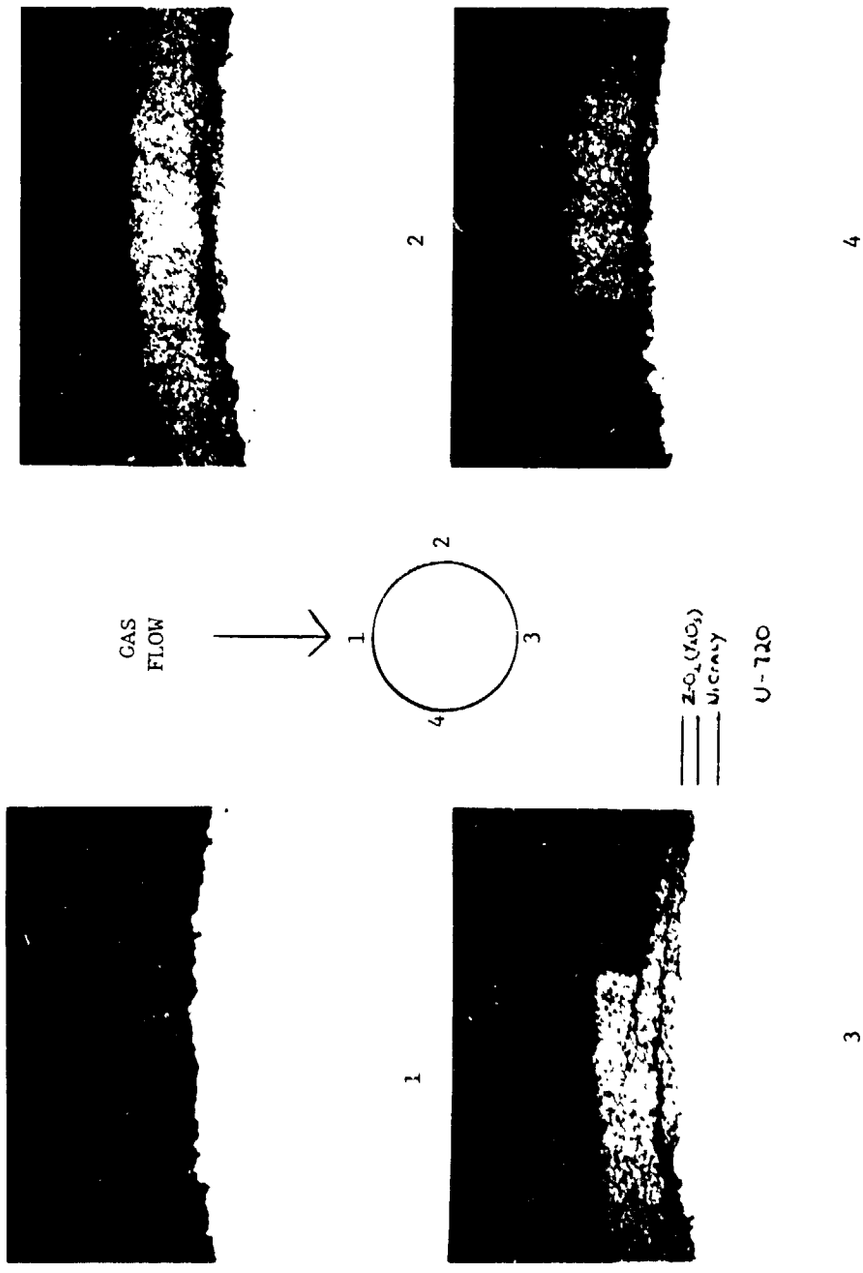

Fig. 15 - Metallographic cross-sections from four different locations of specimen B-3 ($ZrO_2 \cdot 15Y_2O_3$) after 350 hours of exposure in test IA2 (30X)

Surface X-ray diffraction analysis and electron microprobe mapping scans for Zr, Y, S, Mg, P, V, Na, Si, Al, Fe, Ni and Co were also obtained in the cross-sections of some test specimens. It was found that although microprobe analysis failed to identify any condensed impurities, X-ray analysis detected a trace of $Mg_3(PO_4)$ phase on the surface of the 500-hour specimens. This occurred because the clean GT No. 2 fuel actually contained about 0.3 ppm Mg and 0.3 ppm P. A $MgSO_4 \cdot 6H_2O$ phase was also found on the $ZrO_2 \cdot 24.65$ MgO/NiCrAlY specimens. This resulted from the reaction between the sulfur contained in the fuel (about 0.25 wt %) and the MgO in the coating. These $ZrO_2 \cdot 24.65$ MgO coatings also encountered considerable destabilization of the cubic/tetragonal phase. In fact, the 500-hour specimen which did not fail, showed only a small amount of cubic/tetragonal ZrO_2 phase remaining. This observation is in agreement with the fact that from phase equilibria considerations, tetragonal/cubic ZrO_2(MgO) is actually metastable at temperatures below ~900°C. (Ref. 30). Thus it should undergo an eutectoid decomposition and form MgO and monoclinic ZrO_2(MgO) when thermally cycled. The reaction with SO_2/SO_3 merely accelerates the decomposition.

Metallographic cross-sections of three specimens exposed to test 1A1 (1150°C/900°C gas/metal) are shown in Figs. 16-18. It was found that the original fraction of NiCrAlY particles contained in the graded zone of graded coatings (Figs. 16 and 17) was greatly reduced after the test. This clearly demonstrated that the graded zone of both types of graded coatings were extensively oxidized.

Results from X-ray diffraction analysis showed that the major oxidation product in the graded zone was NiO. Minor amounts of Cr_2O_3 as well as traces of Al_2O_3 were also identified. These oxidation products are expected from the NiCrAlY composition used; viz., Ni-20Cr-11Al-0.44Y.

Figure 18 shows the metallographic cross-section of specimen AB1 (D-$ZrO_2 \cdot 8Y_2O_3$, 500 cycles without failure). As may be seen, the specimen has excellent integrity after the test. However, electron microprobe analysis of this specimen showed that the NiCrAlY bond coat surface had oxidized and formed a 0.008 cm thick aluminum-rich surface layer which is presumably Al_2O_3 (Fig. 19b).

From these analyses it can be concluded that although the graded coatings out performed their duplex counterparts at the lower test temperature (800°C), they can encounter failure at higher temperature due to the disruptive internal oxidation of the NiCrAlY contained in the graded zone. A more oxidation resistant alloy is therefore needed for the graded coatings.

ORIGINAL PAGE
BLACK AND WHITE PHOTOGRAPH

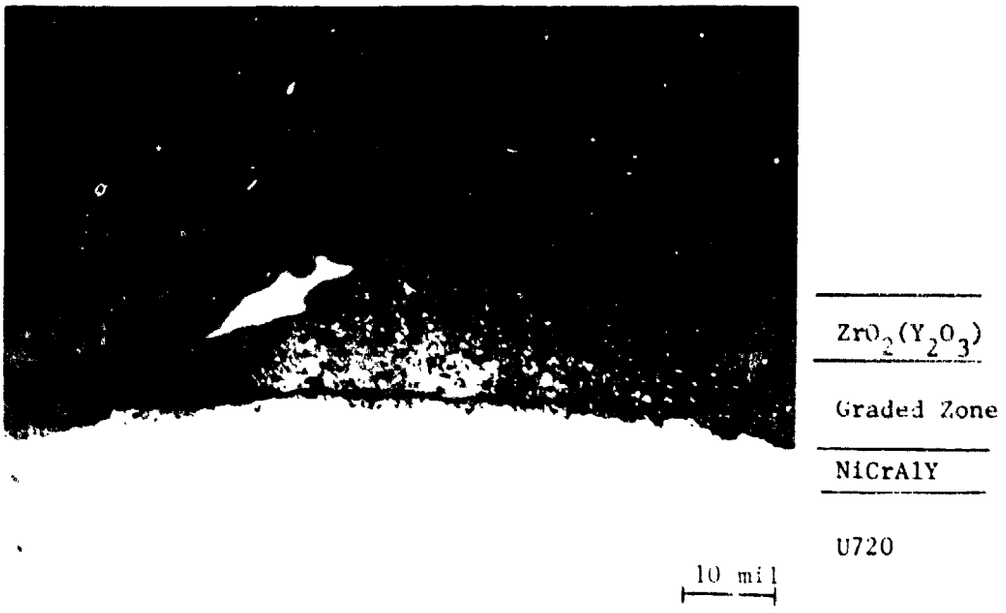

Fig. 16 - Specimen BB2 ($G\text{-}ZrO_2 \cdot 8Y_2O_3$) 133 cycles, Test IA1

ORIGINAL PAGE
BLACK AND WHITE PHOTOGRAPH

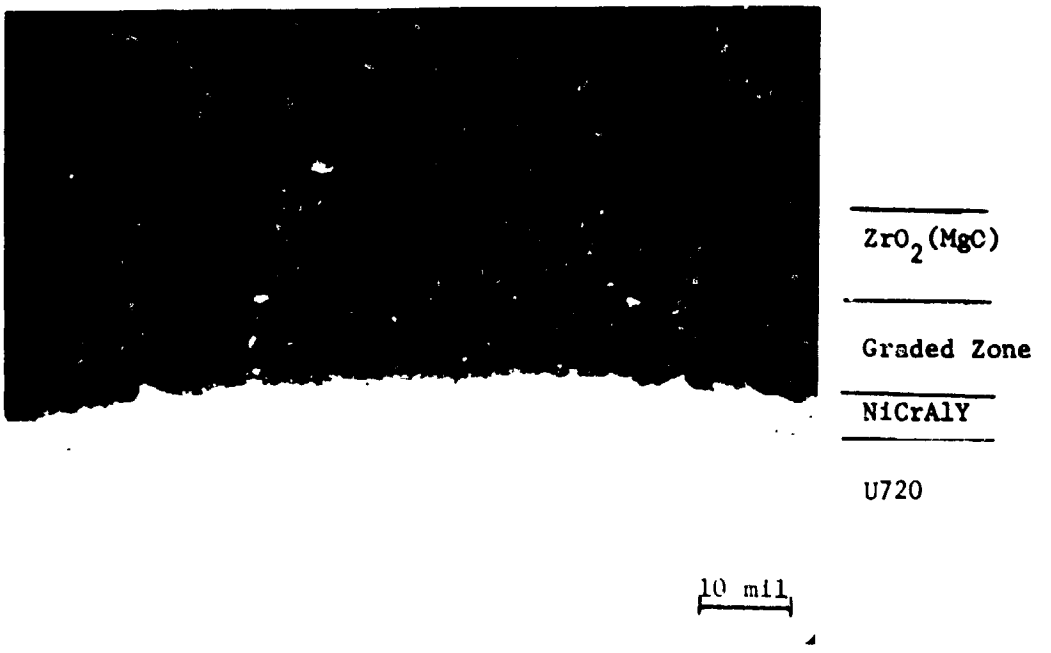

Fig. 17 - Specimen CB2 (G-ZrO_2·24.65 MgO) 350 cycles, Test IA1

ORIGINAL PAGE
BLACK AND WHITE PHOTOGRAPH

Fig. 18 - Specimen AB1 (D-$ZrO_2 \cdot 8Y_2O_3$) 500 cycles, Test IA1

ORIGINAL PAGE
BLACK AND WHITE PHOTOGRAPH

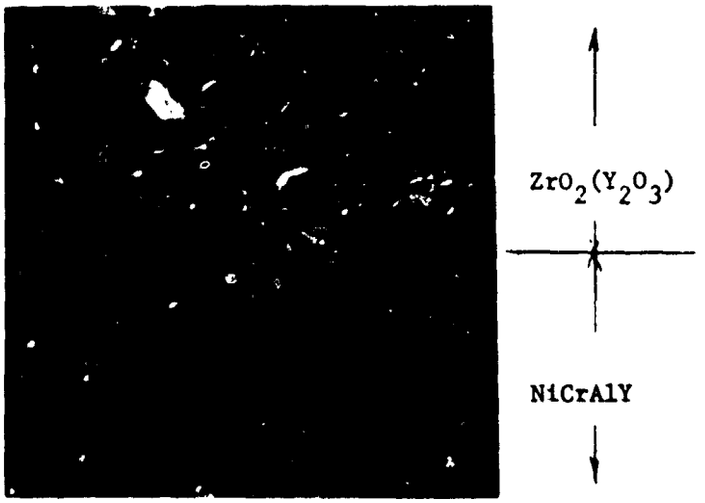

(a)

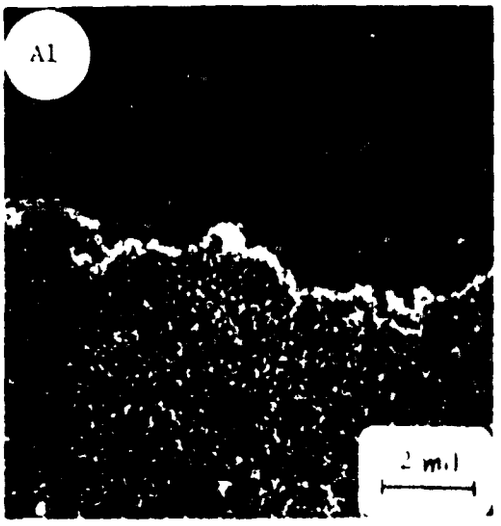

(b)

Fig. 14 - Specimen AB1 (D-$ZrO_2 \cdot 8Y_2O_3$) 500 cycles, Test IA1
(a) SEM picture of region near NiCrAlY
(b) Electron microprobe scan for Al

2.2.3 Task 1B - Fuel Sensitivity Tests

2.2.3.1 Test Results

The fuel sensitivity tests were conducted by maintaining the gas/metal temperature at 1150°C/800°C, respectively. GT No. 2 fuel doped to four levels of impurities to simulate crude and residual oils were used in the tests (Table 10). Following commercial turbine practice, a magnesium additive was added to fuels that contained vanadium (Mg/V = 3). All tests were terminated after 500 one-hour cycles.

Figure 20 shows the results of the burner rig fuel sensitivity tests with V dopants in terms of the minimum number of one-hour cycles to initiate spalling failure. The detailed test observations are listed in Tables 11-14. It is clear from these results that the partially stabilized $ZrO_2 \cdot 8Y_2O_3$ coating performed better than the fully stabilized $ZrO_2 \cdot 15Y_2O_3$ and $ZrO_2 \cdot 20Y_2O_3$ coatings.

A possible explanation for the better performance of the partially stabilized $ZrO_2(Y_2O_3)$ coatings is that with an optimum fraction of monoclinic $ZrO_2(Y_2O_3)$, the microscopically stressed, two phase $ZrO_2(Y_2O_3)$ system can relieve thermal stresses by developing small stable cracks throughout the ceramic (Ref. 31).

Test results shown in Fig. 20 also reveal strikingly that the graded coatings, regardless of their compositions, out performed the duplex counterparts. This reveals the advantage of the presence of a compliant component to prevent crack propagation and subsequent spallation even if the oxide component may be under corrosion attack. While it is clear from Fig. 20 that graded $ZrO_2 \cdot 8Y_2O_3$ and duplex Ca_2SiO_4 coatings performed the best, none of the coating systems tested could survive the most severe test with 180 ppm V. A general result from Fig. 20 is that vanadium appears to be very detrimental to coating life. Accelerated failures occurred with increasing vanadium content even when the Mg/V ratio remained constant.

Results from test 1B6, an accelerated sea salt corrosion test, are shown in Fig. 21. Detailed test observations are listed in Table 15. Note that the duplex coatings were tested at two metal temperatures: 800°C and 900°C. The 900°C was chosen as the higher testing temperature in order to be above the melting point of Na_2SO_4 (884°C).

It is clear from Fig. 21 that none of the coatings tested could survive the severity of the test. In fact, the Ca_2SiO_4 specimen tested at 900°C metal temperature spalled at the top after only seven one-hour cycles. The failed Ca_2SiO_4 specimen surfaces showed a glazed appearance suggesting the possibility of reaction between Ca_2SiO_4 and the combustion gases and/or condensates. Several NiCrAlY coated specimens also encountered severe

Table 10

SUMMARY OF FUEL SENSITIVITY TEST CONDITIONS

Test No.	Gas/Metal Temp (°C)	Fuel
1B4	1150/800	GT No. 2 doped to 1 ppm Na, 2 ppm V, 2 ppm P, 0.5 ppm Ca, 2 ppm Fe, 6 ppm Mg
1B4R	1150/800	GT No. 2 doped to 1 ppm Na, 2 ppm V, 2 ppm P, 0.5 ppm Ca, 2 ppm Fe, 6 ppm Mg
1B5	1150/800	GT No. 2 doped to 1 ppm Na, 50 ppm V, 2 ppm P, 0.5 ppm Ca, 2 ppm Fe, 150 ppm Mg
1BX	1150/800	GT No. 2 doped to 9 ppm Na, 180 ppm V, 18 ppm P, 4.5 ppm Ca, 2 ppm Fe, 594 ppm Mg, and 2.25 wt % S
1B6	1150/800 and 1150/900	GT No. 2 doped to 100 ppm Na, 180 ppm Cl, 13 ppm Mg, 4 ppm Ca, 4 ppm K and 2 wt % S

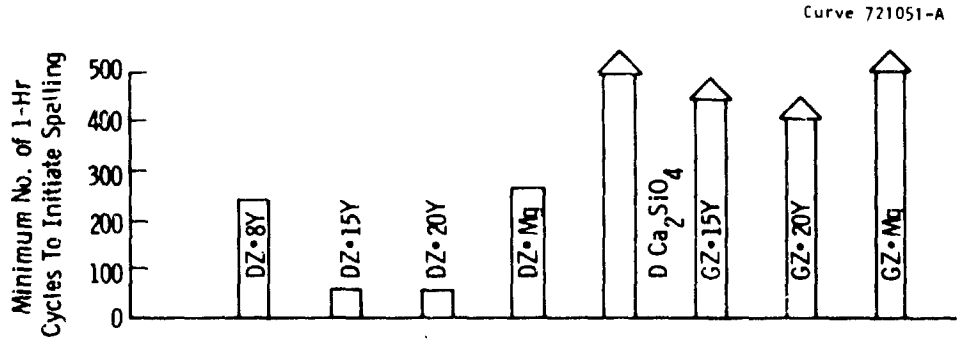

(a) Tests 1B4 and 1B4R
Fuel: GT No. 2 doped to (ppm) 1-Na, 2-V, 2-P, 0.5, Ca, 2-Fe, 6-Mg

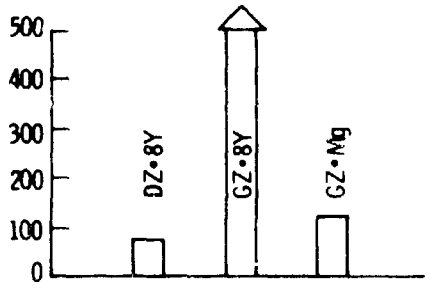

(b) Test 1B5
Fuel: GT No. 2 doped to (ppm)
1-Na, 50-V, 2-P, 0.5-Ca,
2-Fe, 150-Mg

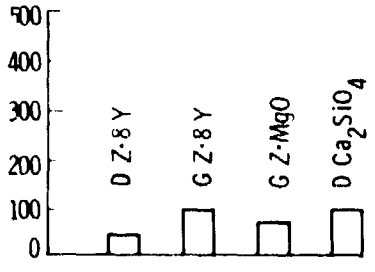

(c) Test 1BX
Fuel: GT No.2 doped to (ppm)
9-Na, 180-V, 18-P,
4.5 Ca, 2-Fe, 594-Mg

Figure 20 - Cycles to failure in 500-hour cycle burner rig tests using doped fuel (1150°C gas/800°C metal)

Table 11

Test IB4 Summary*

Specimen No.	Position	Time (1-hr cycles) In	Time (1-hr cycles) Out	Net Cycles Completed	Failure Description
A-4	3	0	500	500	At 219 hrs, spalled at upper front end
A-5	5	0	150	150	No failure
B-4	6	0	59	59	Spalled at both ends
B-5	4	0	59	59	Spalled at both ends
C-4	7	0	500	500	At 267 hrs, spalled at center front
C-5	1	0	150	150	No failure
U-4	2	0	500	500	"
U-5	8	0	150	150	"
D-1	6	60	500	440	"
B-6	4	60	500	440	Between 156-172 hr (net 96-112 hr) a large crack developed on upper front end and chip fell off at 196 hr (136 hr net)
C-6	1	151	500	350	No failure
A-6	5	151	500	350	"
U-6	8	151	500	350	"

A - $ZrO_2 \cdot 8Y_2O_3$ (duplex)

B - $ZrO_2 \cdot 15Y_2O_3$ (duplex)

C - $ZrO_2 \cdot 24.65$ MgO (duplex)

D - Graded $ZrO_2 \cdot 15Y_2O_3$

U - Uncoated U-720 alloy

*Fuel: GT No. 2 doped to 1 ppm Na, 2 ppm V, 2 ppm P, 0.5 ppm Ca, 2 ppm Fe, 6 ppm Mg.

Temperatures: 1150°C gas/800°C metal

Table 12

Test IB4R Summary*

Specimen No.	Position	Time (1-hr cycles) In	Time (1-hr cycles) Out	Net Cycles Completed	Failure Description
D-5	2	0	95	95	No failure
D-4	8	0	95	95	No failure
E-3	3	0	500	500	No failure
E-4	5	0	50	350	No failure
F-3	6	0	500	500	Chipped at 314 hr, spalled through length of specimen at 421 hours.
F-4	4	0	350	350	Chipped at 265 hours
G-3	7	0	350	350	No failure
G-4	1	0	500	500	No failure
H-1	2	96	189	93	Spalled at upper end at 56 hours
H-3	2	190	350	160	Spalled at 60 hours
K-0	8	96	500	405	No failure
E-6	5	351	500	150	No failure
F-6	4	351	500	150	No failure
D-4	7	351	500	95+150	No failure
K-1	2	351	500	150	No failure

D - Graded $ZrO_2 \cdot 15Y_2O_3$

E - Graded $ZrO_2 \cdot 24.65MgO$

F - Duplex $ZrO_2 \cdot 8Y_2O_3$ (NASA)

G - Duplex Cn_2SiO_4 (NASA)

H - Duplex $ZrO_2 \cdot 20Y_2O_3$

K - Graded $ZrO_2 \cdot 20Y_2O_3$

*Fuel: GT No. 2 doped to 1 ppm Na, 2 ppm V, 2 ppm P, 0.5 ppm Ca, 2 ppm Fe, 6 ppm Mg.

Temperatures: 1150°C gas/800°C metal

Table 13

Test IB5 Summary*

Specimen No.	Position	Time (1-hr Cycles) In	Time (1-hr Cycles) Out	Net Cycles Completed	Failure Description
AB4	3	0	150	150	Chipped at upper end at 78 cycles Spalled at upper end at 137 cycles
AB5	5	0	500	500	Chipped at upper end at 78 cycles
BB4	6	0	500	500	No Failure
BB5	4	0	150	150	" "
CB4	2	0	150	150	Spalled at upper end at 115 cycles
CB5	8	0	500	500	Chipped at upper end at 113 cycles
UB4	7	0	500	500	No Failure
UB5	1	0	150	150	" "
AB6	3	151	500	350	Spalled at upper end at 265 net cycles
BB6	4	151	500	350	No Failure
CB6	2	151	500	350	" "
UB6	1	151	500	350	" "

AB - Duplex $ZrO_2 \cdot 8Y_2O_3$ on U-720 alloy substrate
BB - Graded $ZrO_2 \cdot 8Y_2O_3$ on U-720 alloy substrate
CB - Graded $ZrO_2 \cdot 24.65$ MgO on U-720 alloy substrate
UB - Uncoated U-720 alloy

* Fuel = GT No. 2 doped to 1 ppm Na, 50 ppm V, 2 ppm P, 0.5 ppm Ca, 2.0 ppm Fe, 150 ppm Mg.
Temperature = 1150°C gas/800°C metal

Table 14

Test IBX Summary*

Specimen No.	Position	Time (1-Hr cycles) In	Time (1-Hr cycles) Out	Net Cycles Completed	Failure Description
IA1	3	0	150	150	Spalled at front after 39 cycles
IA2	6	0	150	150	Spalled at front after 98 cycles
IB1	1	0	150	150	Chipped at top after 98 cycles
IB2	7	0	500	500	No failure
IC1	5	0	500	500	Small chip at top after 150 cycles
IC2	4	0	150	150	Chipped at lower front after 59 cycles
IS1	2(3**)	0	500	500	Chipped at top edge after 98 cycles, surface micro-flaking
IN1	8(2**)	0	500	500	No failure
IB3	1	151	500	350	Spalled at bottom after 157 cycles
IC3	4	151	500	350	Chipped to top after 350 cycles
IS2	6	151	500	350	Surface micro-flaking after ~100 cycles chipped at top edge after 350 cycles
WB1	8	151	500	350	Mechanical chipped at top edge after 156 cycles

LA - Duplex $ZrO_2 \cdot 8Y_2O_3$
IB - Graded $ZrO_2 \cdot 8Y_2O_3$
IC - Graded $ZrO_2 \cdot 24.65$ MgO
IS - Duplex Ca_2SiO_4
IN - NiCrAlY (5 mil)
WB - Duplex $ZrO_2 \cdot 8Y_2O_3$ (Westinghouse)

} on U-720 alloy substrate

*Fuel = GT No. 2 doped to 9 ppm Na, 180 ppm V, 18 ppm P, 4.5 ppm Ca, 2 ppm Fe, 596 ppm Mg and 2.25% S.
Temperature = 1150°C gas/800°C metal
**New position after 150 cycles

Curve 728570-A

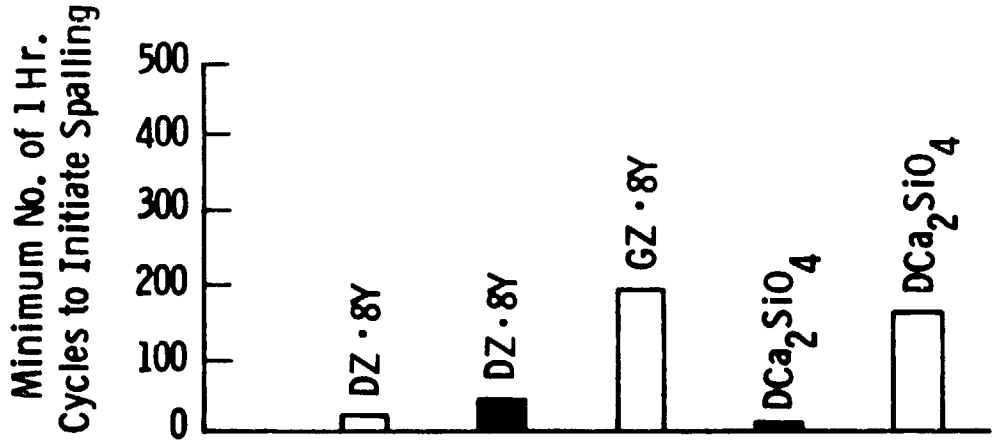

Figure 21 - Cycles to failure in a 300-hour cycle burner rig test (Test 1B6)
Temperature: ▭ 1150°C gas/800°C metal
▬ 1150°C gas/900°C metal
Fuel: GT No. 2 doped to (ppm): 100-Na, 180-Cl, 13-Mg, 4-Ca, 4-K 2 Wt%S

Table 15

TEST 1B6 SUMMARY*

Specimen No.*	Position	Time 1-Hr Cycles In	Time 1-Hr Cycles Out	Net Cycles Completed	Failure Description
A1 (800)	4	0	300	300	small chip at front after 18 cycles
A2 (900)	6	0	151	151	chipped at front bottom after 67 cycles
B1 (800)	1	0	300	300	spalled at middle after 191 cycles
B2 (800)	8	0	151	151	No failure
S1 (900)	2	0	151	151	Spalled at top after 7 cycles
S2 (800)	5	0	300	300	Spalling at front after 163 cycles
N1 (900)	3	0	300	300	Severe hot corrosion
N2 (857)	7	0	151	151	Signs of hot corrosion
A3 (900)	6	152	300	149	Spalled at top after 40 cycles
B3 (800)	8	152	300	149	No failure
N3 (857)	7	152	300	149	Signs of hot corrosion
WB1 (900)	2	152	300	149	Cracked at front after 40 cycles

A - D - $ZrO_2 \cdot 8Y_2O_3$

B - G - $ZrO_2 \cdot 8Y_2O_3$

S - D - Ca_2SiO_4

N - NiCrAlY (5 mil)

WB - D - $ZrO_2 \cdot 8Y_2O_3$ (Westinghouse sprayed)

Fuel = GT No. 2 doped to 100 ppm Na, 180 ppm Cl, 13 ppm Mg, 4 ppm Ca, 4 ppm K, 2 wt% S.

* Temperature = 1150°C gas/metal temperature (°C) in parenthesis.

hot corrosion. Although most of the coatings failed in relatively short testing times, the test was continued to accumulate 300 one-hour cycles in order to gain information on the possible corrosion resistance of failed specimens that still retained a thin coating layer.

The post-test conditions of some representative specimens from these fuel sensitivity tests are shown in Figs. 22-24.

2.2.3.2 Post-test Analysis

Metallographic examination of the contaminated fuel tested specimens showed that the duplex coatings always spalled in the ceramic coating very close to the ceramic/NiCrAlY interface. The cross-section of a D-$ZrO_2 \cdot 8Y_2O_3$ specimens failed in the 50 ppm V test (1B5) is shown in Fig. 25 as an example. This is similar to the failure locations of the clean fuel tested specimens mentioned in section 2.2.2.2. However, for graded specimens tested in contaminated fuels, cracking and eventual spalling occurred only near the oxide/graded zone interface. Thus a graded zone which can provide some protection was left adhering to the specimen. A typical cross-section of a graded specimen failed in a contaminated fuel test is shown in Fig. 26. This is different from the failure mode of the graded coatings encountered in clean fuel tests at higher metal temperatures (845 and 900°C) where failures occur at the graded zone/NiCrAlY bond coat interface as shown earlier in Figs. 16, 17.

Detailed post-test analyses, which included X-ray diffraction, chemical as well as electron microprobe analysis showed that chemical and physical interactions between the ceramic coatings and the combustion gases and/or condensates played a critical role in coating degradation. Detailed findings from the post-test analysis for each coating system are described below.

(a) $ZrO_2 \cdot Y_2O_3$/NiCrAlY coating systems

Post-test analysis on $ZrO_2(Y_2O_3)$ coatings exposed to combustion environments containing vanadium impurities revealed that the coating degradation was closely related to the destabilization of $ZrO_2(Y_2O_3)$ induced by the reaction with combustion condensates.

$ZrO_2 \cdot 8Y_2O_3$ specimens (both graded and duplex) that failed in the vanadium doped tests invariably showed an increase of monoclinic $ZrO_2(Y_2O_3)$, (greater amounts with increased vanadium contamination). Using careful sampling procedures, this destabilization process of tetragonal/cubic $ZrO_2(Y_2O_3)$ to monoclinic $ZrO_2(Y_2O_3)$ has been examined in detail. Table 16 shows the results of post-test X-ray analysis on a failed graded $ZrO_2 \cdot 8Y_2O_3$ specimen exposed in Test 1BX for 350 one-hour cycles. X-ray samples were taken at various depths of the coating from both leading and trailing edges.

ORIGINAL PAGE
BLACK AND WHITE PHOTOGRAPH

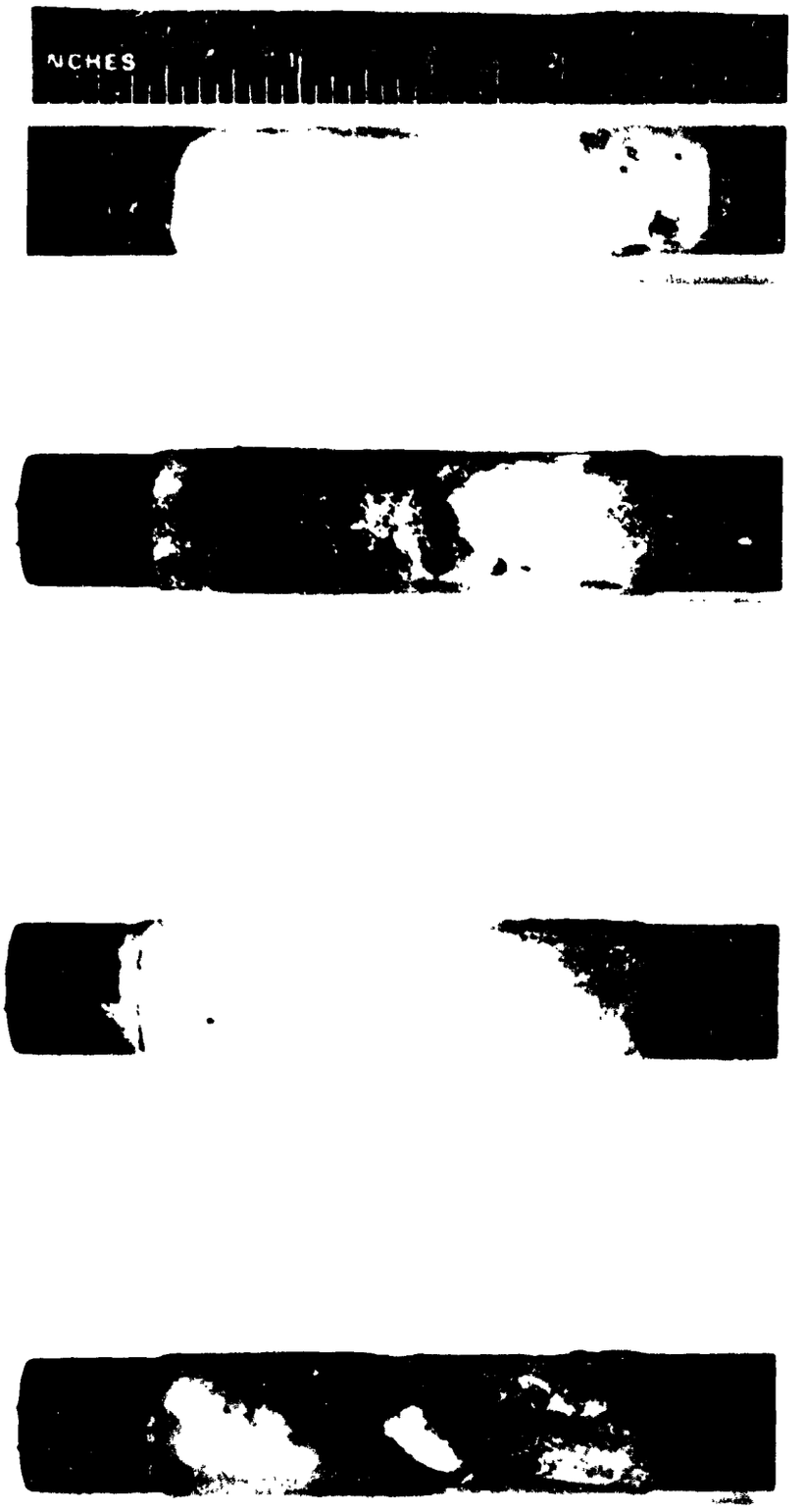

Fig. 22 - Exposed specimens from test IB5
Fuel: GT No. 2 doped to (ppm): 1-Na, 50-V, 2-P, 0.5-Ca, 2-Fe, 150 Mg
Temperature: 1150°C gas/800°C metal

ORIGINAL PAGE
BLACK AND WHITE PHOTOGRAPH

Fig. 23 - Exposed specimens from Test IBX
Fuel: CT No. 2 doped to (ppm): 9-Na, 180-V, 18-P, 4.5 Ca, 2-Fe, 594 Mg
and 2.25 wt % S
Temperature: 1150°C Gas/800°C metal

N-2 NiCrAlY
1575°F Metal
~1575°F Surface

A-3 D-$ZrO_2 \cdot 8Y_2O_3$
1650°F Metal
~1760°F Surface

B-3 G-$ZrO_2 \cdot 8Y_2O_3$
1475°F Metal
~1650°F Surface

S-1 D-Ca_2SiO_4
1650°F Metal
~1760°F Surface

WB-1 D-$ZrO_2 \cdot 8Y_2O_3$
1650°F Metal
~1760°F Surface

ORIGINAL PAGE
BLACK AND WHITE PHOTOGRAPH

Fig. 24 - Exposed specimens from Test IB6
Fuel: GT No. 2 doped to (ppm): 100-Na, 180-Cl, 13-Mg, 4-Ca, 4-K and 2 wt % S
Temperature: 1150°C gas/800-900°C (1475-1650°F) metal

ORIGINAL PAGE
BLACK AND WHITE PHOTOGRAPH

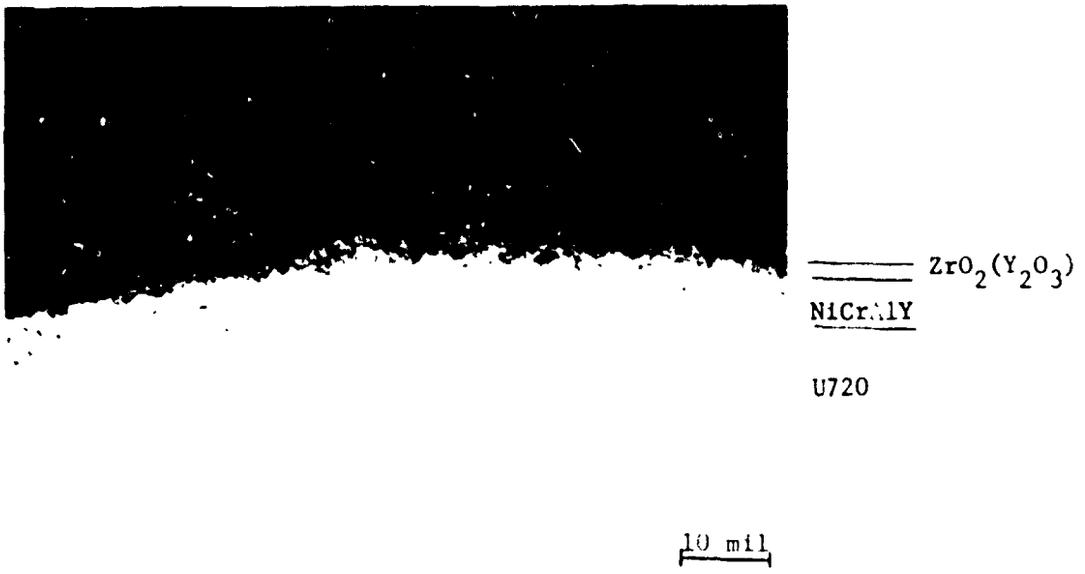

Fig. 25 - Specimen AB4 (D-$ZrO_2 \cdot 8Y_2O_3$) 150 cycles, Test IB5

ORIGINAL PAGE
BLACK AND WHITE PHOTOGRAPH

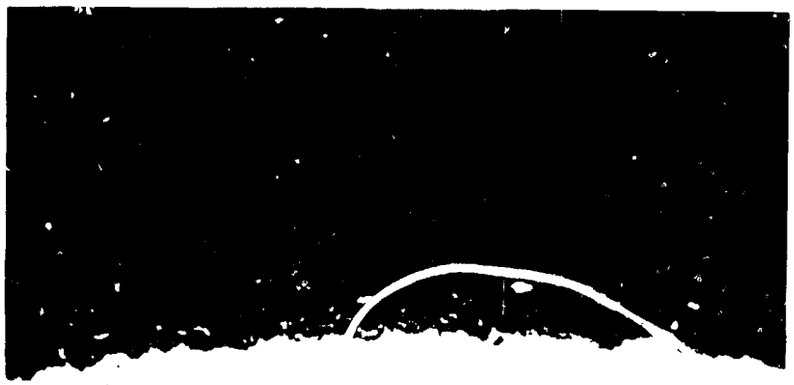

Fig. 26 - Specimen CB4 (C-ZrO_2·24.65 MgO) 150 cycles, Test IB5

Table 16

X-Ray Results on a G-$ZrO_2 \cdot 8Y_2O_3$ Specimen
Exposed for 350 cycles in Test 1BX

X-Ray Sample	Pre-Test Phase	Post-Test Phase
Surface deposits (L.E.)	-	M - $MgSO_4.6H_2O$
		m - MgO, $Mg_3V_2O_8$
Coating surface just below deposits (L.E.)	M-$ZrO_2(Y_2O_3)$(tetra/cubic)	M - $ZrO_2(Y_2O_3)$(monoclinic)
	m-$ZrO_2(Y_2O_3)$(monoclinic)	m - $ZrO_2(Y_2O_3)$ (tetra/cubic)
		T - $MgSO_4$
Deep coating interior (L.E.)	M-$ZrO_2(Y_2O_3)$(tetra/cubic)	M - $ZrO_2(Y_2O_3)$(tetra/cubic)
	m-$ZrO_2(Y_2O_3)$(monoclinic)	m - $ZrO_2(Y_2O_3)$(monoclinic)
Back of spalled chip(L.E.)	M-$ZrO_2(Y_2O_3)$(tetra/cubic)	M - $ZrO_2(Y_2O_3)$(tetra/cubic)
	m-$ZrO_2(Y_2O_3)$(monoclinic)	m - $ZrO_2(Y_2O_3)$(monoclinic)
Surface deposits (T.E.)		T - $MgSO_4.6H_2O$
Coating surface just below deposit (T.E.)	M-$ZrO_2(Y_2O_3)$(tetra/cubic)	M - $ZrO_2(Y_2O_3)$(tetra/cubic)
	m-$ZrO_2(Y_2O_3)$(monoclinic)	m - $ZrO_2(Y_2O_3)$(monoclinic)

L.E. = leading edge

T.E. = trailing edge

M = Major
m = Minor

T = Trace

*Test Temperature = 1150°C gas/800°C metal

Fuel: GT No. 2 doped to (ppm) Na - 9, V-180, p - 18,
Ca - 4.5, Fe - 2, Mg - 594, S - 2.25%

Test Time - 350 one-hour cycles

As may be seen from Table 16 the destabilization of tetragonal/cubic $ZrO_2(Y_2O_3)$ occurred predominantly at regions close to the surface while the coating interior remained unaffected. It is also evident that the destabilization reaction occurred preferentially at the specimen leading edge where more combustion condensates ($Mg_3V_2O_8$, $MgSO_4$ and MgO) are collected. Another important observation was that the back of a chip spalled from the leading edge showed no observable destabilization. These observations suggest that in combustion environments containing vanadium impurity, destabilization of tetragonal/cubic zirconia occurs as the result of chemical reactions with combustion deposits collected on the specimen surface.

It is well known that monoclinic ZrO_2 undergoes phase transformation on heating and cooling with an associated disruptive volume change reported between 4 to 6%. This destabilization reaction can therefore initiate coating cracking and eventually lead to failure (spallation).

Post-test analysis of specimens exposed to the Na doped fuel tests revealed that the condensation of molten Na_2SO_4 was the main cause of coating failure. Figure 27 shows the EMP mapping for D-$ZrO_2 \cdot 8Y_2O_3$/NiCrAlY that was exposed to the 100 ppm Na, 2 wt % S doped fuel test (Test 1B6) for 151 one-hour cycles. It can be seen that Na_2SO_4 has penetrated deeply into the cracks and pores of the $ZrO_2 \cdot Y_2O_3$ coating.

Figure 28 shows the EMP scans on the same D-$ZrO_2 \cdot 8Y_2O_3$/NiCrAlY specimen on an area near the NiCrAlY bond coat. Examination of this figure demonstrates that the Na_2SO_4 condensate can penetrate into the porous $ZrO_2 \cdot Y_2O_3$ coating as far as the $ZrO_2 \cdot Y_2O_3$/NiCrAlY interface.

It is important to point out that this Na_2SO_4 penetration can even occur at temperatures below the melting point of Na_2SO_4 (884°C), because fuel impurities such as Mg can depress the sulfate melting point by forming low melting eutectics such as Na_2SO_4-$MgSO_4$. This is illustrated by the EMP scans of a failed D-$ZrO_2 \cdot 20Y_2O_3$ specimen (Fig. 29) exposed to the (1 ppm Na, 6 ppm Mg test at 800°C metal temperature (Test 1B4R).

The deep penetration of Na, Mg and S into the porous oxide coating has been connected to the formation and penetration of a liquid Na_2SO_4-$MgSO_4$ salt. Chemical analysis of water-washed samples showed that the soluble condensate consisted of $Na_2SO_4 \cdot MgSO_4$ in the molar ratio of 0.72, assuming that the soluble sodium and magnesium were present as sulfates. According to the Na_2SO_4-$MgSO_4$ phase system (Ref. 32), this mixed salt should be molten at 765°C. Since the highest temperature gradient in the oxide samples is 900°C surface and 300°C bond coat, the salt was molten during testing where these conditions prevailed.

It is interesting to note that neither X-ray nor EMP analyses showed any indication of Na-S-Y or Na-S-Zr type compound formation. This suggested that the effect of the Na_2SO_4-$MgSO_4$ on $ZrO_2(Y_2O_3)$ coating is probably

ORIGINAL PAGE
BLACK AND WHITE PHOTOGRAPH

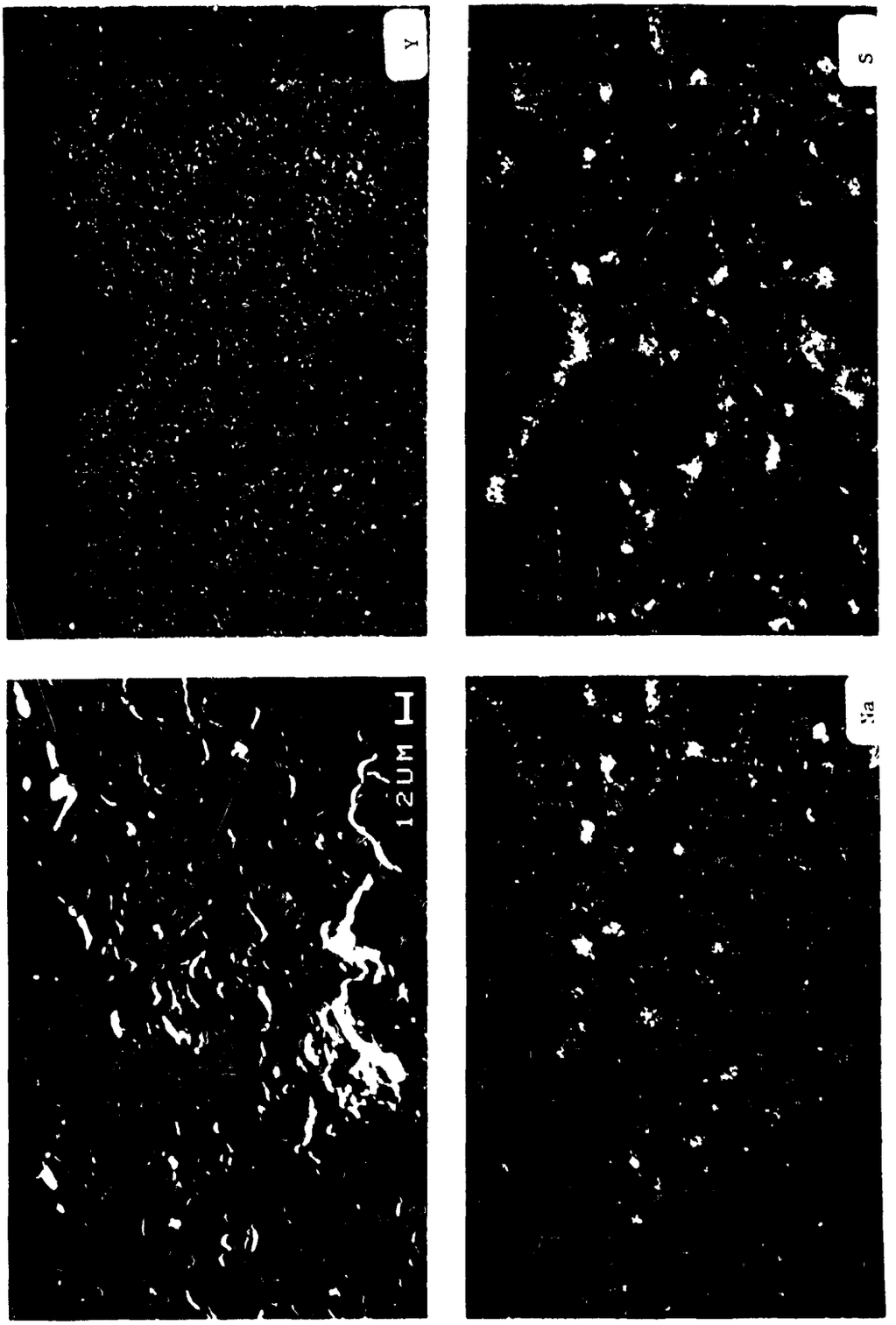

Fig. 27 - EMP scans on specimen 1A2 (D-ZrO_2·$8Y_2O_3$) 151 cycles, Test 1B6

ORIGINAL PAGE
BLACK AND WHITE PHOTOGRAPH

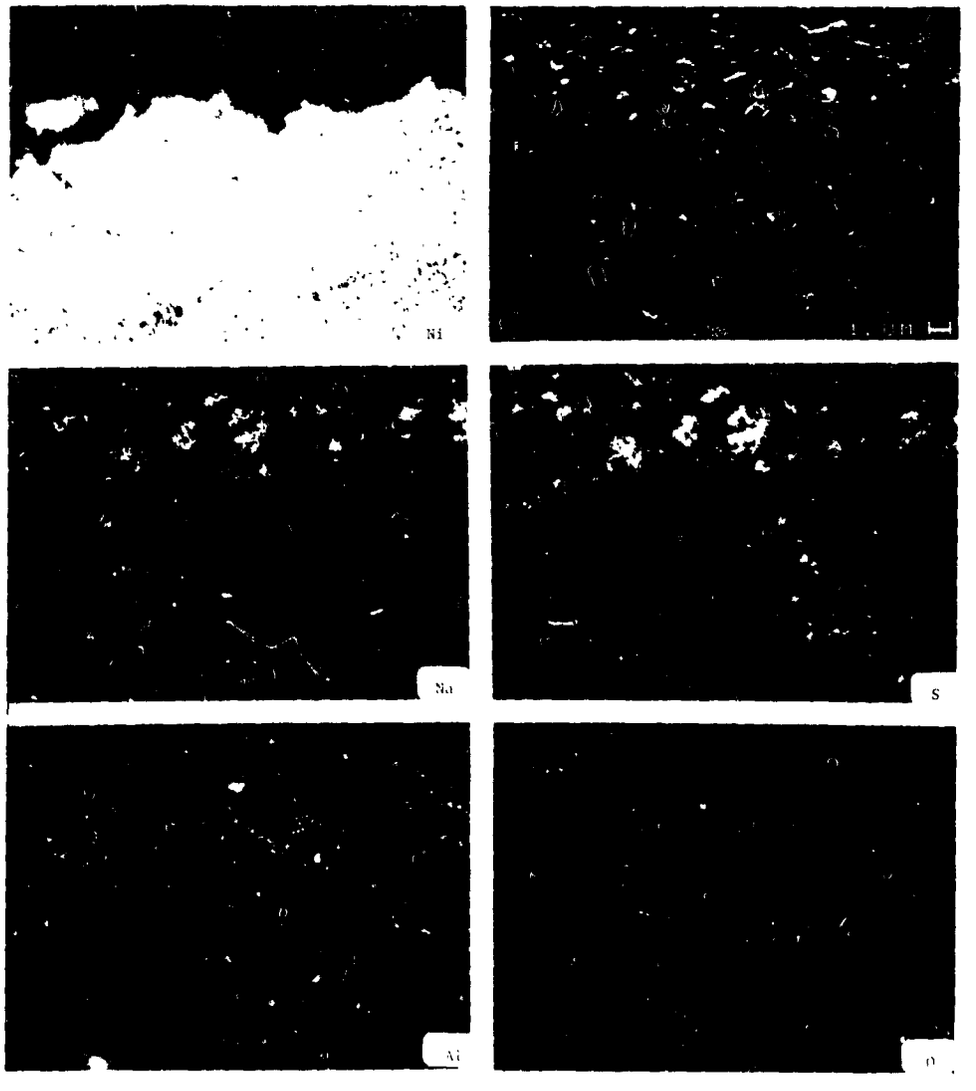

Fig. 28 - EMP scans on specimen A2 (D-$ZrO_2 \cdot 8Y_2O_3$) 151 cycles, Test 1B6 (area near bond coat)

ORIGINAL PAGE
BLACK AND WHITE PHOTOGRAPH

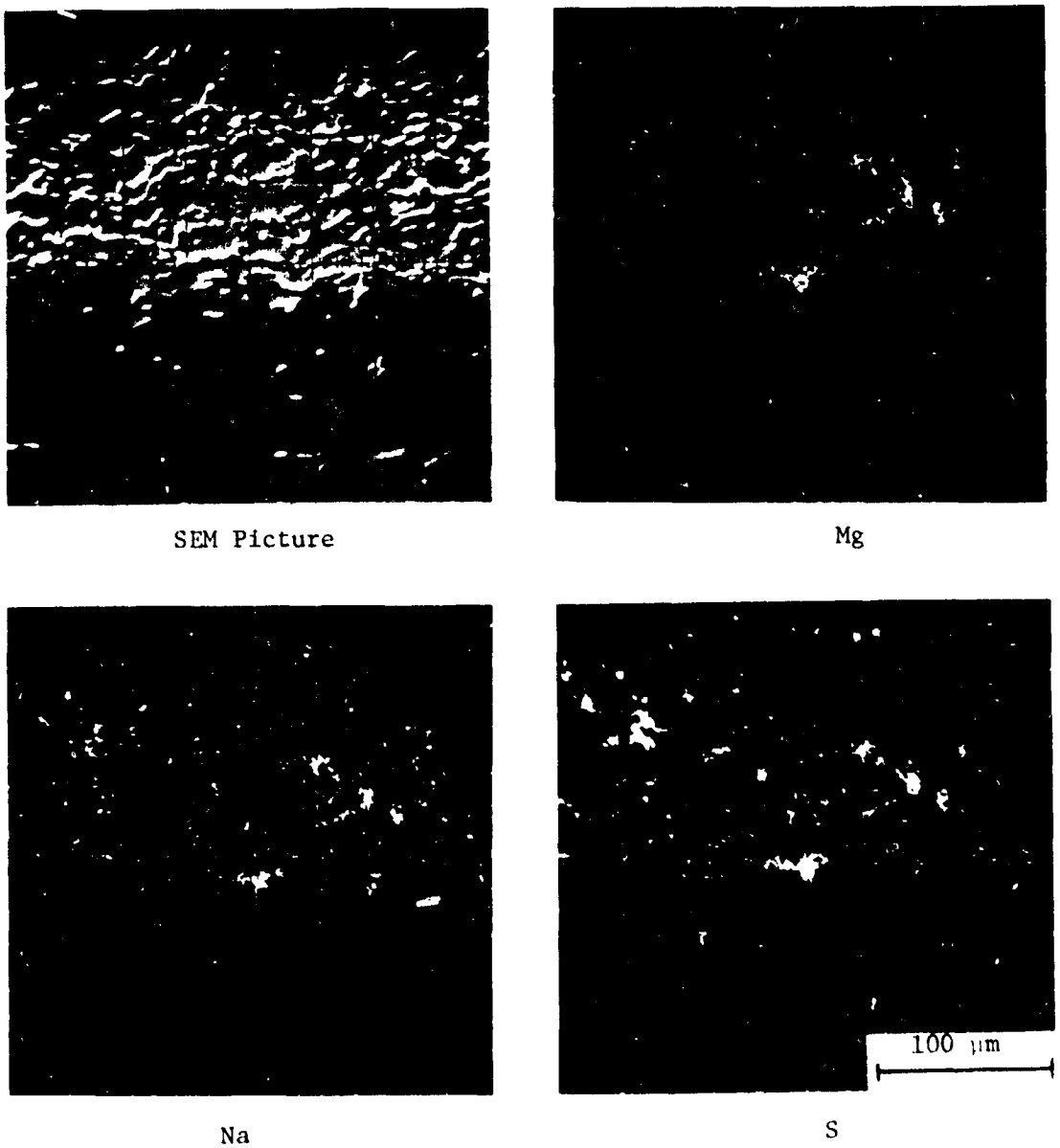

Fig. 29 - EMP scans on specimen H-3 (D-ZrO_2•20Y_2O_3) 160 cycles, Test IB4R

mechanical in nature. Several possible mechanisms relating molten sulfate penetration to $ZrO_2(Y_2O_3)$ coating failure will be discussed in a later section. Among these mechanisms, the one that involves the thermal expansion mismatch between the $ZrO_2(Y_2O_3)$ coating and the entrapped solidified salt condensate is the most probable.

(b) $ZrO_2 \cdot 24.65$ MgO coating systems

X-ray diffraction analysis revealed that in both the vanadium and sodium-doped tests a large fraction of MgO contained in the original duplex and graded $ZrO_2 \cdot 24.65$ MgO coatings had reacted with SO_2/SO_3 (g) in the combustion gases to form $MgSO_4$. Fig. 30 shows the EMP scans on a G-$ZrO_2 \cdot 24.65$ MgO specimen that was exposed for 500 hrs. in Test 1B4R. $MgSO_4$ was found throughout the outer three-quarters of the coating thickness.

A result of removing MgO stabilizer from the ZrO_2(MgO) solid solution was destabilization of ZrO_2(MgO) according to the reaction:

$$ZrO_2 \cdot a\ MgO + x\ SO_3 \rightarrow ZrO_2 \cdot (a-x)\ MgO + x\ MgSO_4$$

(Tetragonal/cubic) (Monoclinic)

This is clearly illustrated by the X-ray diffraction analysis results obtained on several $ZrO_2 \cdot 24.65$ MgO specimens exposed to Test 1B4 for various times (Table 17). The monoclinic ZrO_2(MgO) phase changed from a trace phase into a major phase in less than 350 hrs.

This observed destabilization as well as the volume change associated with the $MgSO_4$ formation were the major contributors responsible for the coating failure.

(c) Ca_2SiO_4 coating system

X-ray and electron microprobe results on the duplex Ca_2SiO_4 coating, which performed quite well in most of the burner rig tests, suggested the occurrence of chemical reactions. In both the vanadium and sodium-doped fuel tests, Ca_2SiO_4 was found to be susceptible to the attack of SO_3/SO_2 gas. A soft and powdery $CaSO_4$ phase was generally found throughout the coating. The reaction that occurred was:

$$Ca_2SiO_4 + 2SO_3(g) = 2CaSO_4 + SiO_2$$

Fig. 31 shows the EMP scans on an interior region of a D-Ca_2SiO_4 specimen that was exposed to the sodium doped test (Test 1B6) for 151 cycles. The extensive formation of $CaSO_4$ is clearly evident.

There is also evidence that a ternary magnesium-calcium silicate may have formed on the Ca_2SiO_4 coating surface after exposure to the combustion environments containing magnesium-vanadium impurities (Fig. 32). Although X-ray diffraction analysis could not identify the exact reaction product because broad amorphous peaks were obtained, the overlapping of

ORIGINAL PAGE
BLACK AND WHITE PHOTOGRAPH

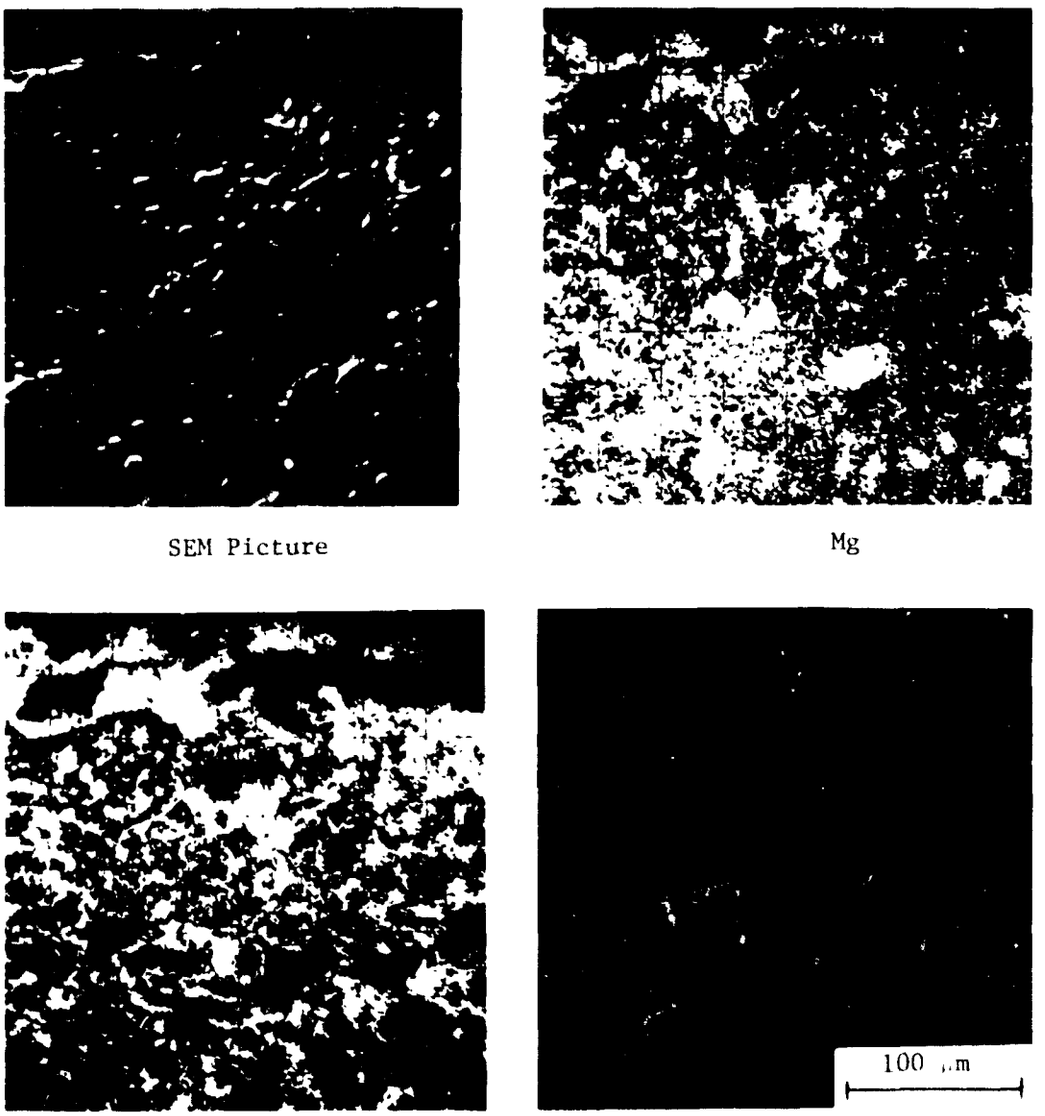

Fig. 30 - EMP scans on specimen L3 (G-ZrO_2·24.65 MgO)
500 cycles, Test IB4R

Table 17

X-RAY RESULTS ON $ZrO_2 \cdot 24.65$ MgO SPECIMENS EXPOSED TO TEST 1BX

Exposed Time	
0	M - Tetragonal/cubic ZrO_2(MgO) m - MgO T - Monoclinic ZrO_2(MgO)
150 hrs	M - Tetragonal/cubic ZrO_2(MgO) m - MgO, $Mg_3(PO_4)_2$ Monoclinic ZrO_2(MgO)
350 hrs	M - Monoclinic ZrO_2(MgO) m - Tetragonal/cubic ZrO_2(MgO) MgO, $MgSO_4 \cdot 6H_2O$ $Mg_3(PO_4)_2$
500 hrs	M - Monoclinic ZrO_2(MgO) m - Tetragonal/cubic ZrO_2(MgO) $MgSO_4 \cdot 6H_2O$, $Mg_3(PO_4)_2$

M = major
m = minor
T = trace

ORIGINAL PAGE
BLACK AND WHITE PHOTOGRAPH

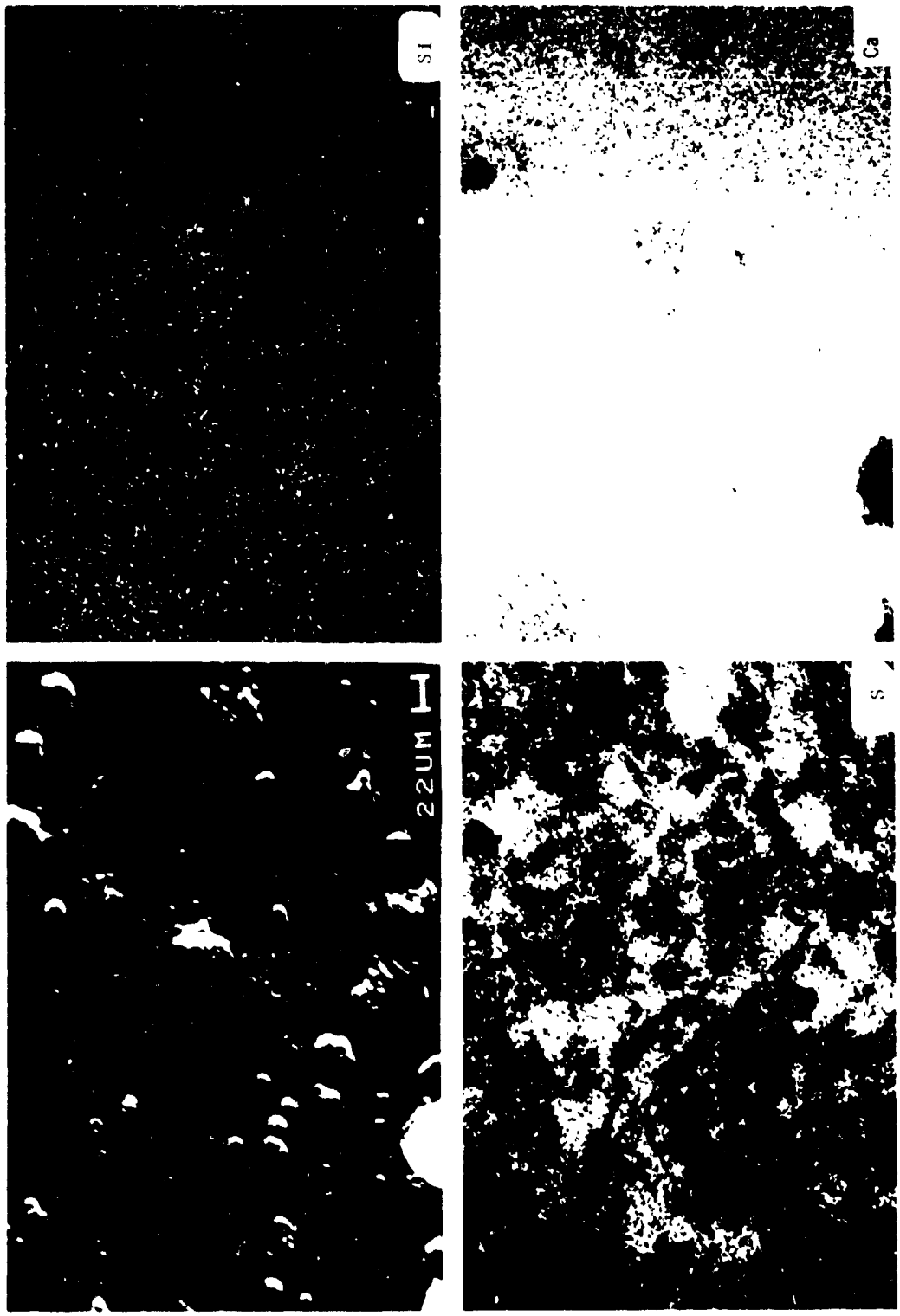

Fig. 31 - EMP scans on specimen S2 ($D\text{-}Ca_2SiO_4$) 300 cycles. Test IB6

ORIGINAL PAGE
BLACK AND WHITE PHOTOGRAPH

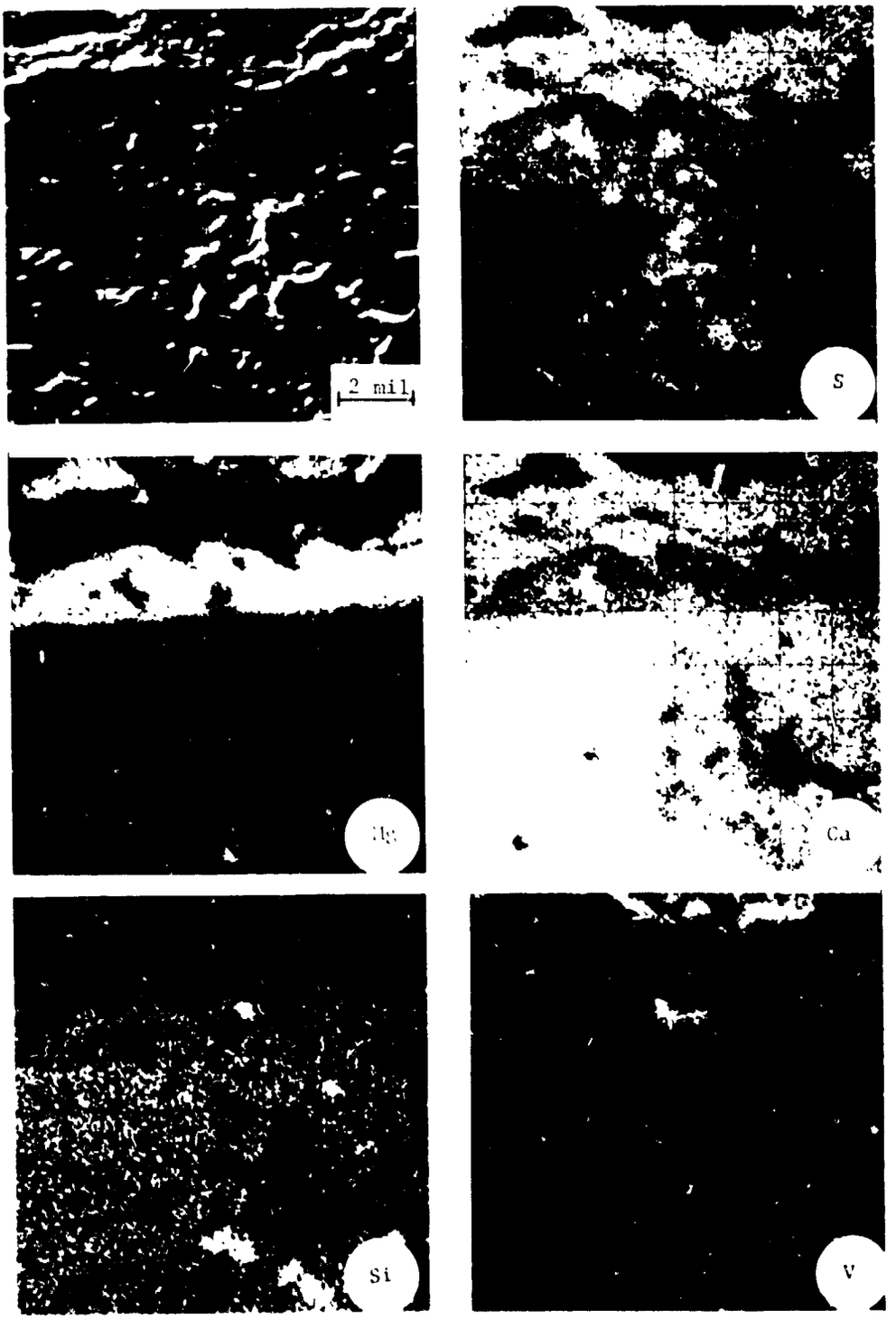

Fig. 32 - EMP scans on specimen SV1 (D-Ca_2SiO_4) 500 cycles, Test IC2

Mg, Si and Ca concentrations (Fig. 32) strongly suggests the formation of a magnesium-calcium silicate. These findings demonstrate that Ca_2SiO_4 is chemically reactive with turbine condensates such as $Mg_3V_2O_8$ and $MgSO_4$.

(d) NiCrAlY coated and uncoated specimens

Most of the NiCrAlY coated and uncoated specimens encountered insignificant attack during the tests. Even those exposed to the 180 ppm V fuel test (Test 1BX) exhibited no noticeable hot corrosion. This is attributed to the inhibition effect of the Mg additives. The only exceptions were those specimens exposed to the high Na-doped fuel test (Test 1B6). In this case some of the NiCrAlY coated specimens were attacked so badly that the 1/8 inch thick metal substrate wall was completely corroded.

Figure 33 shows the cross-section of a NiCrAlY coated specimen exposed for 151 cycles to Test 1B6 at 857°C metal temperature. Extensive hot corrosion attack is clearly demonstrated. An area that suffered a complete loss of the plasma sprayed NiCrAlY coating is shown in Fig. 33b. The cross-section of an unfailed G-$ZrO_2 \cdot 8Y_2O_3$/NiCrAlY specimen that was exposed for the same 151 cycles (but at a metal temperature of 800°C) is shown in Fig. 34. There is no evidence of any hot corrosion attack even in the graded zone. Since these two specimens were tested at the same gas temperature and same cooling rate, results shown in Figs. 33 and 34 clearly illustrate the benefits of the lower metal temperature that resulted from the use of the thermal barrier coatings.

Another important finding is that the NiCrAlY bond coats, exposed after the spalling of the $ZrO_2 \cdot 8Y_2O_3$ and Ca_2SiO_4 overcoats, encountered markly different corrosion attack at the same testing conditions. The exposed NiCrAlY bond coat of a NASA prepared specimen (D-Ca_2SiO_4/NiCrAlY) was corroded so badly after 151 cycles of exposure at 900°C that complete loss of NiCrAlY coating was observed in some areas (Fig. 35a). As a result, even the substrate was corroded (Fig. 35b). However, the exposed NiCrAlY bond coat of the Linde prepared specimen D-$ZrO_2 \cdot 8Y_2O_3$ specimen tested at the same temperature for the same number of cycles experienced no observable hot corrosion (Fig. 36).

There are several reasons to account for this difference in corrosion attack. One reason is that the oxide overcoat on the Ca_2SiO_4/NiCrAlY specimen was lost earlier, so that the NiCrAlY bond coat was exposed for a longer period. Another possible reason is that a residual $ZrO_2(Y_2O_3)$ layer remained on the NiCrAlY bond coat of $ZrO_2 \cdot 8Y_2O_3$/NiCrAlY specimen whereas no residual oxide layer remained in the case of the Ca_2SiO_4/NiCrAlY specimen. However, another and perhaps more important reason for the difference in corrosion resistance of these specimens is related to the microstructure of the NiCrAlY bond coats. It can be seen from Fig. 37 that the NASA sprayed NiCrAlY bond coat exhibits a porous layered-type structure. However, the spraying parameters and post-sprayed

ORIGINAL PAGE
BLACK AND WHITE PHOTOGRAPH

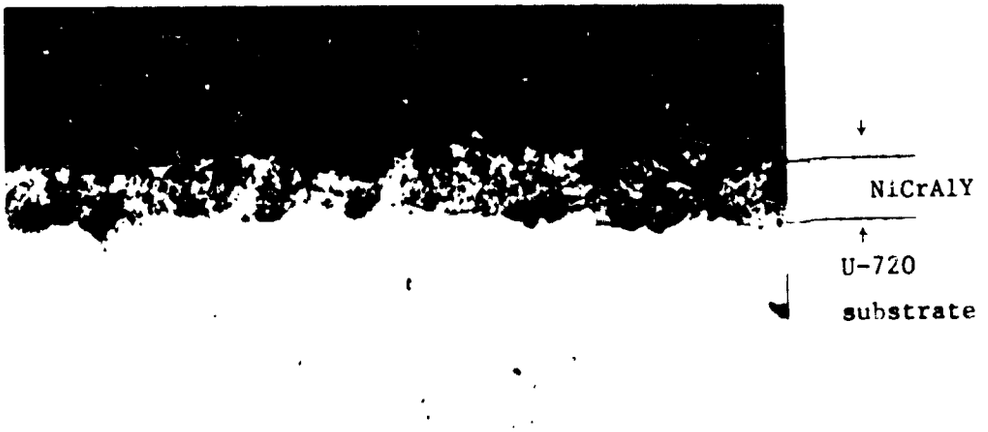

(a)

(b)

Fig. 33 - Specimen N-2 (NiCrAlY) 151 cycles, Test 1B6
1150°C gas/857°C metal
(100X)

ORIGINAL PAGE
BLACK AND WHITE PHOTOGRAPH

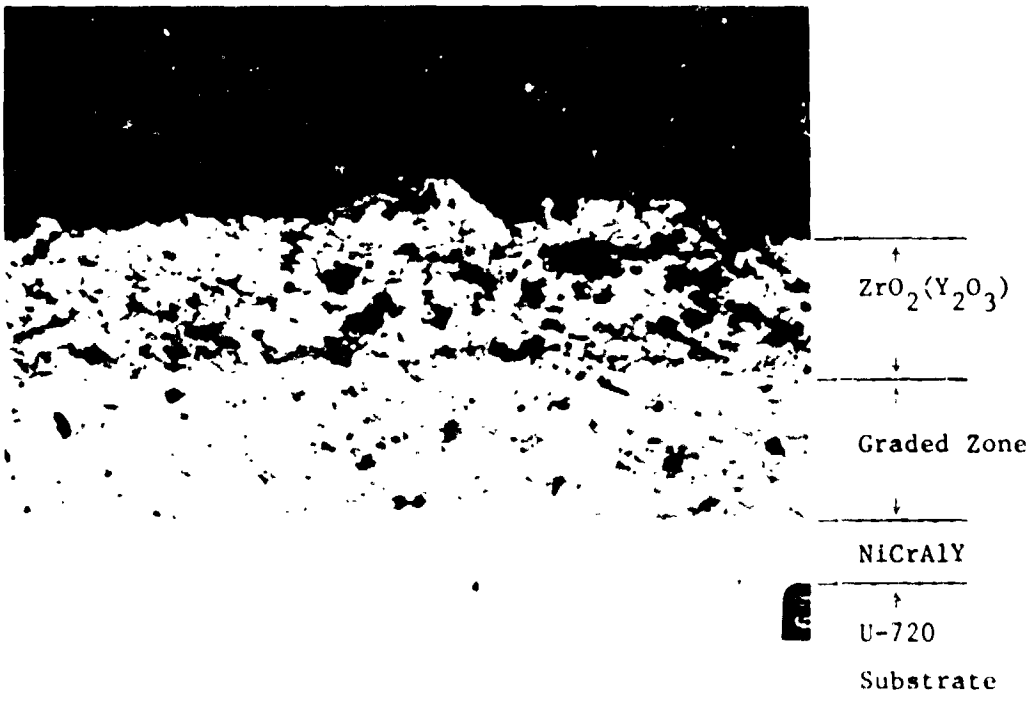

Fig. 34 - Specimen B-2 ($G\text{-}ZrO_2 \cdot 8Y_2O_3$) 151 cycles, Test 1B6
1150°C gas/800°C metal
(100X)

ORIGINAL PAGE
BLACK AND WHITE PHOTOGRAPH

(a)

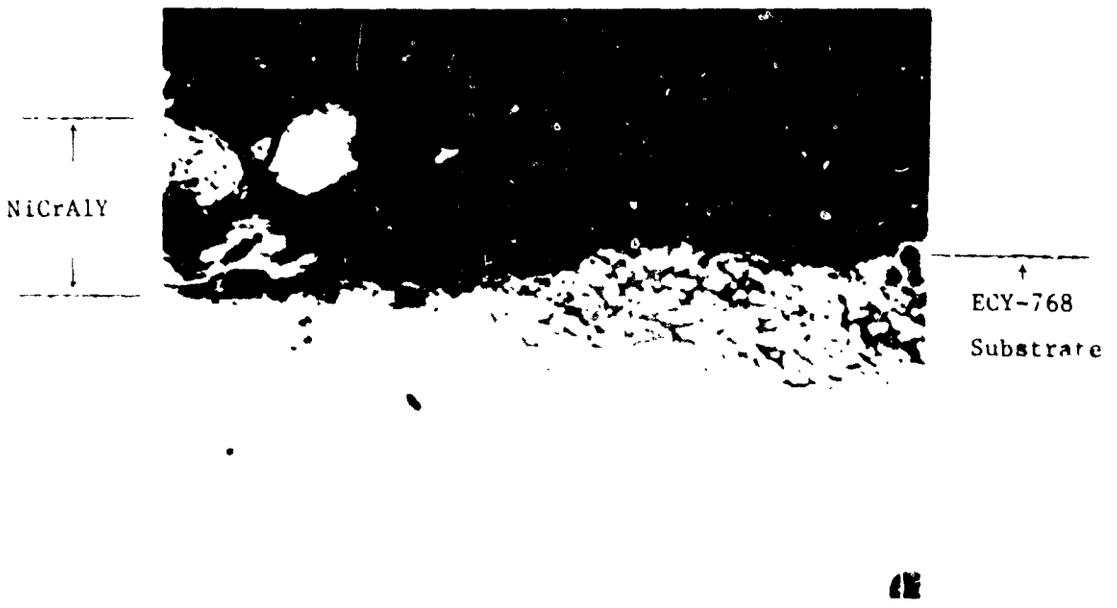

(b)

Fig. 35 - Specimen S-1 (D-Ca_2SiO_4) 151 cycles, Test 186
1150°C gas/900°C metal
(100X)

ORIGINAL PAGE
BLACK AND WHITE PHOTOGRAPH

Fig. 36 - Specimen A-2 ($D\text{-}ZrO_2 \cdot 8Y_2O_3$) 151 cycles, Test 1B6
1150°C gas/900°C metal
(400X)

ORIGINAL PAGE
BLACK AND WHITE PHOTOGRAPH

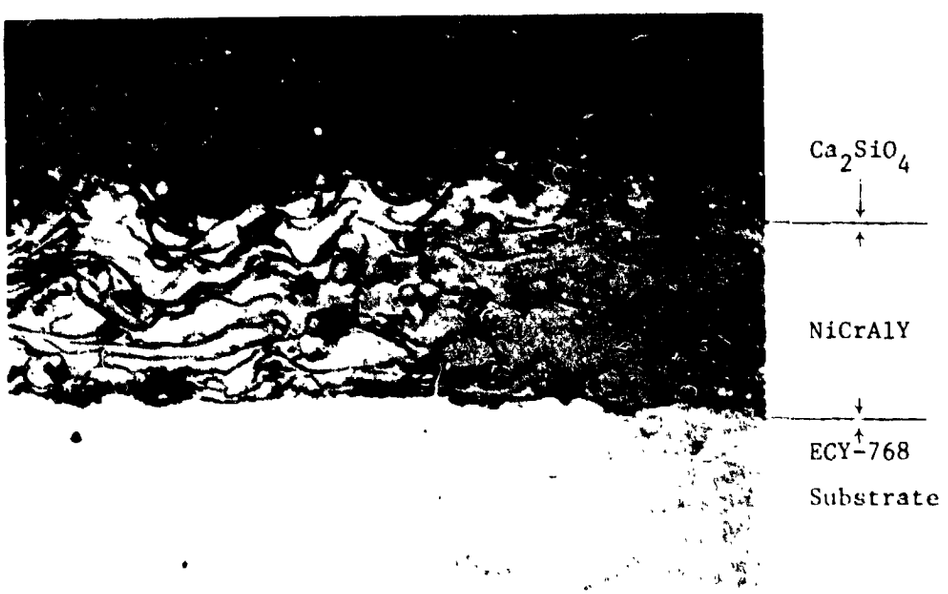

Fig. 37 - NASA sprayed NiCrAlY bond coat (200X)

treatments employed by Linde have resulted in a highly dense structure (Fig. 36). Thus although the porous nature of the NASA NiCrAlY bond coat may offer good thermomechanical performance, it also provides easy paths for corrodants to penetrate into the coating and thereby enhance hot corrosion attack. These results suggest that in order to have both chemical and thermomechanical stability, the microstructure of the NiCrAlY coats still need to be optimized.

2.2.4 Task 1C - Water Washing Sensitivity Tests

2.2.4.1 Test Results

The objective of conducting these tests was to evaluate the coating sensitivity to turbine clean-up (water washing procedures). The first water washing sensitivity test (Test 1C1) was conducted using the same contaminated fuel as that in Test 1B5: GT No. 2 fuel doped to 1 ppm Na, 50 ppm V, 2 ppm P, 0.5 ppm Ca, 2 ppm Fe, and 150 ppm Mg. The fuel simulated a water washed residual oil treated with a magnesium-containing fuel additive. The gas and metal temperature were 1150°C and 800°C, respectively (Table 18).

The sample measurements and water washing schedule for Test 1C1 were as follows:

0 hour	Weigh
50 hour	Weigh, wash, weigh
100 hour	Wash
150 hour	Wash and replace new specimen
250 hour	Wash
350 hour	Wash
450 hour	Weigh, wash, weigh
500 hour	Weigh

At the end of the first fifty one-hour cycles of burner rig exposure, none of the specimens showed signs of failure. They were removed from the holder and weighed individually to determine the amount of deposit accumulated. The results are shown schematically in Fig. 38 where it is interesting to note that although the specimens were randomly located, coatings of the same kind gathered very similar amounts of deposit. Thus, the amount of deposit was more a function of coating system than of specimen location. It is also interesting to note that the duplex Ca_2SiO_4/NiCrAlY and the graded $ZrO_2 \cdot 24.65$ MgO/NiCrAlY coating systems gained about two to three times more weight than that of the duplex $ZrO_2 \cdot 8Y_2O_3$/NiCrAlY coating system. This may reflect the fact that the former two coatings readily react with sulfur and oxygen from the environment to form $MgSO_4$ and $CaSO_4$ as previously described. The possible

Table 18

Summary of Water Washing Sensibility Test Conditions

Test No.	Gas/Metal Temp. (°C)	Fuel
1C1	1150/800	GT No. 2 doped to 1 ppm Na, 50 ppm V, 2 ppm P, 0.5 ppm Ca, 2.0 ppm Fe, 150 ppm Fe
1C2	1150/800	GT No. 2 doped to 1 ppm Na, 20 ppm V, 2 ppm P, 0.5 ppm Ca, 2 ppm Fe, 66 Mg and 0.25% S

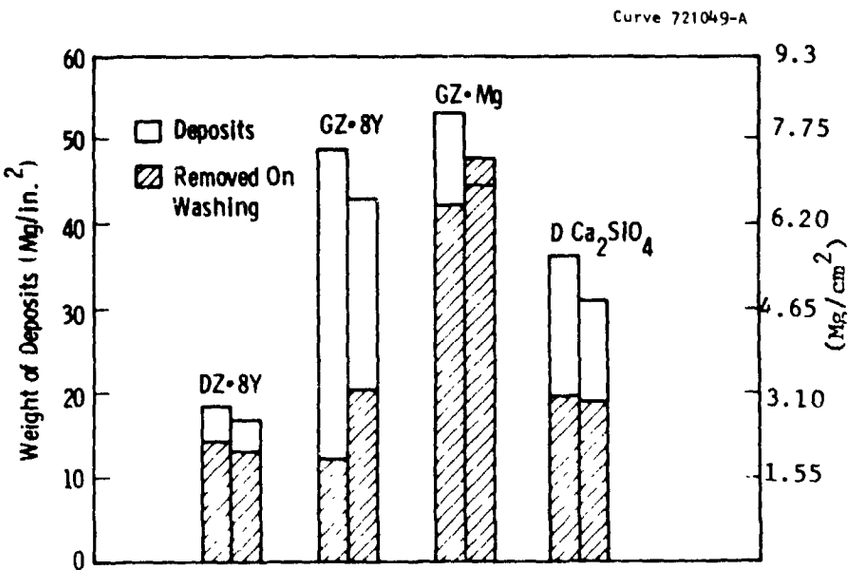

Figure 38 - Weight of deposits accumulated in a 50-hour cyclic burner rig test (1Ci)

reason for the greater weight gained by the graded $ZrO_2 \cdot 8Y_2O_3$/NiCrAlY systems is that the former coatings experienced internal (NiCrAlY) oxidation.

After weight gain determinations, the specimens were reassembled into the specimen holder and placed in front of a metal duct encasing a spray nozzle. Water washing was conducted using deionized water containing 5 ppm Na+K. The flow rate of the water spray was controlled at 0.5 gallon/minute, which represents the laboratory reduced scale version of actual turbine washing procedures. After ten minutes of washing, the specimens were dried with a hot air gun for ten minutes. It was observed that most of the surface deposits were washed away during the first two to three minutes. The specimens were again disassembled and reweighed after three such washing and drying cycles. Since the resulting weight measurements showed that some wash water was still retained by several specimens, it was necessary to place the specimens into an oven (150°C) for 1.5 hours to assure that they were dried completely. The amount of deposits removed from each specimen is also shown in Fig. 38. In the case of one G-$ZrO_2 \cdot 24.65$ MgO/NiCrAlY specimen, the removal was >100% which indicated coating material as well as deposit removal.

The weight of deposit accumulation as a function of time was obtained by combining the data obtained from both Tests 1C1 and 1B5 and is plotted in Fig. 39. The G-$ZrO_2 \cdot 8Y_2O_3$/NiCrAlY specimen was selected as an example because this was the only coating system that did not suffer a spalling failure in Test 1B5. The important information conveyed by Fig. 39 is that although the initial deposit accumulation is proportional to exposure time, it soon reaches a maximum value after about 150 one-hour cycles. Subsequently, a kinetic equilibrium is established wherein the deposition and presumably flaking rates are about equal to each other.

The result of Test 1C1 is shown in Fig. 40. For comparison purposes, the results of Test 1B5 where water washing was not used are also shown. The detailed test observations are listed in Table 19. It appears that the water washing improved the durability of the G-$ZrO_2 \cdot 24.65$ MgO/NiCrAlY coatings most. A graded $ZrO_2 \cdot 8Y_2O_3$/NiCrAlY specimen developed a small chip at the top end after 450 cycles. Since this coating system did not fail in the earlier 1B5 test, it is not certain whether the observed chipping represents a detrimental influence of water washing or merely an edge effect. Not shown in Fig. 40 is the D-Ca_2SiO_4/NiCrAlY specimen which survived the test.

To determine the effect of retained water in the coatings after the specimens were washed at the end of 450 cycles, only four specimens were dried. The other four specimens were returned to the burner rig soaked with water. The result of this brief experiment was that retained water from washing did not initiate failure of specimens that were not previously spalled or cracked. However, the two wet specimens that contained previously chipped areas appeared to have spalled much more after 50 cycles.

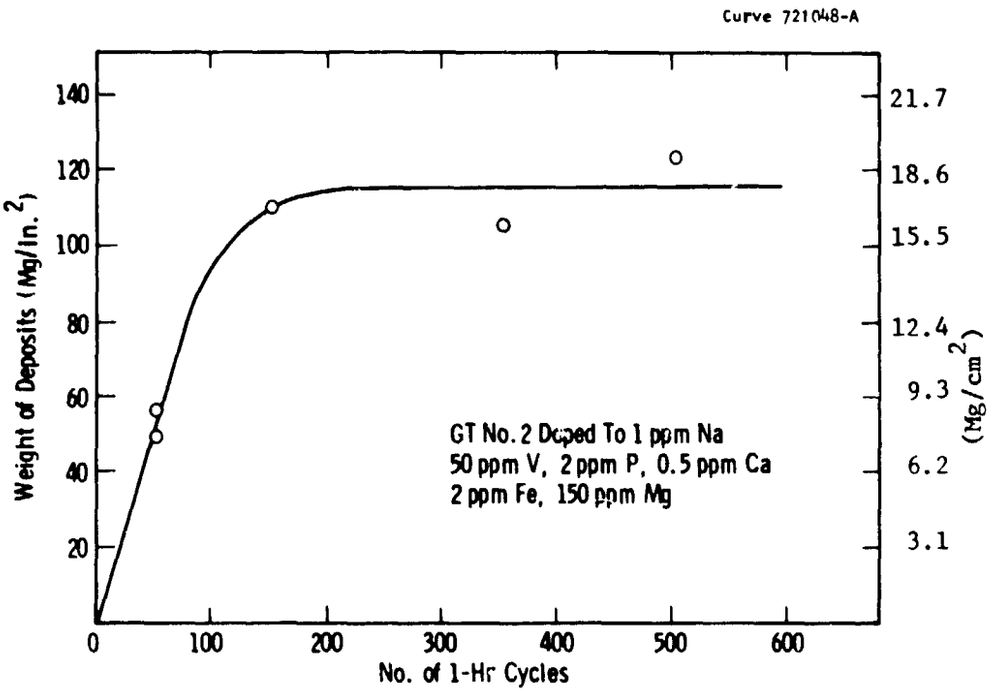

Figure 39 - Rate of deposit accumulation on G-ZrO_2 $8Y_2O_3$ specimens in a cyclic burner rig (Tests 1C1 & 1B5)

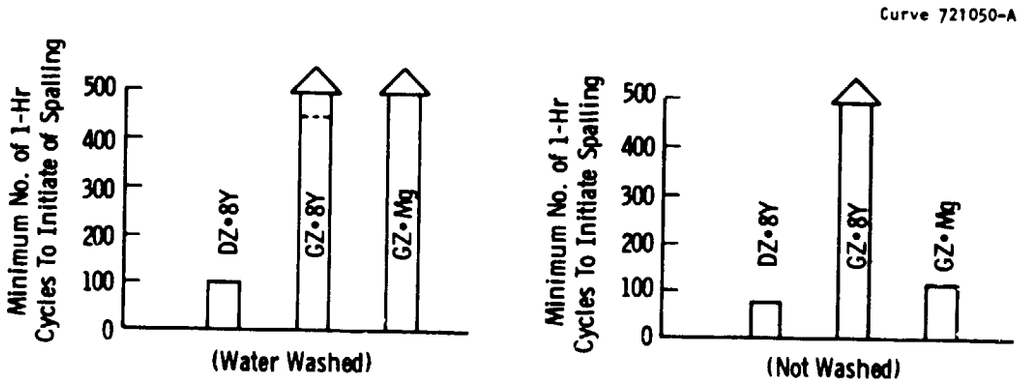

Figure 40 - Effect of water washing on number of cycles to failure
(Tests 1C1 and 1B5)
Temperature: (1150°C gas/800°C metal)
Fuel: GT No. 2 doped to (ppm): 1-Na, 50-V, 2-P,
0.5-Ca, 2-Fe, 150-Mg

Table 19

Test IC1 Summary*

Specimen No.	Position	Time (1-hr Cycles) In	Time (1-hr Cycles) Out	Net Cycles Completed	Failure Description
AB1	3	0	500	500	Chipped at top end at 150 cycles
AB2	8	0	150	150	Spalled at top end at 100 cycles
BB1	4	0	150	150	No Failure
BB2	6	0	500	500	Small chip at top end at 450 cycles
CB1	1	0	150	150	Chipped at bottom end at 150 cycles
CB2	7	0	500	500	No Failure
SB1	2	0	500	500	" "
SB2	5	0	150	150	" "
AB3	8	151	500	350	Spalled at top and bottom ends at 300 cycles
BB3	4	151	500	350	No Failure
CB3	1	151	500	350	" "
SB3	5	151	500	350	" "

AB - Duplex $ZrO_2 \cdot 8Y_2O_3$ on U-720 alloy substrate

BB - Graded $ZrO_2 \cdot 8Y_2O_3$ on U-720 alloy substrate

CB - Graded $ZrO_2 \cdot 24.65MgO$ on U-720 alloy substrate

SB - Duplex Ca_2SiO_4 on U-720 alloy substrate

*Fuel = GT No. 2 doped to 1 ppm Na, 50 ppm V, 2 ppm P, 0.5 ppm Ca, 2.0 ppm Fe, 150 ppm Mg
Temperature = 1150°C gas/800°C metal

This suggests that the water washing of damaged specimens without drying will lead to more pronounced spalling on further exposure to the hot combustion gases.

Test 1C2 was a second water-washing sensitivity test using the same fuel as that planned for pressurized passage tests (Task II); i.e., GT No. 2 fuel doped to contain 1 ppm Na, 20 ppm V, 2 ppm P, 0.5 ppm Ca, 2 ppm Fe, 66 ppm Mg and 0.25% S (Table 18). The main objective of running Test 1C2 was to obtain a comparison between tests conducted in the atmospheric burner rig with those in the pressurized passage. Test 1C2 specimens were washed at 150 to 200 hr. intervals. Fig. 41 shows the results of Test 1C2. Detailed observations made during the test are listed in Table 20.

The D-$ZrO_2 \cdot 8Y_2O_3$/NiCrAlY specimens chipped and spalled at the hot ends after 150 one-hour cycles before the water washing was conducted. Results obtained on the graded $ZrO_2 \cdot 24.65$ MgO/NiCrAlY specimens were mixed. Spalling occurred on two of three specimens after 150 test cycles, whereas the remaining specimen survived 500 cycles without failure. Compared to the failures observed in the 1B5 test where higher vanadium/magnesium contents (50/150 ppm) were used, it is evident that coating life increases with a decrease in vanadium/magnesium levels contained in the fuel. Fig. 42 shows the post-test conditions of representative specimens from 1C2 test.

2.2.4.2 Post-Test Analysis

Detailed post-test analysis, which included X-ray diffraction, metallographic, scanning electron microscopic as well as electron microprobe analysis, were conducted on representative specimens from the water washing sensitivity tests. Most of the results obtained were similar to those described in section 2.2.3.2 for the fuel impurity sensitivity tests.

X-ray diffraction analysis on post-test specimen revealed that the surface deposits collected on most specimens evaluated in 1C1 and 1C2 tests contained MgO, $MgSO_4$ (or $MgSO_4 \cdot 6H_2O$-hydrated after burner rig exposure) as the major phases, and $Mg_3V_2O_8$ as the minor phase. There were also local variations. For instance, MgO was usually found to be the major phase in X-ray samples collected from areas that were directly facing the flame (highest temperature), while $MgSO_4$ was the major phase found on the backs and sides of the specimens (lower temperature). These observations are consistent with the fact that in the chemical equilibrium,

$$MgO + SO_3 \rightleftarrows MgSO_4$$

the formation of $MgSO_4$ is thermodynamically more favorable at lower temperatures. The effect of water washing was primary to remove these deposits, which in some cases could affect the performance of the

Table 20

Test IC2 Summary *

Specimen No.	Position	Time (1-Hr cycles) In	Time (1-Hr cycles) Out	Net Cycles Completed	Failure Description
AB1	2	0	150	150	Spalled at top end after 150 cycles
AB2	5	0	500	500	Cracked at top after 500 cycles
BB1	1	0	150	150	No failure
BB2	8	0	500	500	No failure
CB1	4	0	150	150	Chipped at top after 150 cycles
CB2	7	0	500	500	No failure
SV1	3	0	500	500	No failure
1A23	6	0	500	500	Chipped at top end after 256 cycles
AB3	4	151	500	350	Chipped at top end after 150 net cycles
BB3	2	151	500	350	No failure
CB3	1	151	500	350	Chipped at top end after 150 net cycles

AB - Duplex $ZrO_2 \cdot 8Y_2O_3$ on U-720 alloy substrate

BB - Graded $ZrO_2 \cdot 8Y_2O_3$ on U-720 alloy substrate

CB - Graded $ZrO_2 \cdot 24.5MgO$ on U-720 alloy substrate

SV - Duplex Ca_2SiO_4 on ECY-768 alloy substrate

1A23 - NASA spray duplex $ZrO_2 \cdot 8Y_2O_3$ on U-720 alloy substrate

---

* Fuel = GT No. 2 doped to 1 ppm Na, 20 ppm V, 2 ppm P, 0.5 ppm Ca, 2 ppm Fe, 66 ppm Mg and 0.25% S.

Temperature = 1150°C gas/800°C metal

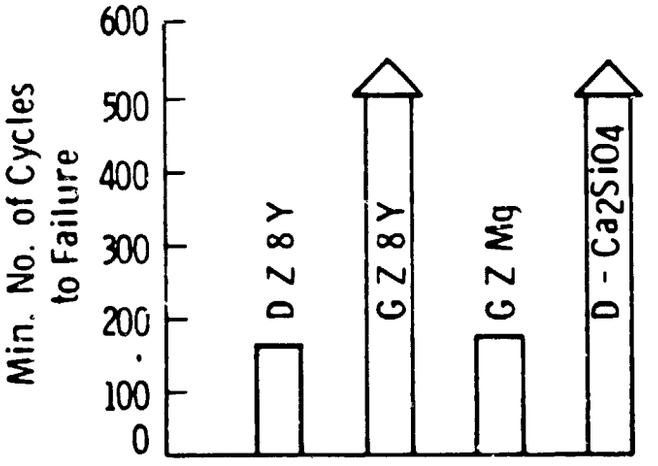

Figure 41 - Cycle to failure in burner rig water washing sensitivity test (1C2)
Temperature: (1150°C gas/800°C metal)
Fuel: GT No. 2 doped to (ppm): 1-Na, 20-V, 2-P, 0.5-Ca, 2-Fe, 66-Mg

ORIGINAL PAGE
BLACK AND WHITE PHOTOGRAPH

Fig. 42 - Representative exposed specimens from test 1C2
Fuel - GT No. 2 doped to (ppm): Na-1, V-20, P-2, Ca-0.5, Fe-2, Mg-66
Temperature - 1150°C gas/800°C metal

coatings.

An important observation from the X-ray analysis was that unlike the results obtained on the higher vanadium tested (1C1) specimens, the 1C2 tested specimens showed no significant change in the ratio of monoclinic $ZrO_2(Y_2O_3)$ to tetragonal/cubic $ZrO_2(Y_2O_3)$; i.e., little or no yttrium leaching had occurred. This may be the primary reason for the better coating performance in the 1C2 test.

X-ray analysis on D-Ca_2SiO_4/NiCrAlY specimens showed $MgSO_4$ (or $MgSO_4 \cdot 6H_2O$) and $CaSO_4$ as major phases and $Mg_3V_2O_8$, MgO as minor phases. There was also evidence of an amorphous phase which is likely silica or a silica-rich phase. Electron microprobe scans of these D-Ca_2SiO_4/NiCrAlY specimens showed conclusively that sulfur has penetrated deeply into the coating interior (Fig. 43).

Of the three graded $ZrO_2 \cdot 24.65$ MgO specimens tested in 1C2 test, it was mentioned earlier that two failed after 150 cycles while the third survived 500 cycles without spalling. However a metallographic examination of the survivor (Fig. 44) clearly revealed that large cracks developed inside the coating. It was also evident from microstructure examinations that internal oxidation of the NiCrAlY particles within the graded zone had occurred.

2.3 TASK II - HIGH PRESSURE EFFECTS

2.3.1 Test Facility

For pressurized passage testing, a rig capable of operating at pressures up to twelve atmospheres was used (Fig. 45).

The test section consisted of six 1.27 cm diameter test specimens mounted in an electrically actuated traveler assembly (Fig. 46). The actuator could be operated manually or on an automatic timing cycle. The specimens were mounted horizontally in two rows. The top to bottom spacing were staggered to limit wake effects in the gas stream approaching the back row.

The test section flow passage was 10.7 cm high and 4.8 cm wide. Five 3.18 mm diameter thermocouples were located in the gas stream immediately upstream of the test section. These thermocouples were used to measure the combustion gas temperature. Two thermocouples were mounted in the wall of each test specimen to measure the metal temperature during operation. These thermocouples were located approximately 6.25 mm from the passage wall.

ORIGINAL PAGE
BLACK AND WHITE PHOTOGRAPH

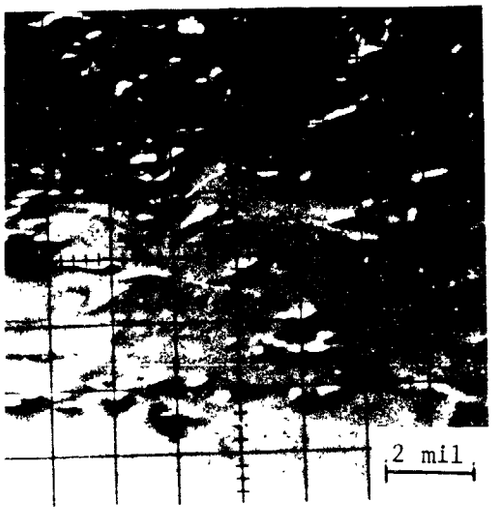

SEM Picture

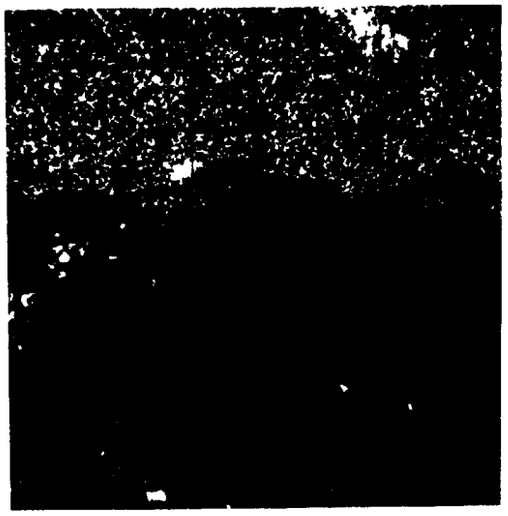

Si

Ca

S

Fig. 43 - EMP scans on specimen SV1 (D-Ca_2SiO_4) 500 cycles, Test IC2

C-2

ORIGINAL PAGE
BLACK AND WHITE PHOTOGRAPH

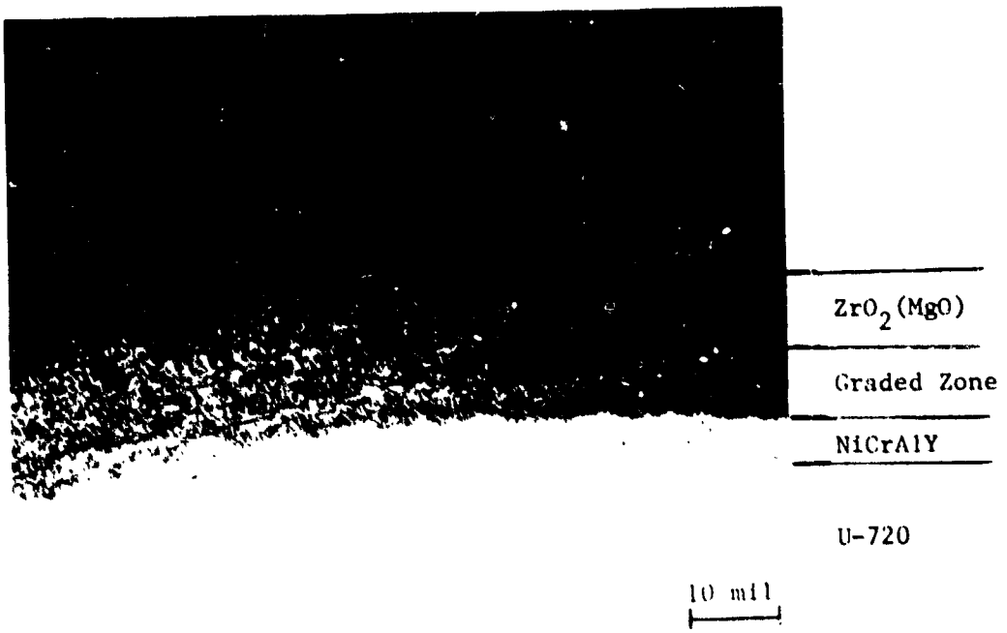

Fig. 44 - Specimen CB2 (G-ZrO_2•24.65 MgO) 500 cycles, Test 1C2

ORIGINAL PAGE
BLACK AND WHITE PHOTOGRAPH

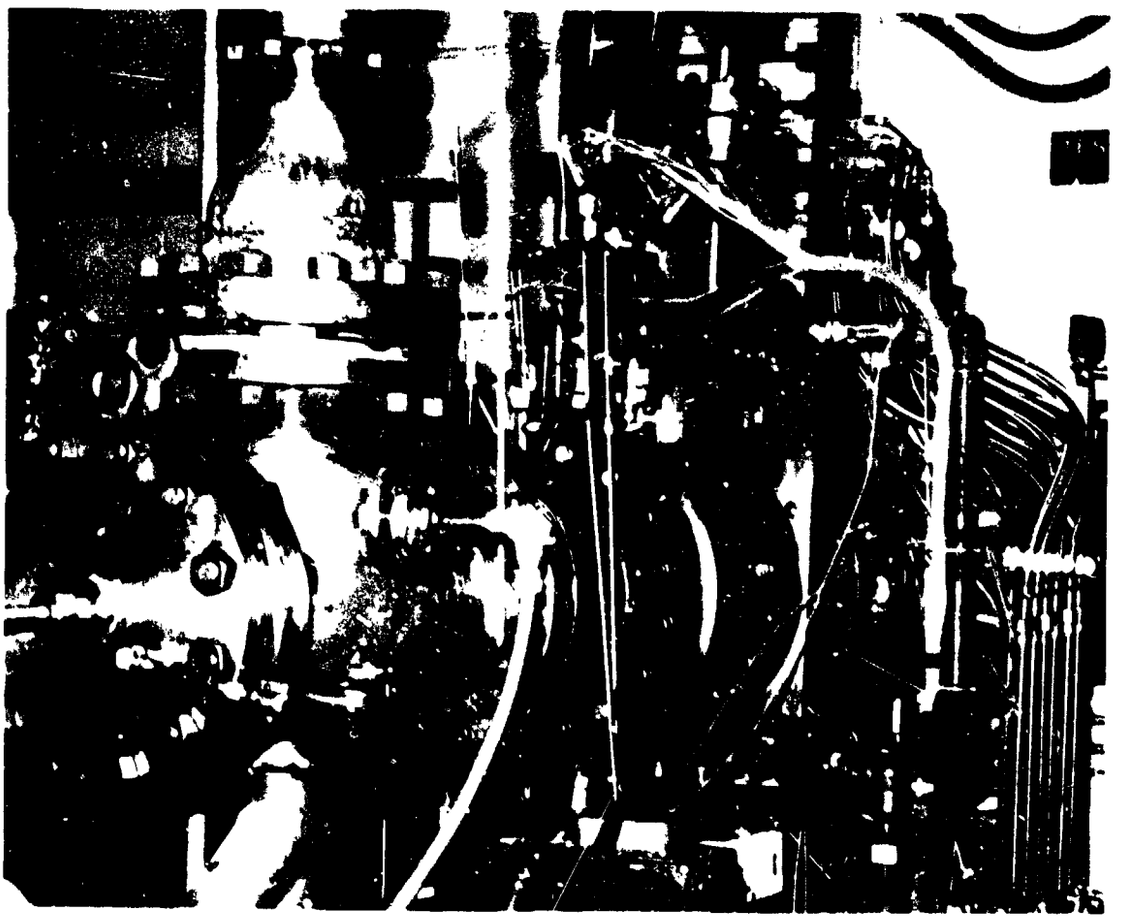

Fig. 45 - Pressurized test passage

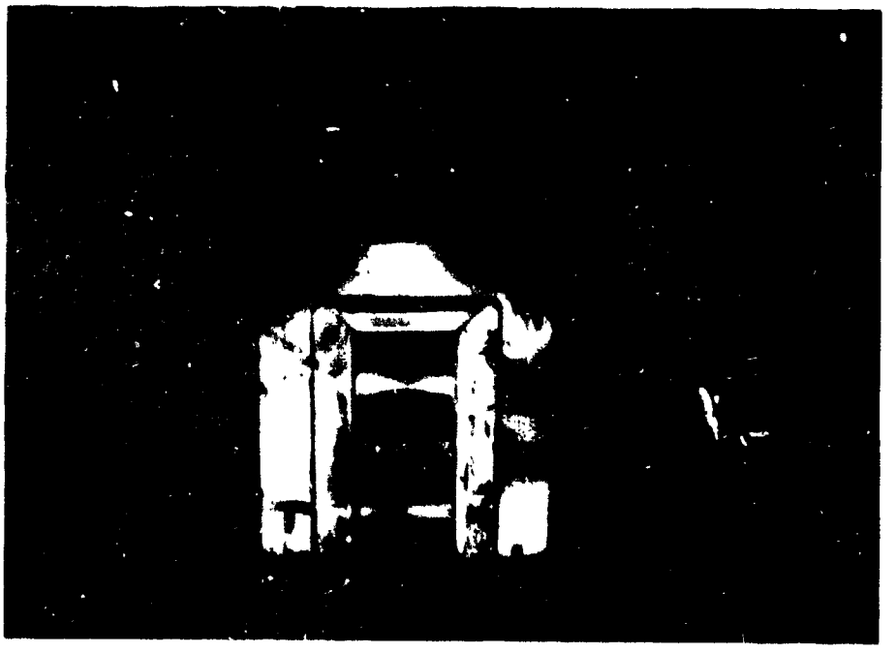

Fig. 46 - Pressurized passage test specimens mounted in the electrically actuated traveler assembly

The test specimens were cooled by internal air flow. Individual cooling air tubes permitted the specimen metal temperatures to be adjusted externally during test passage operation. The rig allowed a maximum temperature difference of 280°C between the combustion gas temperature and the test specimen maximum metal temperature. Under normal conditions, the maximum metal temperature for all six test specimens were maintained within $\pm$ 11°C during steady state operation.

Combustion was achieved using a cut-down version of the Westinghouse 1/4 scale B-4 combustor and fuel nozzle used successfully on other test programs. Ignition was achieved using a propane ignitor. A fireye infra-red flame detection system was used as a safety interlock on the fuel system.

Two 400 gallon day tanks were used to supply fuel for passage operation. The tanks were operated independently and isolated from the fuel system to permit refilling with #2 fuel oil and the mixing of fuel additives without shutting down the passage.

In order to increase the speed and accuracy of data recording and retrieval, the test passage instrumentation was tied into the Test and Development DEC PDP-11 computer data acquisition system to digitize and record test temperature data on magnetic tape. All passage data channels were read sequentially in less than a second. The normal intervals between scans for the tests were 15 seconds. Longer or shorter intervals may be specified. To obtain a better definition of the thermal shock, which occurs during traveler insertion and retraction, two second intervals were used during several heat up and cool down cycles.

Two different levels of thermal cycling were used. The first consisted of inserting the specimen traveler assembly directly into the gas stream held at 1066°C and keeping the metal temperature at 800°C for a total exposure time of 55 minutes. The specimens were then extracted and allowed to cool to 90-150°C for five minutes before they were reinserted into the gas stream. The thermal transient experienced by specimens during this operation was far more severe than the normal start-up and shut-down transients expected for turbine blades in an operating utility gas turbine.

The second level of thermal transient conditions was more realistic. It involved air/fuel flow and temperature ramps to closely simulate the normal start-up and shut-down transients expected in actual gas turbines. Each cycle consisted of a 30 minute heating up and 20 minute cooling down period. The time at steady-state with specimen temperature at 800°C was 40 minutes. The operating procedure was essentially divided into the following seven steps:

(1) Insert specimen into gas stream which was held at 593°C (1100°F) and 2 lb/sec air flow.

(2) Maintaining 593°C (1100°F) passage temperature, increase air flow from 2 lb/sec to 4 lb/sec gradually over a 5-minute period.

(3) Increase passage temperature from 593°C (1100°F) to ∿1066°C (1950°F) at an approximate rate of 20°C/minute over a 25-minute period by increasing fuel flow.

(4) Maintain steady state for 40 minutes. Adjust passage temperature and specimen cooling air as required to maintain all specimens at 800°C (1475°F).

(5) Decrease passage temperature from 1066°C (1950°F) to 893°C (1100°F) at an approximate rate of 31°C/min over a period of 15 minutes by decreasing fuel flow.

(6) Maintain 1066°C (1100°F), reduce air flow from 4 lb/sec to 2 lb/sec gradually over a 5-minute period.

(7) Retract specimens and let cool to 90-150°C (200-300°F) in antechamber for 5 minutes before again inserting into gas stream.

Figure 47 shows the schematic representation of the thermal cycles used in the pressurized passage tests. The calculated heat flux history for the pressurized passage test specimens are shown in Fig. 48 (dotted line - convection and radiation heat transfer modes are considered; dash line - only convection is considered). For comparison purposes, the heat flux history for the actual W501D row 1 turbine blades is also included (solid lines in Fig. 48). Under similar conditions, the heat flux of the test specimens and row 1 turbine blades were 400-435 KW/M^2 and 320 KW/M^2, respectively. The ramp rate was reasonably similar for both, hence the test profile was conservative; i.e., it was at least 25% more severe than that of the actual turbines.

Due to the physical constraints of the testing passage, direct measurement of specimen coating surface temperatures was impossible. Therefore, they were calculated from heat transfer data instead. An iterative procedure using Newton's method showed that under the testing conditions of 1066°C gas temperature (actual temperature varied between 980-1090°C) and 800°C metal temperature, the coating surface temperature was about 870-925°C.

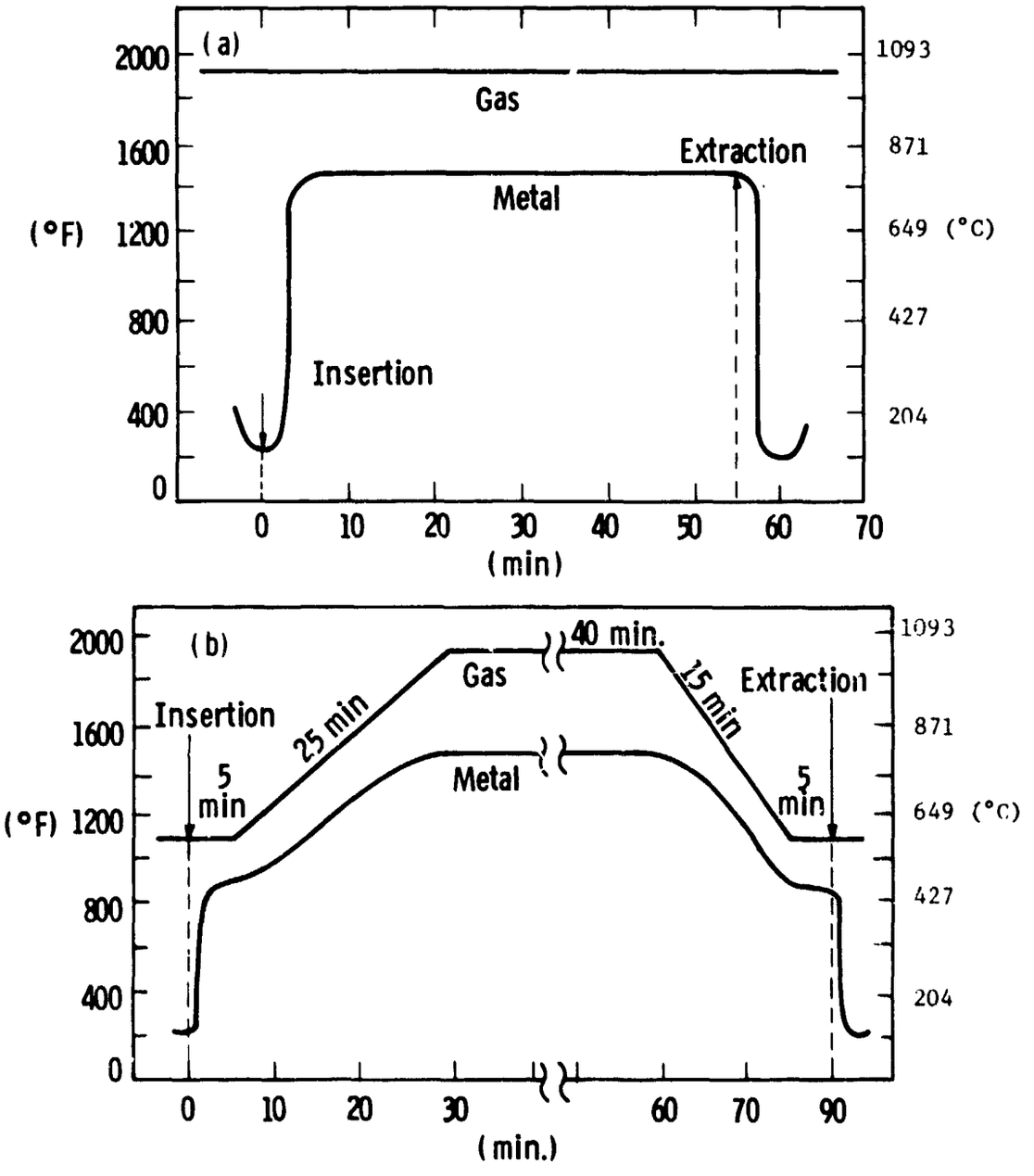

Figure 47 - Thermal cycles for test pins in pressurized passage

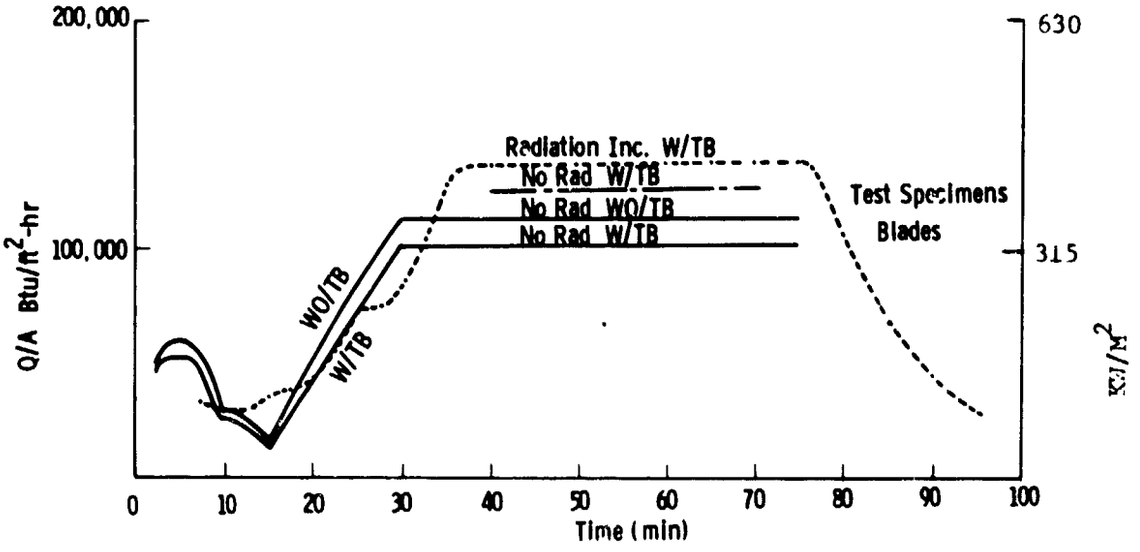

Figure 48 - Heat flux history for W501-D turbine blades and pressurized passage test specimens

2.3.2 Test Results

All pressurized passage tests were conducted at the nominal steady-state condition of 135 psig, 1066°C gas temperature and 800°C metal temperature. The gas velocity was 130 M/sec, which was almost 40 times faster than than in the burner rig but very similar to those found in an actual utility gas turbine. Table 21 lists the comparison of pertinent conditions used in the burner rig and pressurized passage tests. Those found in the commercial W501D turbine are also listed for reference.

As in atmospheric burner rigs, both clean fuel and impurity-doped fuel sensitivity tests were conducted. Clean fuel tests were conducted using GT No. 2 fuel. Impurity-doped fuel tests were conducted using GT No. 2 fuel doped to 1 ppm Na, 20 ppm V, 2 ppm P, 0.5 ppm Ca, 2 ppm Fe, 66 ppm Mg and 0.25% S (Table 22). This was the same fuel used for Test 1C2 of the atmospheric burner rig tests. Six specimens which included two each of duplex $ZrO_2 \cdot 8Y_2O_3$, graded $ZrO_2 \cdot 8Y_2O_3$ and duplex Ca_2SiO_4 were evaluated in each test. After 20 cycles, the specimens were extracted for examination. Due to the high operating cost, all the pressurized passage tests were terminated after 50 cycles.

Results of pressurized passage tests are shown in Figures 49(a-b). Regardless of which thermal cycle was used, all three coating systems tested in the undoped GT No. 2 fuel passed the 50 cycles without failure. However, in the contaminated fuel test, they all encountered gross coating spalling after testing for less than 20 cycles.

Besides clean and doped No. 2 fuel tests, a test using a coal-derived fuel was also conducted. Synfuels such as those derived from coal are projected by some to be the major available fuels for combustion turbines in the future. Although many of these fuels appear to contain low to insignificant quantities of corrodants such as vanadium, other elemental impurities such as Na, K, P, Fe, S and Cl are often present in significant quantities. The main objective of running this test was to determine the effects of these elemental impurities on the durability of thermal barrier coatings and thus extending our test data base on ceramic coatings to synfuels.

The fuel used in test II-4 was SRC-2 (2.9 middle distillate/1 heavy distillate) that had the following analyzed elemental impurities: Ca - 1.5 ppm, V - 0.43 ppm, Na - 2 ppm, Pb - 2.7 ppm, Ti - 0.66 ppm, Fe - 17.7 ppm and K - 1.3 ppm. This fuel also contained 0.0094 wt % ash. The test was concluded after 20 cycles for which all six specimens survived without failure. They were covered with a reddish brown deposit, which was later identified to be iron oxide (Fe_2O_3). Post-test measurements revealed that the deposition rate ranged from 0.08 to 0.3 $mg/cm^2/hr$. It was also found that coating thickness changes were negligible, indicating that within the test period erosion was not a problem. This

Table 21

COMPARISON OF TESTING CONDITIONS IN BURNER RIG AND PRESSURIZED PASSAGE

	Gas Temp (°C)	Metal Temp (°C)	P_{O_2} (Atm)	P_{SO_3} (Atm) (0.24% S)	Gas Velocity (M/Sec)	Btu/Hr-Ft^2 (KW/M^2)
Burner Rig	1150	800	0.11	1.23×10^{-6}	3.7	(158)
Pressurized Passage (135 psig)	1066	800	1.48	4.16×10^{-5}	130	(400)
W501D (170 psig)	1066	843	1.66	6.53×10^{-5}	153	(320)

Table 22

SUMMARY OF HIGH PRESSURE EFFECT TESTS
(135 psig)

Test No.	Gas/Metal Temp. (°C)	Fuel
II-1	1066/800	GT No. 2 doped to 1 ppm Na, 20 ppm V, 2 ppm P, 0.5 ppm Ca, 2 ppm Fe, 66 ppm Mg
II-2	1066/800	Ditto
II-3B*	1066/800	Ditto
II-2	1066/800	GT No. 2
II-3*	1066/800	GT No. 2
II-4*	1066/800	SRC-2

*Thermal cycle involved air/fuel flow and temperature ramps

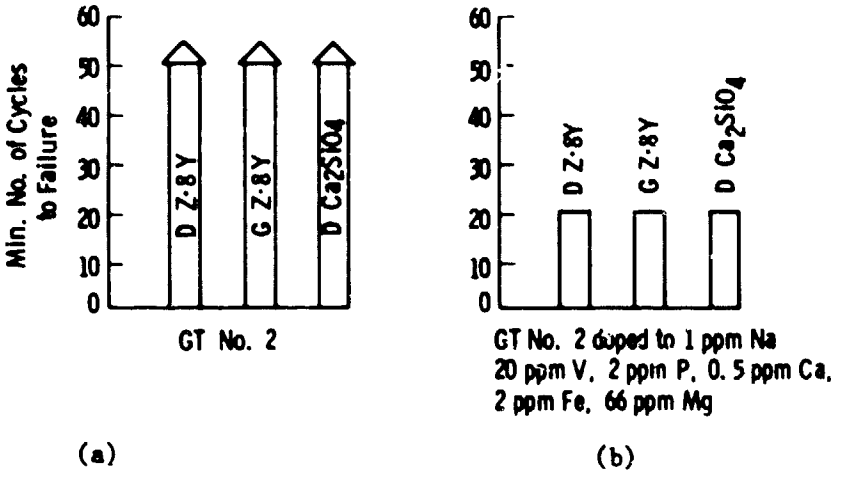

Figure 49 - Cycles to failure in pressurized passage tests
Temperature: 1066°C gas/800°C metal
Pressure: 135 psig

(a) Tests II-2, II-3
(b) Tests II-1, II-1B, II-3B

preliminary test was very encouraging since the coating systems tested with the SRC-2 fuel did not encounter either erosion or corrosion problems. However, the long term durability of the coatings with coal derived fuel has yet to be demonstrated.

The post test conditions of specimens tested in the pressurized passage are shown in Figs. 50-52.

Comparison between pressurized passage and atmospheric burner rig tests conducted using the same fuel (Figure 41 vs. Figure 49) clearly illustrates the greater severity of the pressurized passage test. Due to the higher total pressure, the impurity elements have a much higher partial pressure in the pressurized passage and likely accounts for the accelerated initiation of failures. Indeed, by using higher dopant levels, the failure times observed in atmospheric burner rig Test IBX (Figure 20) approached those observed in the pressurized passage test (Figure 49). Figure 53 shows the post-test conditions of two graded $ZrO_2 \cdot 8Y_2O_3$ specimens. It can be seen that the specimen tested for only 20 cycles in the pressurized passage has suffered more extensive damage than the one tested for 350 cycles in the burner rig using a fuel with 9X dopant concentrations. The difference can be attributed to the higher gas velocity, mass flow rate, and thermal stress condition that existed in the pressurized tests. These factors are important in imparting damage once failures initiate due to reactions with the condensate. In the clean fuel test failure did not initiate and hence extensive coating damage did not occur.

2.3.3 Post-test Analysis

Detailed post-test analyses on the pressurized test specimens showed in general that their chemical behavior towards the combustion gases was qualitatively similar to that observed in the burner rig tests.

X-ray diffraction analysis showed that the deposits formed in the impurity-doped fuel, pressurized passage test were MgO, $MgSO_4$ ($MgSO_4 \cdot 6H_2O$) and $Mg_3V_2O_8$. These were very similar to those formed in the atmospheric burner rig tests using the vanadium-magnesium doped fuels. A significant difference was that the deposits formed in the pressurized passage were more massive and more dense.

Metallographic cross-sections of post-test specimens were also examined. Figure 54 shows the front and back cross-sections of a D-$ZrO_2 \cdot 8Y_2O_3$ specimen. It can be seen that while gross spalling occurred at the front of the specimen, the back of the specimen did not spall although it showed some cracking. Similar failure patterns were observed in the outer non-graded zone of the G-$ZrO_2 \cdot 8Y_2O_3$ specimens (Fig. 55). Thus, it is interesting to note that for the G-$ZrO_2 \cdot 8Y_2O_3$ specimen, cracking and

ORIGINAL PAGE
BLACK AND WHITE PHOTOGRAPH

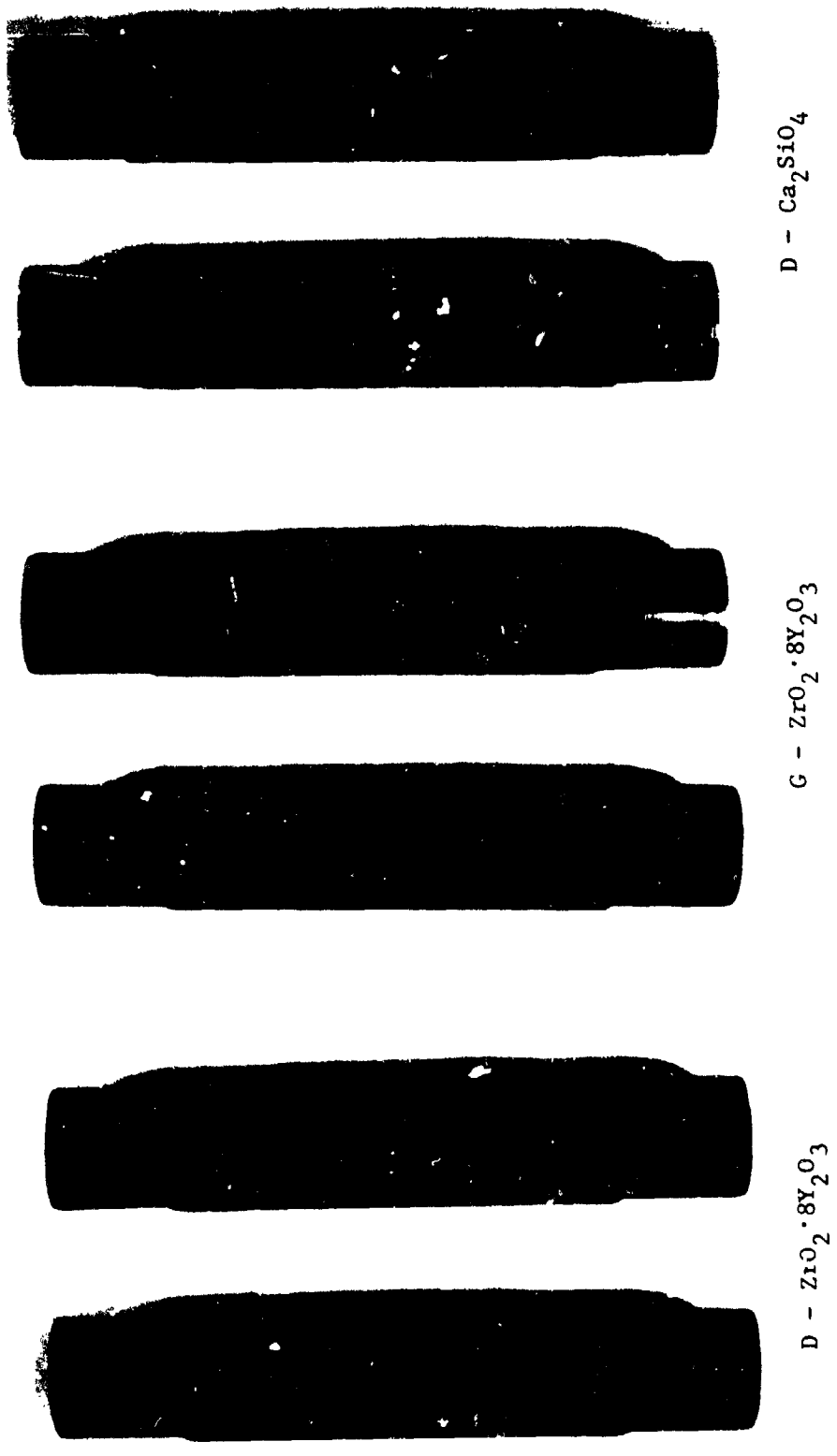

Fig. 50 - Exposed specimens from pressurized passage test (II-3)
Fuel - GT No. 2
Temperature - 1066°C gas/800°C metal
Cycles - 50

ORIGINAL PAGE
BLACK AND WHITE PHOTOGRAPH

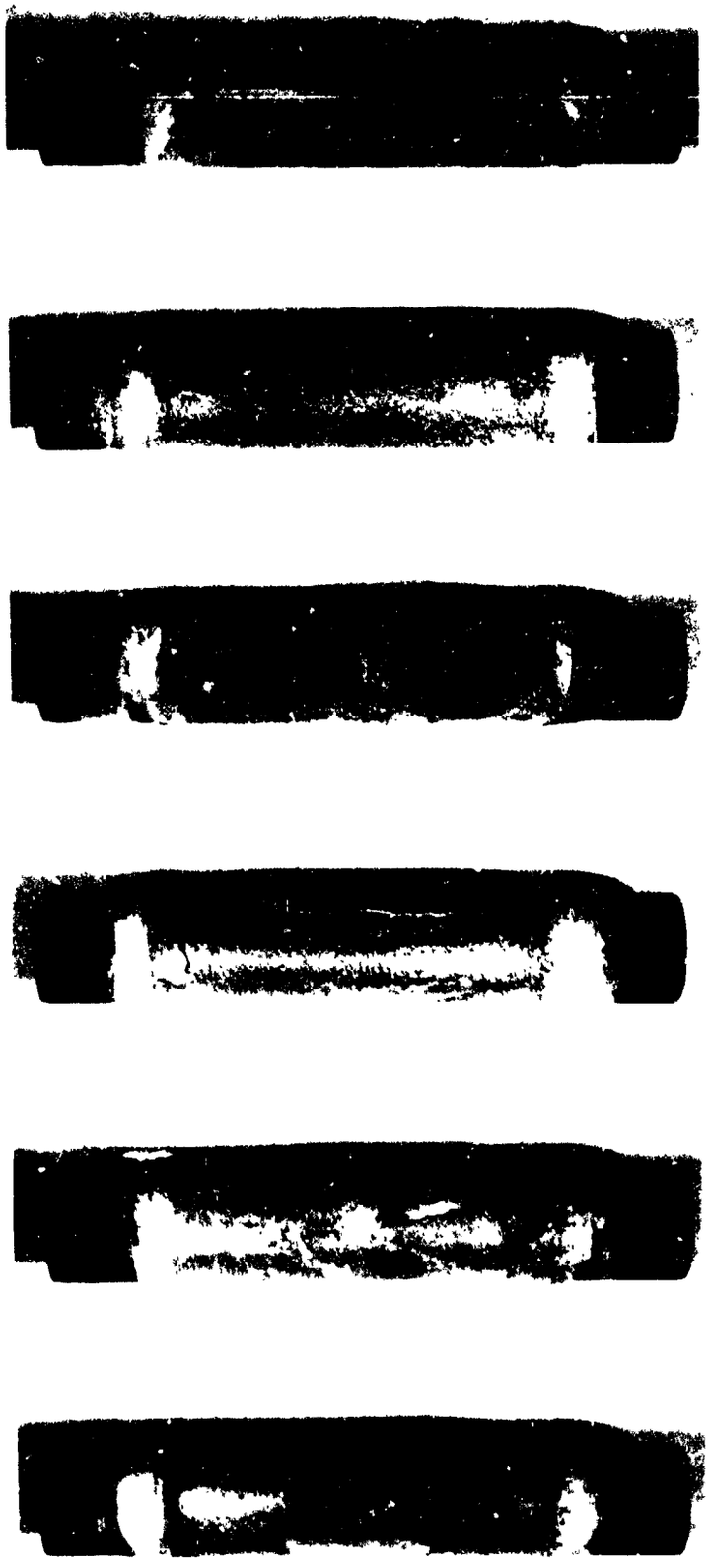

Fig. 51 - Leading edges of exposed specimens from pressurized passage test (II-3B)
Fuel - GT No. 2 doped to (ppm): 1-Na, 20-V, 0.5 Ca, 2-Fe, 66-Mg and 0.25 wt % S
Temperature: 1066°C gas/800°C metal
Cycles - 20

ORIGINAL PAGE
BLACK AND WHITE PHOTOGRAPH

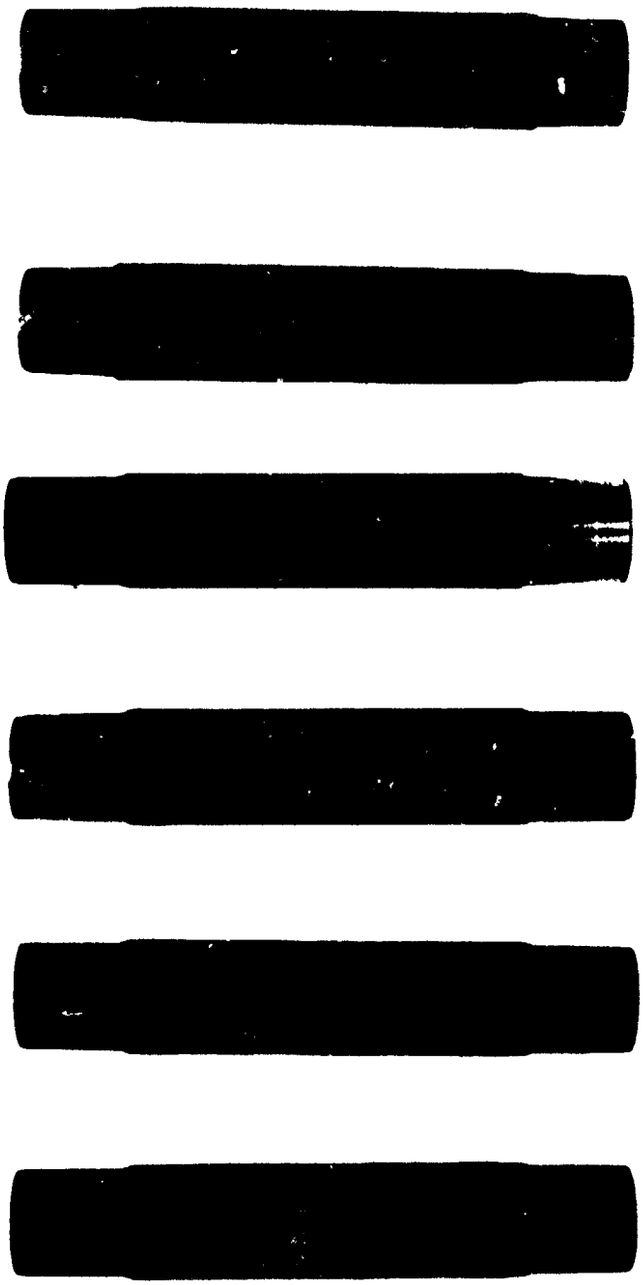

Fig. 52 - Leading edges of exposed specimens from pressurized passage test (II-4)
Fuel - SRC-2 synfuel
Temperature - 1066°C gas/800°C metal
Cycles - 20

ORIGINAL PAGE
BLACK AND WHITE PHOTOGRAPH

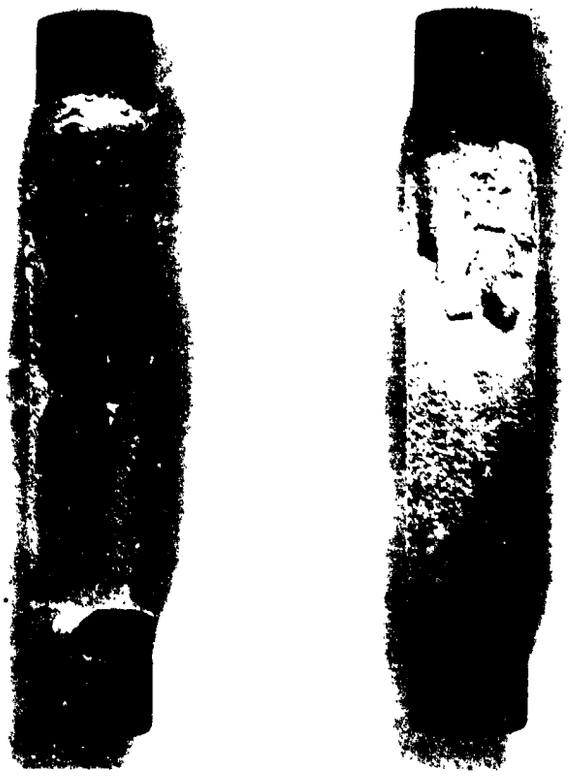

(a) (b)

Fig. 53 - Post-test conditions of G-$ZrO_2 \cdot 8Y_2O_3$/NiCrAlY specimens from
(a) pressurized passage test II-3B, 20 cycles
(b) burner rig test 1BX, 350 cycles

ORIGINAL PAGE
BLACK AND WHITE PHOTOGRAPH

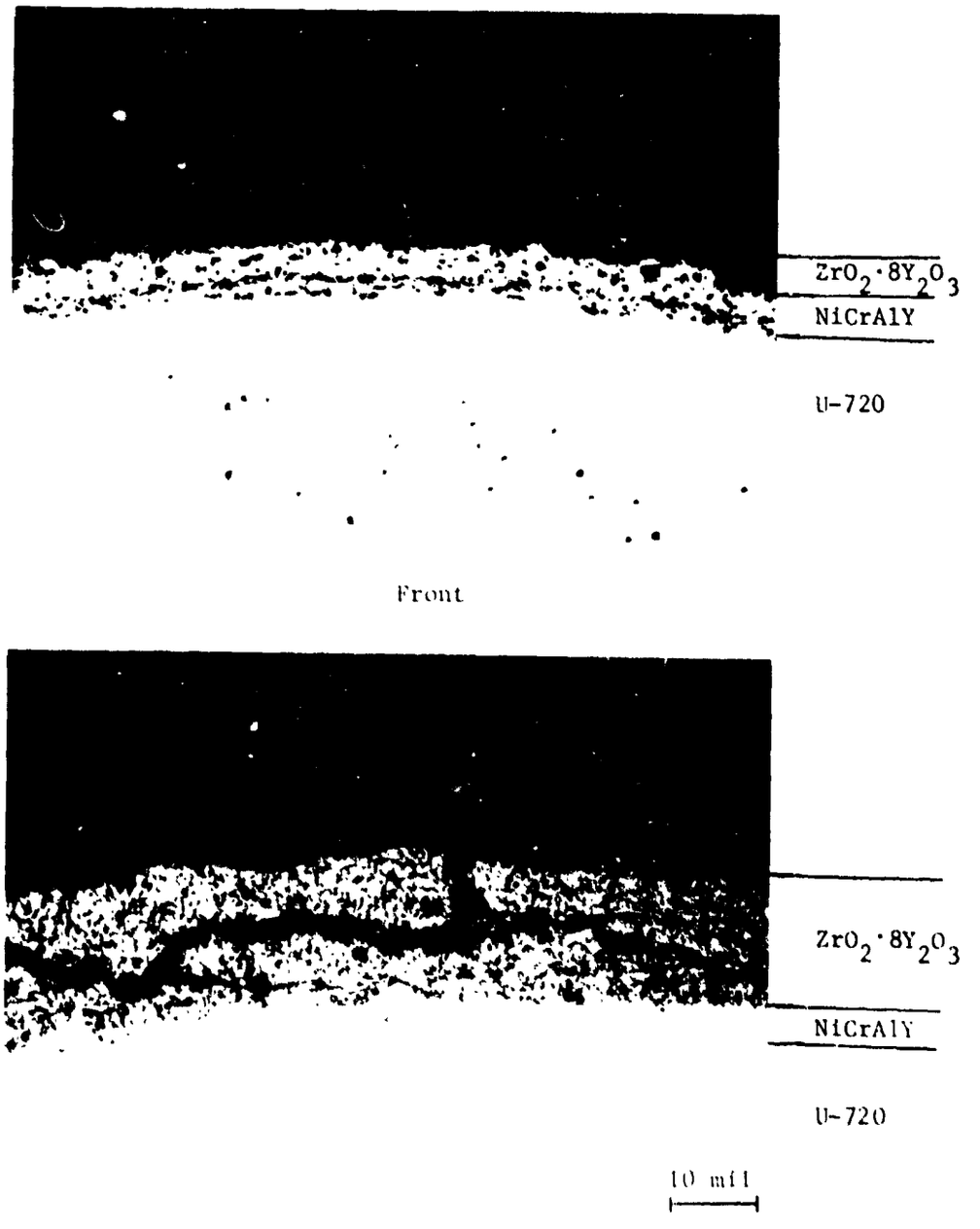

Fig. 54 - D-$ZrO_2 \cdot 8Y_2O_3$ 50 cycles, Test 11-1B

ORIGINAL PAGE
BLACK AND WHITE PHOTOGRAPH

Leading edge

Trailing edge

Fig. 55 - G-$ZrO_2 \cdot 8Y_2O_3$/NiCrAlY, 20 cycles, Test II-3B

eventual spalling occurred at or near the oxide/graded zone interface, and as a result, a protective graded zone is left adhering to the specimen. This is very similar to the failure encountered by graded coatings in the high vanadium atmospheric burner rig test described previously.

X-ray analysis of $ZrO_2 \cdot Y_2O_3$ specimens exposed to the impurity-doped test showed that the fraction of monoclinic $ZrO_2(Y_2O_3)$ has significantly increased. At some coating locations just beneath the deposits, the monoclinic $ZrO_2(Y_2O_3)$ fraction increased from the original 15-20% to almost 50%. This suggested that the $ZrO_2 \cdot 8Y_2O_3$ coating degradation mechanism in the pressurized passage test was similar to that proposed for the high vanadium atmospheric burner rig test, i.e., destabilization of $ZrO_2(Y_2O_3)$ caused by the reaction with combustion condensates.

Metallographic examination of the D-Ca_2SiO_4 specimens was very interesting. A reaction layer formed on the coating surface below the combustion deposits (Fig. 56). EMP analysis on this specimen suggested that the reaction layer was a calcium-magnesium vanadate formed by the reaction between Ca_2SiO_4 and the vanadium containing deposits (Fig. 57).

Post-test analysis was also conducted on clean fuel-tested specimens. The metallographic cross-sections of the D-$ZrO_2 \cdot 8Y_2O_3$/NiCrAlY, G-$ZrO_2 \cdot 8Y_2O_3$/NiCrAlY and D-Ca_2SiO_4/NiCrAlY specimens are shown in Figs. 58-60. Measurements using a calibrated filar eye piece showed no noticeable coating thickness change after the test, indicating that there was no significant erosion problem associated with the high velocity pressurized passage test. It should however be cautioned that the testing time was only 50 cycles.

As may be seen in Figure 59, the G-$ZrO_2 \cdot 8Y_2O_3$/NiCrAlY specimen did not exhibit destructive internal oxidation/sulfidation after being tested for 50 cycles under the high P_{O_2} and P_{SO_3} conditions that existed in the pressurized passage (Table 21). However, the coating behavior for longer term exposures remains to be studied.

The Ca_2SiO_4/NiCrAlY specimen that performed very well in previous atmospheric burner rig tests also survived the 50 cycle clean fuel test without spalling. However, a series of small cracks (both radial and circumferential) developed in the coating (Figure 60). Electron microprobe analysis showed also that significant sulfur concentrations penetrated into the coating (Figure 61). Since this sulfur is not associated with the calcium, it is clear that $CaSO_4$ formed according to the following reaction:

$$Ca_2SiO_4 + 2SO_3 \rightarrow 2CaSO_4 + SiO_2$$
$$(2SO_2 + O_2)$$

It thus appears that even in the relatively clean GT No. 2 fuel combustion environments, Ca_2SiO_4 is chemically reactive.

ORIGINAL PAGE
BLACK AND WHITE PHOTOGRAPH

Front

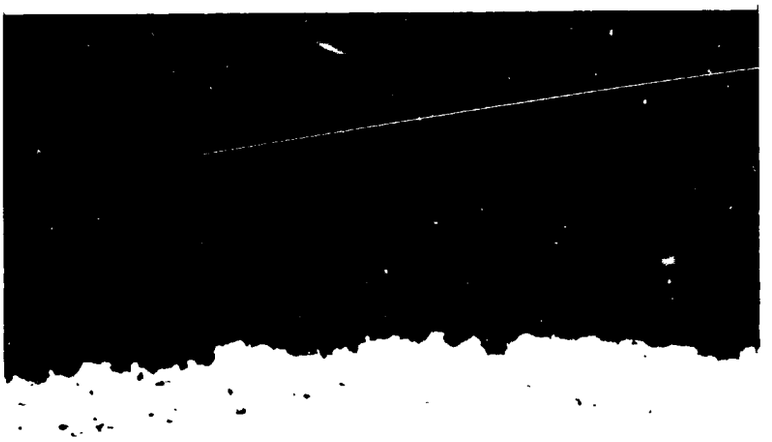

Back

Fig. 56 - D-Ca_2SiO_4, 20 cycles, Test II-3B

ORIGINAL PAGE
BLACK AND WHITE PHOTOGRAPH

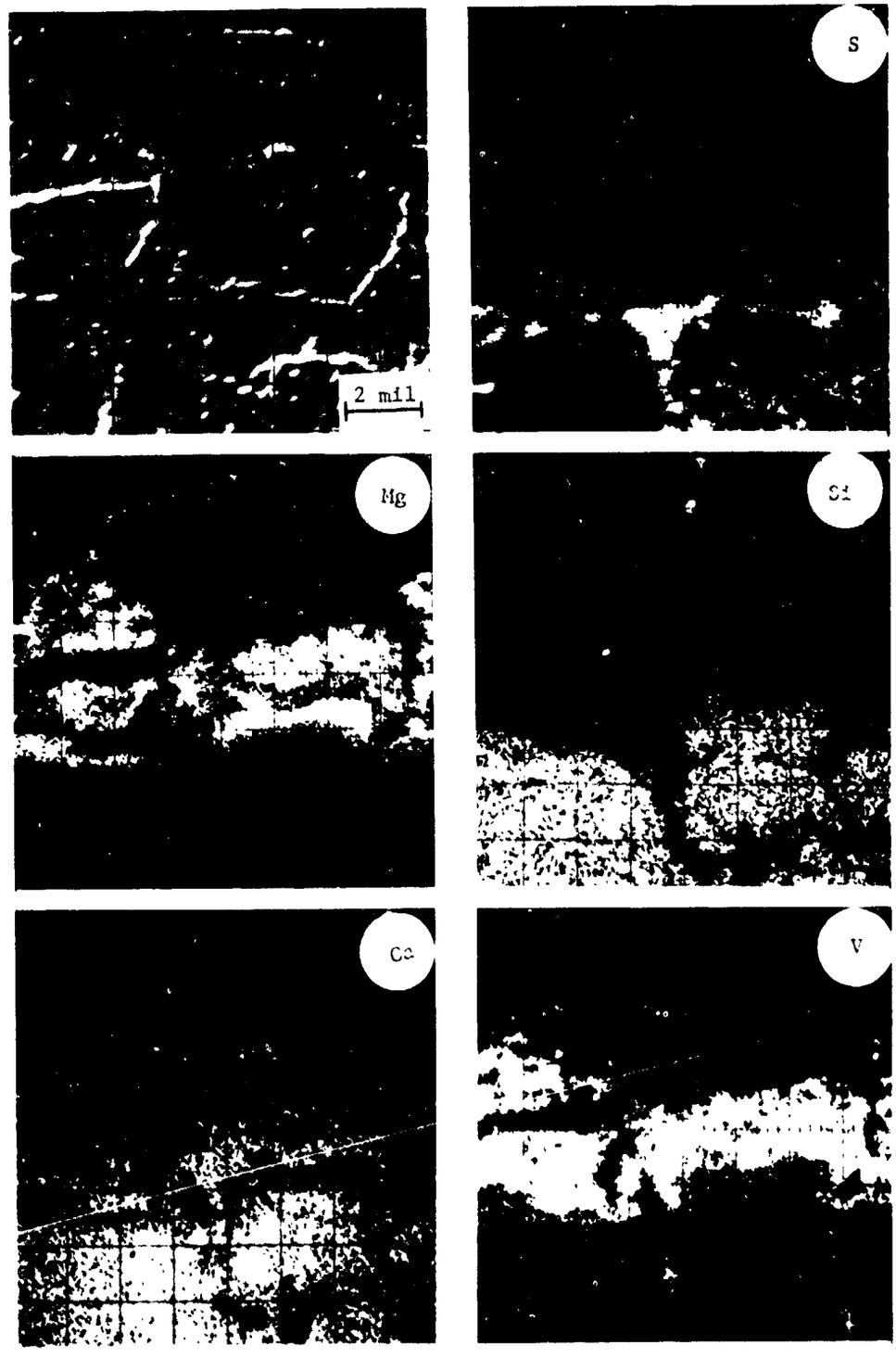

Fig. 57 - EMP scans on specimen 3S6 (D-Ca_2SiO_4) 20 cycles, Test II-3B

ORIGINAL PAGE
BLACK AND WHITE PHOTOGRAPH

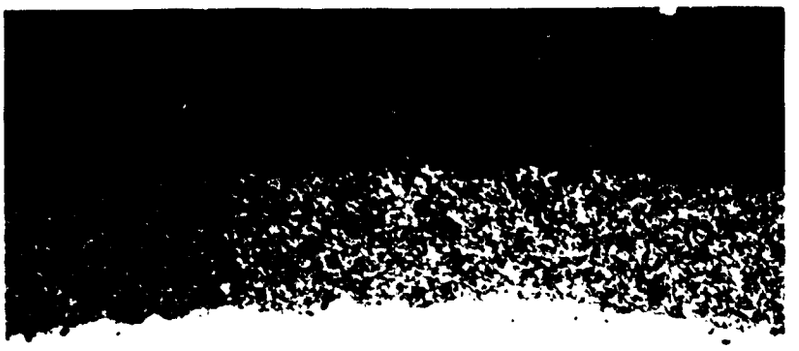

Fig. 58 - D-$ZrO_2 \cdot 8Y_2O_3$, 50 cycles, Test II-3 (50X)

ORIGINAL PAGE
BLACK AND WHITE PHOTOGRAPH

Fig. 59 - G-$ZrO_2 \cdot 8Y_2O_3$, 50 cycles, Test II-3 (50X)

ORIGINAL PAGE
BLACK AND WHITE PHOTOGRAPH

Fig. 60 - D-Ca_2SiO_4, 50 cycles, Test II-3 (50X)

ORIGINAL PAGE
BLACK AND WHITE PHOTOGRAPH

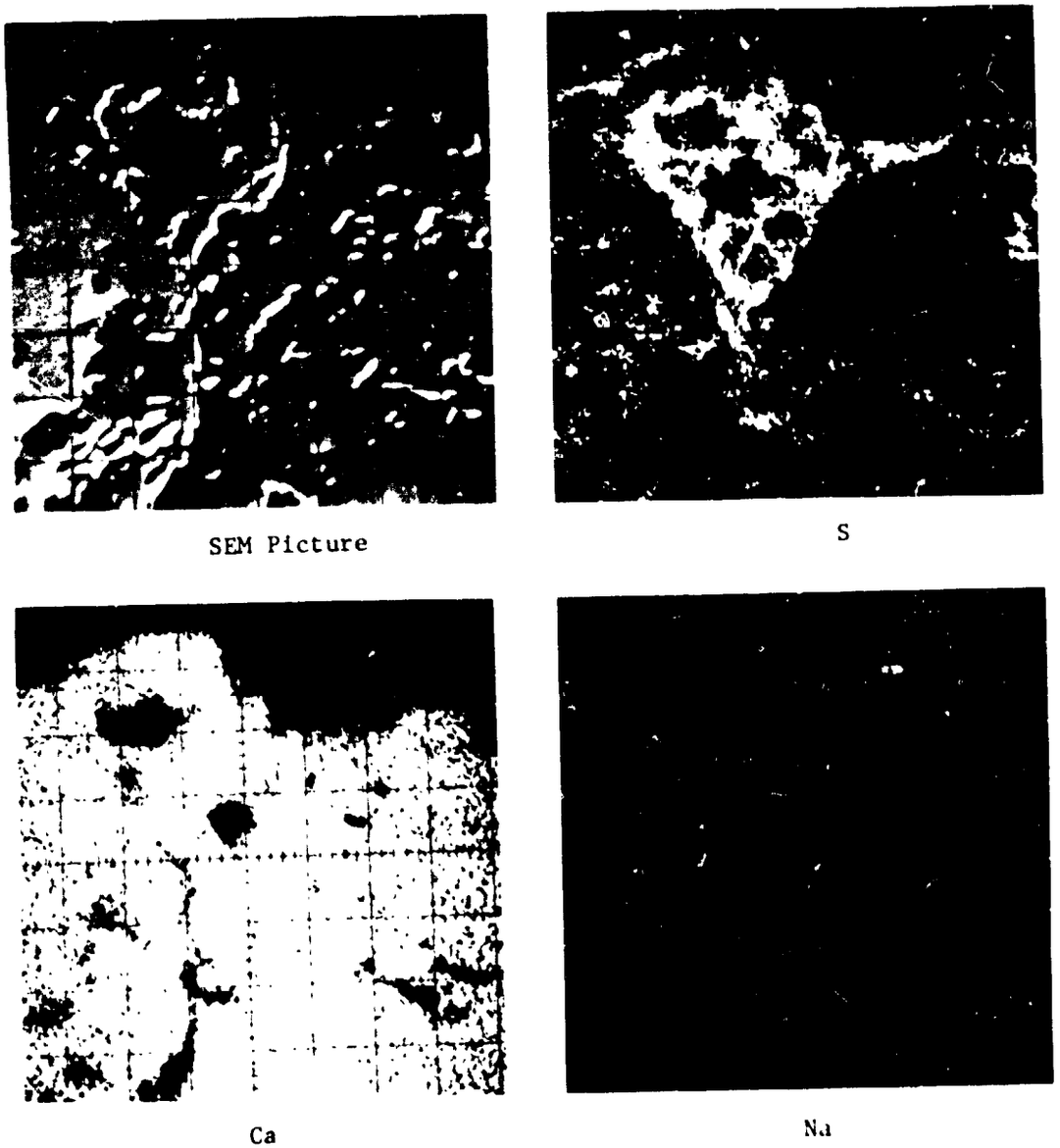

Fig. 61 - EMP scans on specimen 3S1, 50 cycles, Test 11-3

2.4 TASK III - ENDURANCE TEST

2.4.1 Test Facility

The 4000 hr. endurance test was conducted in an atmospheric burner rig. The test equipment and procedure were the same as those described in Task 1, section 2.2.1.

2.4.2 Test Conditions and Results

Four coating systems were selected for the 4000 cycle endurance test: D-$ZrO_2 \cdot 8Y_2O_3$/NiCrAlY, G-$ZrO_2 \cdot 8Y_2O_3$/NiCrAlY, D-Ca_2SiO_4/NiCrAlY and Linde sprayed NiCrAlY (5 mil). The gas temperature was 1150°C and the metal temperature was 800°C with the exception of the NiCrAlY coated specimens which were tested at 857°C. The fuel used was undoped GT No. 2 fuel. The test plan was to start with two specimens for each coating system. After 1500 one-hour cycles, one specimen for each coating system would be extracted and a new one then inserted so that on the completion of 4000 cycles, specimens that had been exposed for 1500, 2500 and 4000 one-hour cycles would be available for evaluation and analysis. However, for scheduling convenience the specimen change planned at the 1500 cycle was changed to 1428 cycles.

The post-test conditions of the four specimens extracted after 1428 cycles are shown in Fig. 62. It should be noted that the chip at the bottom of the D-$ZrO_2 \cdot 8Y_2O_3$/NiCrAlY specimen was not test-related i.e., this specimen was mechanically damaged at the beginning of the test. It may be seen that the G-$ZrO_2 \cdot 8Y_2O_3$ specimen also shows some damage; viz. a circumferential chip developed at the top of the specimen. This apparently resulted from the detrimental internal oxidation of NiCrAlY particles in the graded zone. The D-Ca_2SiO_4 specimen exhibited signs of surface micro-chipping at the hot end. This is attributed to flaking of $CaSO_4$ formed from the attack of SO_3 gas on Ca_2SiO_4.

During the 2200th cycle, a compressor failure occurred and the loss of cooling air caused a serious metal temperature excursion. During a period of 15 to 45 minutes, most of the specimens experienced metal temperatures as high as 1177°C. The two graded $ZrO_2 \cdot 8Y_2O_3$/NiCrAlY specimens spalled extensively, but the duplex specimens showed no apparent failure. This accidental occurrence clearly demonstrated that the duplex specimens can tolerate temperature excursions better than the graded ones. Another graded $ZrO_2 \cdot 8Y_2O_3$/NiCrAlY specimen was apparently not subjected to as high a temperature excursion since it survived the accident. Several representative specimens that were extracted after the temperature excursion are shown in Fig. 63. The test was restarted

ORIGINAL PAGE
BLACK AND WHITE PHOTOGRAPH

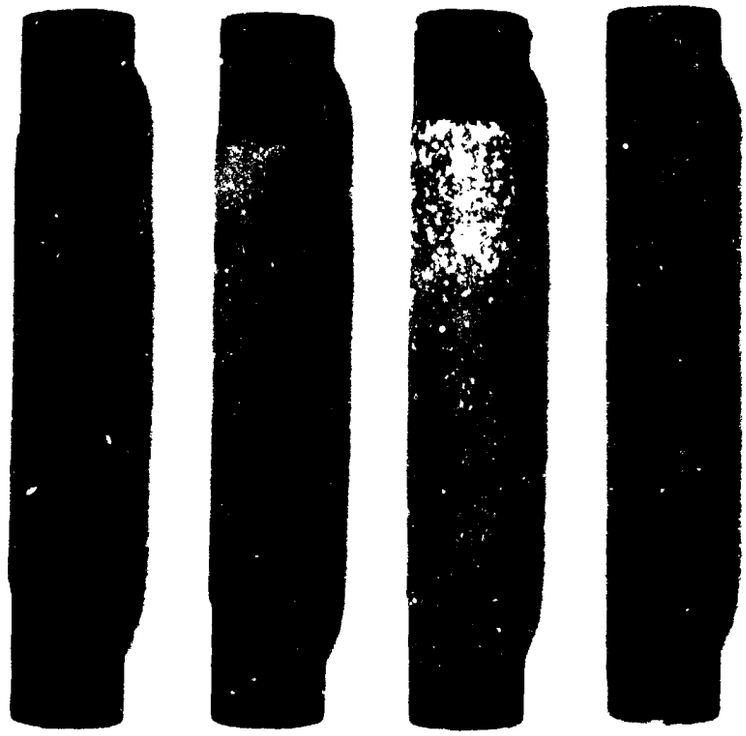

A-1
D-Z·8Y

B-1
G-Z·8Y

S-2
D-Ca_2SiO_4

N-1
NiCrAlY

Fig. 62 - Post-test conditions of some specimens from Test III (Endurance Test)
Fuel: GT No. 2
Temperature: 1150°C gas/800°C metal except N-1 (857°C)
Cycles: 1428

ORIGINAL PAGE
BLACK AND WHITE PHOTOGRAPH

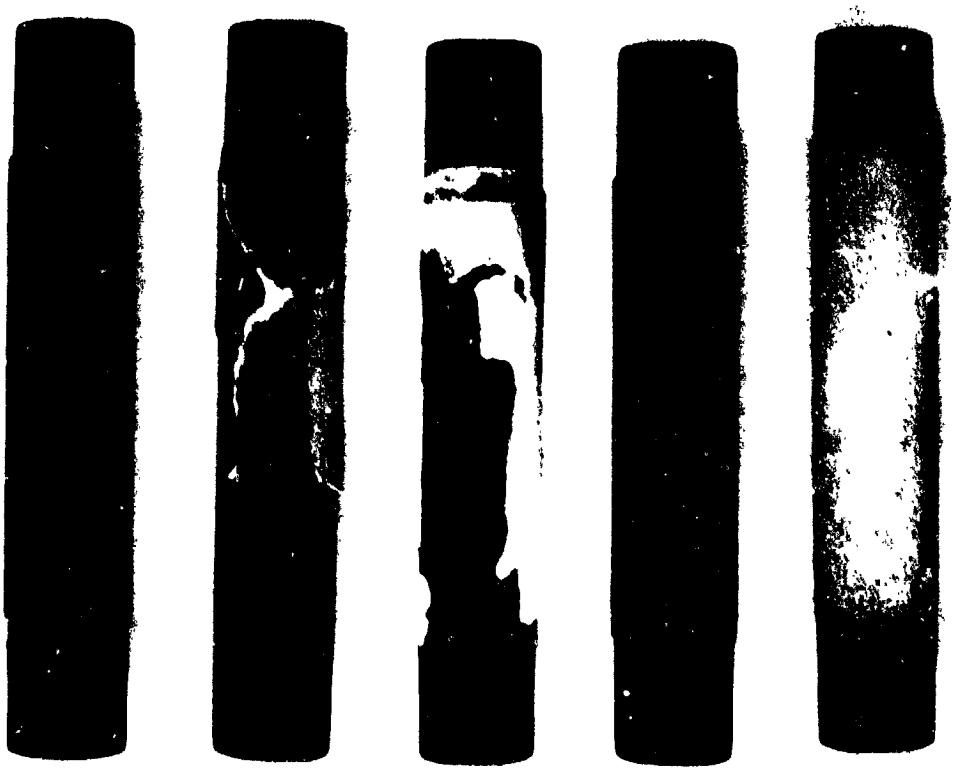

D-Z•8Y	CZ•8Y	CZ•8Y	CZ•8Y	D-Ca_2SiO_4
772 cycles	2200 cycles	190 cycles	772 cycles	190 cycles

Fig. 63 - Specimens exposed to accidental temperature excursion in Test 111

after replacing these accidentally damaged specimens. As a result of this temperature excursion incident, the maximum exposure time for the normally tested specimens was reduced to 3228 one-hour cycles instead of the planned 4000 cycles. The results of the endurance test in terms of minimum number of cycles to cause a spalling failure are shown in Fig. 64.

Detailed test descriptions both before and after the accidental temperature excursion are listed in Tables 23 and 24. Note that some of the specimens had been previously exposed for 1428 cycles. They were inserted into the test to replace those damaged by the accidental temperature excursion. 123 cycles after the test was restarted Specimen A_2 (D-$ZrO_2 \cdot 8Y_2O_3$/NiCrAlY, 2323 net cycles) developed a long crack at the back face, bottom location. This presumably was the result of the earlier temperature excursion. This same specimen later exhibited massive spalling on further thermal cycling (Fig. 65). However, the other D-$ZrO_2 \cdot 8Y_2O_3$/NiCrAlY specimen (A1), which was not subjected to the temperature excursion, showed no signs of failure after a total exposure time of 3228 one-hour cycles. This indicates that the failure of specimen A-2 was indeed premature (Fig. 65).

It was mentioned earlier that specimen A1 (D-$ZrO_2 \cdot 8Y_2O_3$/NiCrAlY) had suffered a mechanical chip at its bottom backface at the beginning of the test. However, after a total exposure time of 3228 one-hr cycles, this chip did not enlarge. Fig. 66 shows the condition and stability of this mechanical chip after various periods of exposure.

Specimen B1 (G-$ZrO_2 \cdot 8Y_2O_3$/NiCrAlY) that had previously developed a circumferential chip at its top end during the first 1428 cycles of exposure, spalled at that location after being tested for an additional 806 cycles. At the same time the other G-$ZrO_2 \cdot 8Y_2O_3$/NiCrAlY specimen (B5), developed circumferentail chipping at its top edge after 806 cycles of exposure. This result indicates that internal oxidation of the NiCrAlY particles used in the graded zone was the life determining factor and hence a more oxidation-resistant MCrAlY is needed for the graded coatings. Fig. 67 shows the development sequence of the circumferential chips on graded $ZrO_2 \cdot 8Y_2O_3$/NiCrAlY specimens after various periods of exposure.

The two D-Ca_2SiO_4/NiCrAlY specimens showed no signs of catastrophic failure. However, surface microchipping was evident - (Fig. 68). This again was due to the formation of the friable $CaSO_4$.

The condition of the NiCrAlY coated specimens is shown in Fig. 69. Some signs of oxidation are evident.

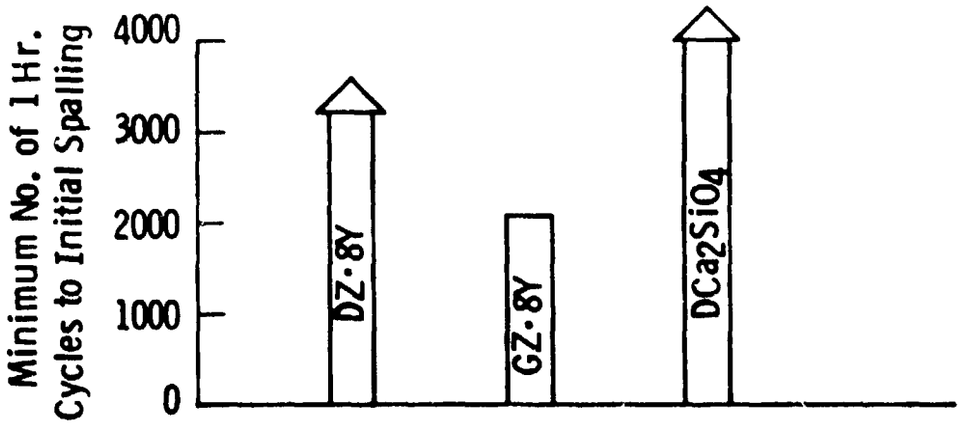

Figure 64 - Cycles to failure in the endurance tests
Temperature: 1150°C gas/800°C metal
Fuel: GT No. 2

Table 23

Endurance Test Summary* (Before Temperature Excursion)

Specimen No.	Position	Time (1-Hr Cycles) In	Time (1-Hr Cycles) Out	Net Cycles Completed	Failure Description
A1	4	0	1428	1428	Mechanical chip at bottom
A2	6	0	-	2199	No failure
B1	1	0	1428	1428	Small chip at top
B2	8	0	-	2199	Large spall at top after 2055 cycles
S1	2	0	-	2199	No failure
S2	5	0	1428	1428	No failure
N1	3	0	1428	1428	No failure
N2	7	0	-	2199	No failure
A3	4	1429	-	771	No failure
B3	1	1429	-	771	Small chip at top
S3	5	1429	2009	580	Mech. chip when put in top spalled after 580 cycles
N3	3	1429	2009	580	No failure
B4	3	2010	-	189	No failure
S4	5	2010	-	189	No failure

A - D-$ZrO_2 \cdot 8Y_2O_3$

B - G-$ZrO_2 \cdot 8Y_2O_3$

S - D-Ca_2SiO_4

N - NiCrAlY (5 mil)

*Fuel = GT No. 2
Temperature = 1150°C gas/800°C metal except for N1, N2 and N3 (857°C)

Table 24

Endurance Test* Summary (after temperature excursion)

Specimen Number	Position	Time (1-Hour Cycles) In	Time (1-Hour Cycles) Out	Net Cycles Completed	Failure Description
A1**	2	0	1800	1428 + 1800	No Failure
A2***	5	0	1800	2200 + 1800	Cracked at bottom after 2323 cycles then developed into large spalling
B1**	4	0	1800	1428 + 1800	Spalled at top after 2334 cycles
B5	6	0	1800	1800	Circumferential chip at top after 806 cycles
S1***	1	0	1800	2200 + 1800	Surface microchipping
S2**	8	0	1800	1428 + 1800	" "
N1**	3	0	1800	1428 + 1800	No Failure
N2***	7	0	1800	2200 + 1800	" "

A - D-$ZrO_2 \cdot 8Y_2O_3$

B - G-$ZrO_2 \cdot 8Y_2O_3$

S - D-Ca_2SiO_4

N - NiCrAlY (5 Mil)

*Fuel = GT No. 2
Temperature = 1150°C gas/800°C metal except for N1 and N2 (857°C)

**Previously exposed for 1428 cycles

*** Previously subjected to accidental temperature excursion at the 2200th cycle

ORIGINAL PAGE
BLACK AND WHITE PHOTOGRAPH

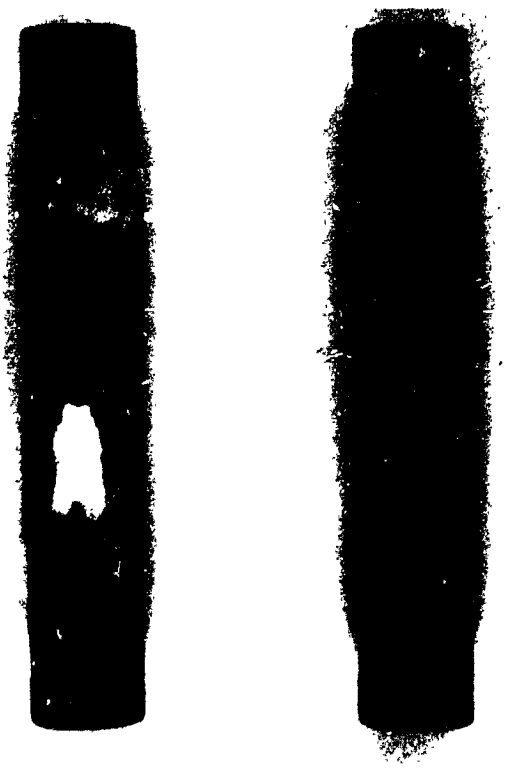

A-2* A-1

4000 cycles 3228 cycles

Fig. 65 - Post-test conditions of D-$ZrO_2 \cdot 8Y_2O_3$ specimens
Fuel - GT No. 2
Temperature - 1150°F gas/800°C metal

*subjected to accidental temperature excursion

ORIGINAL PAGE
BLACK AND WHITE PHOTOGRAPH

1428 cycles 2334 cycles 2757 cycles 3228 cycles

Fig. 66 - Mechanically chipped D-ZrO_2•$8Y_2O_3$ specimen (A-1) after various exposure periods (trailing edge)

Fuel - GT No. 2

Temperature - 1150°C gas/800°C metal

ORIGINAL PAGE
BLACK AND WHITE PHOTOGRAPH

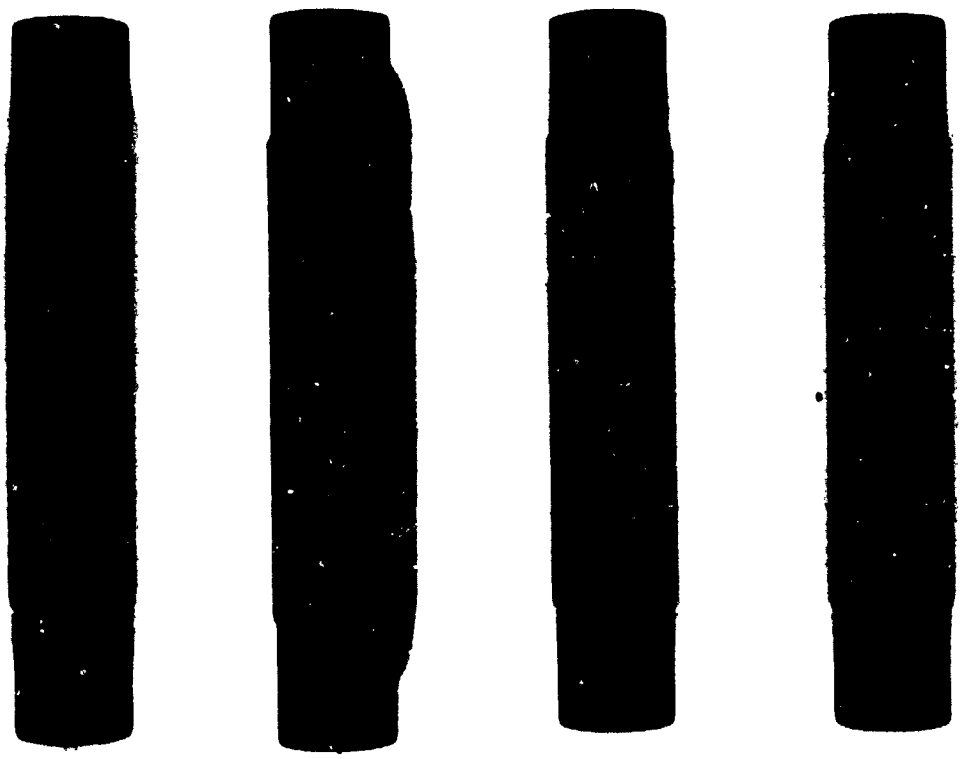

B-5	B-1	B-1	B-1
806 cycles	1428 cycles	2334 cycles	3228 cycles

Fig. 67 - Graded $ZrO_2 \cdot 8Y_2O_3$/NiCrAlY specimens after various exposure times

Fuel - GT No. 2

Temperature - 1150°C gas/800°C metal

ORIGINAL PAGE
BLACK AND WHITE PHOTOGRAPH

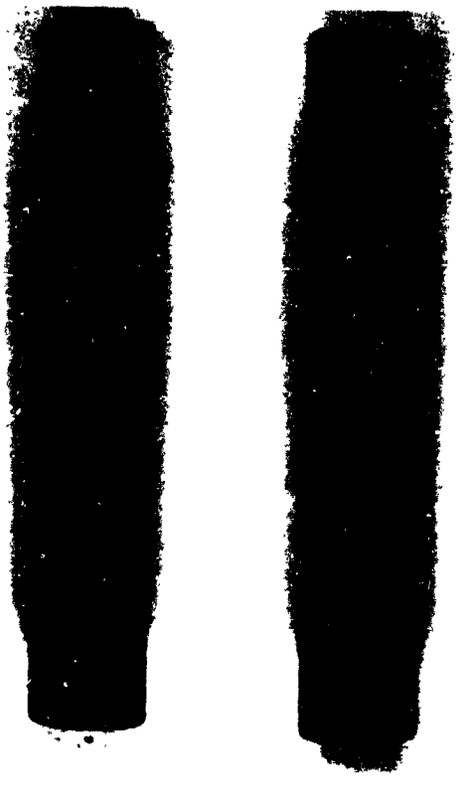

S-1* S-2

4000 cycles 3228 cycles

Fig. 68 - Post-test conditions of D-Ca_2SiO_4 specimens
Fuel - GT No. 2
Temperature - 1150°C gas/800°C metal

*subjected to accidental temperature excursion

ORIGINAL PAGE
BLACK AND WHITE PHOTOGRAPH

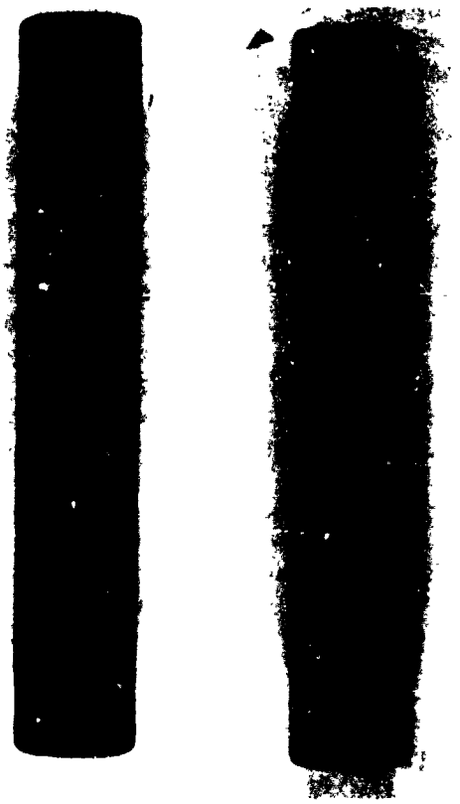

N-1 N-2*

3228 cycles 4000 cycles

Fig. 69 - Post-test conditions of NiCrAlY coated specimens
Fuel - GT No. 2
Temperature - 1150°C gas/800°C metal

*subjected to accidental temperature excursion

2.4.3 Post-Test Analysis

Detailed post-test analysis of the endurance tested specimens which included metallographic and electron microprobe analysis were conducted.

The metallographic cross-sections of two D-$ZrO_2 \cdot 8Y_2O_3$/NiCrAlY specimens are shown in Fig. 70. Specimens A2 (4000 cycles), the one that had encountered the accidental temperature excursion, exhibits extensive coating damage. The other normally tested specimen (A1), however, shows excellent coating integrity after a total exposure of 3228 one-hour cycles. EMP scans on these two specimens (Figs. 71, 72) reveal that specimen A2 did not actually encounter excessive oxidation of its NiCrAlY bond coat. In fact, both specimens show very similar behavior. An aluminum and oxygen rich layer (likely Al_2O_3) was formed on the surface of the NiCrAlY bond coat. Thus, the accelerated failure of specimen A-1 is apparently due to a more severe thermal stress condition brought about by the accidental temperature excursion rather than the oxidation of the NiCrAlY bond coat.

Figure 73 shows the metallographic cross-section of specimen B4 (G-$ZrO_2 \cdot 8Y_2O_3$/NiCrAlY) that also encountered the accidental temperature excursion. Although this specimen was only exposed for 189 one-hour cycles, it experienced extensive oxidation at both its graded zone and bond coat. It also appears that the metal substrate was oxidized as well.

A G-$ZrO_2 \cdot 8Y_2O_3$/NiCrAlY specimen that was not subjected to the accidental temperature excursion also showed signs of oxidation. This may be seen in Fig. 74 where most of the NiCrAlY particles have been depleted in the graded zone. EMP scans of this specimen showed further that a large portion of the oxygen concentration was associated with the formation of Al_2O_3, NiO or Cr_2O_3 (Fig. 75); i.e., oxidation products of NiCrAlY.

Metallographic cross-sections of the D-Ca_2SiO_4 specimens are again very interesting (Fig. 76). Irrespective of whether the specimen was exposed to the accidental temperature excursion or not, a surface reaction layer was formed. EMP scans revealed that this surface reaction layer was rich in sulfur (Figs. 77 and 78), and hence a $CaSO_4$ layer formed by the reaction of Ca_2SiO_4 with the SO_2/SO_3 gas contained in the combustion environment. This also explains why surface microchipping was observed during the test. It is also interesting to note from Fig. 77 that a ternary compound may have formed below the $CaSO_4$ layer. However, the exact composition of this ternary compound was not determined.

These observations of $CaSO_4$ and/or ternary compound formation clearly reveal the fact that although the Ca_2SiO_4 specimens performed very well during the endurance test, there is definitely a potential chemical stability problem on long term exposures that may affect its performance.

ORIGINAL PAGE
BLACK AND WHITE PHOTOGRAPH

A-2* (4000 cycles)

A-1 (3228 cycles)

Fig. 70 - Cross sections of D-$ZrO_2 \cdot 8Y_2O_3$/NiCrAlY specimens from endurance test (50X)

*Exposed to accidental temperature excursion

ORIGINAL PAGE
BLACK AND WHITE PHOTOGRAPH

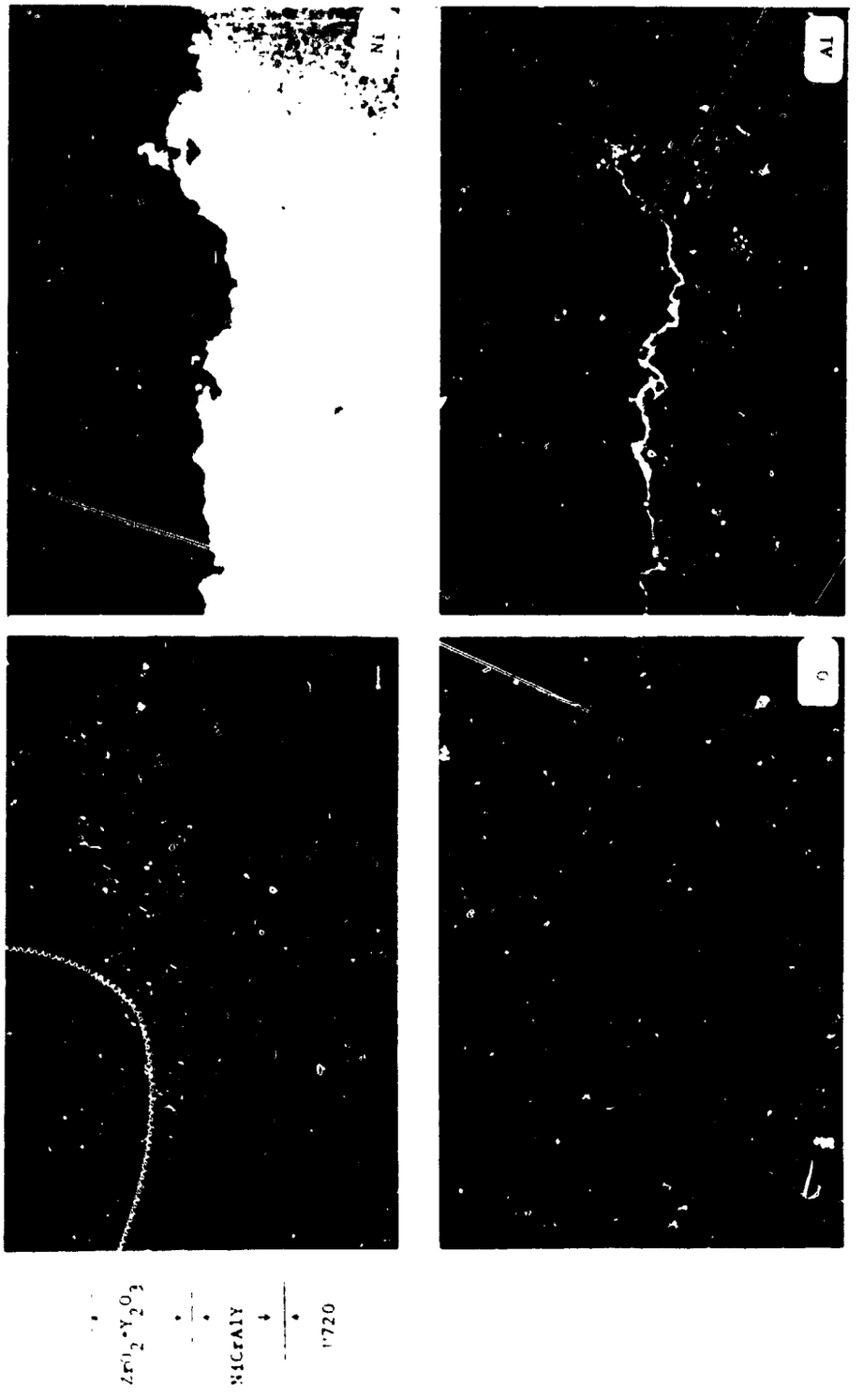

Fig. 71 - EMP scans on Specimen A-2* ($D\text{-}ZrO_2 \cdot 8Y_2O_3$), 4000 cycle, endurance test

*subjected to accidental temperature excursion

ORIGINAL
BLACK AND WHITE PHOTOGRAPH

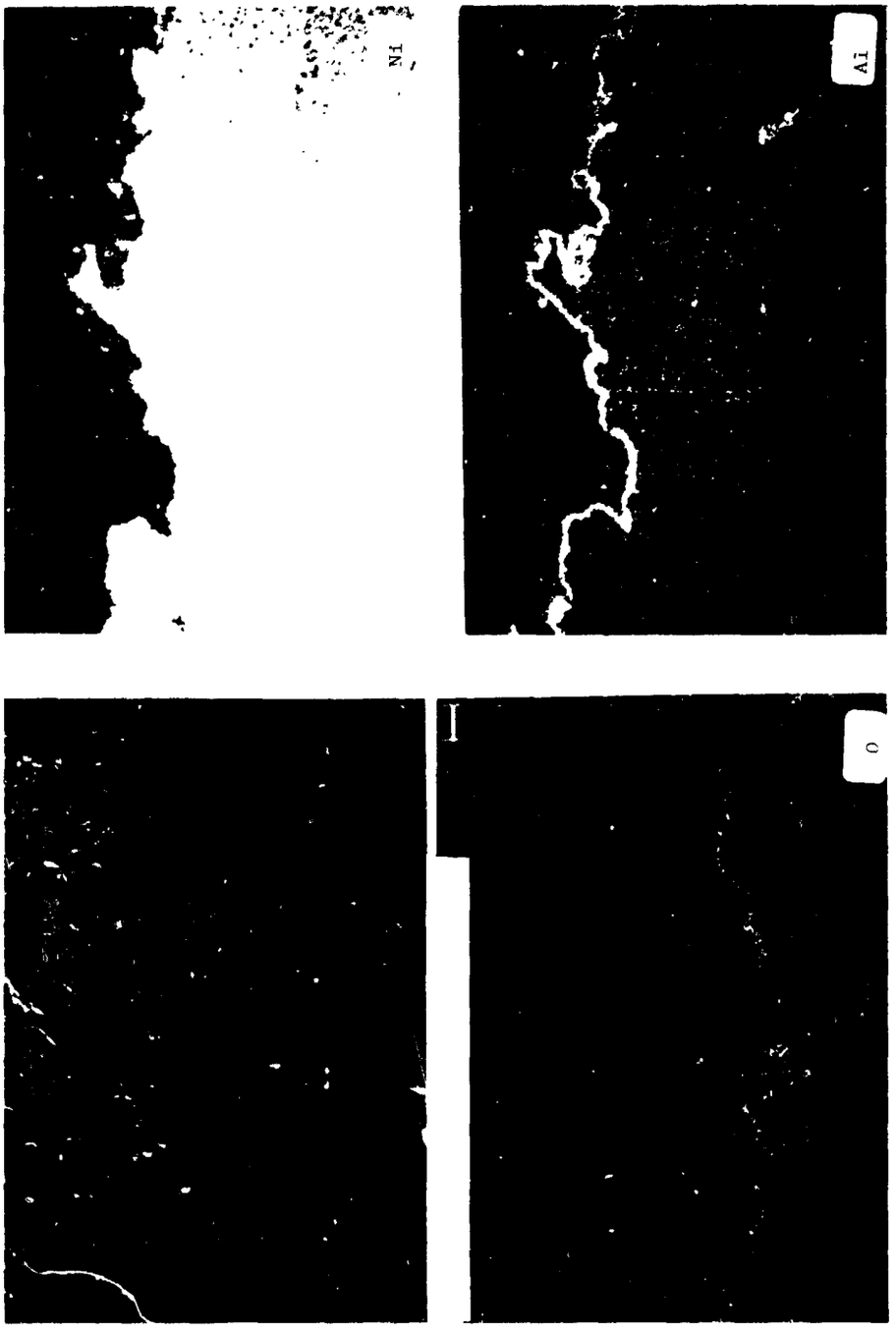

Fig. 72 - EMP scans on specimen A-1 ($D\text{-}ZrO_2 \cdot 8Y_2O_3$), 3228 cycles, endurance test

ORIGINAL PAGE
BLACK AND WHITE PHOTOGRAPH

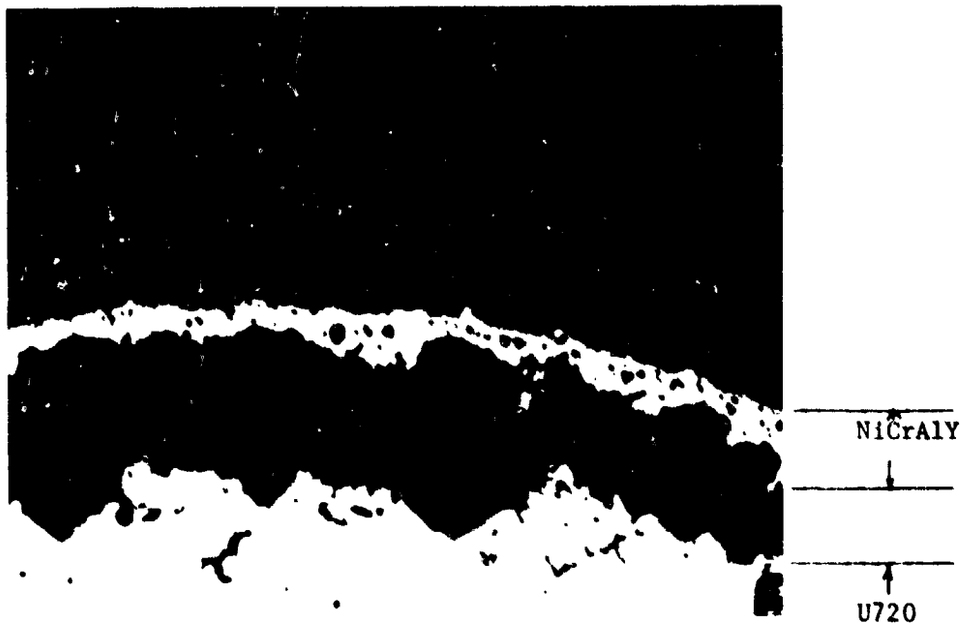

Front

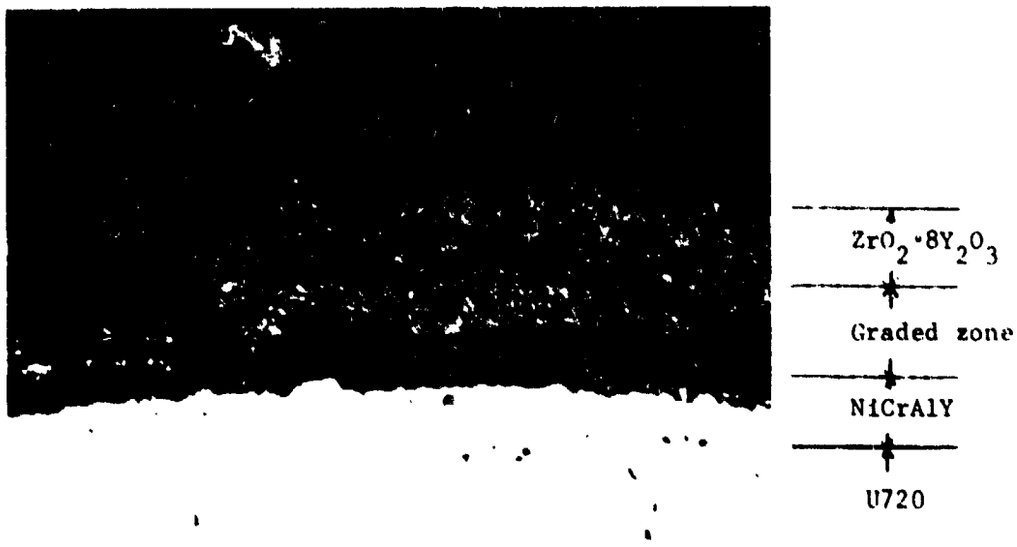

Back

Fig. 73 - Cross section of specimens B4*(G-$Zr_2 \cdot 8Y_2O_3$/NiCrAlY) 189 cycles, endurance test (50X)

*subjected to accidental temperature excursion

ORIGINAL PAGE
BLACK AND WHITE PHOTOGRAPH

Fig. 2a - Cross-section of specimen B-1* (ZrO_2*$8Y_2O_3$/NiCrAlY), 1228 cycles, endurance test (50X)

*was not subjected to temperature excursion

ORIGINAL PAGE
BLACK AND WHITE PHOTOGRAPH

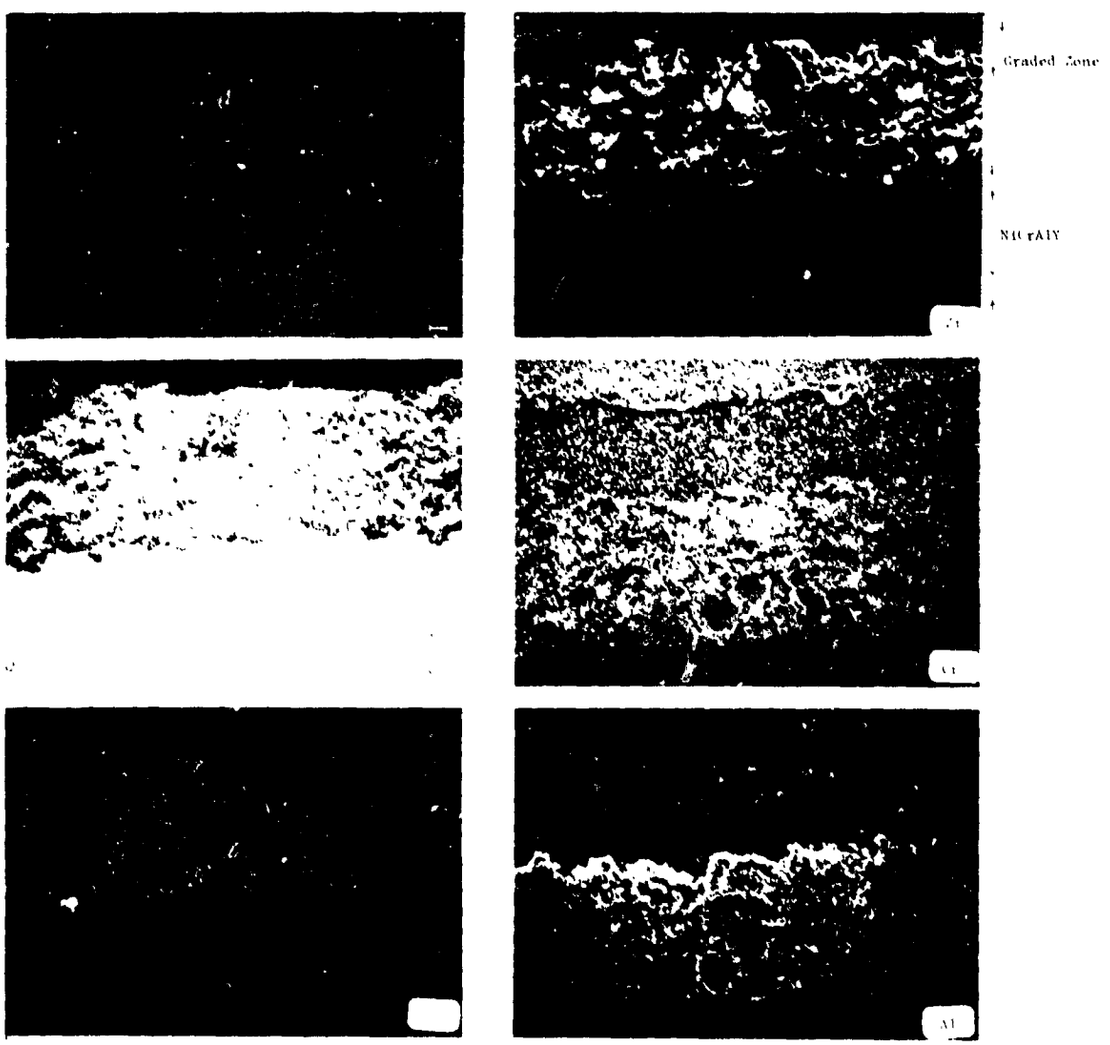

Fig. 75 - EMP scans on specimen B1 (G-ZrO_2·$8Y_2O_3$/NiCrAlY), 3228 cycle, endurance test

ORIGINAL PAGE
BLACK AND WHITE PHOTOGRAPH

Fig. 76 - Cross-section of specimen S1 ($D\text{-}Ca_2SiO_4$), 4000 cycles, endurance test (50X)

ORIGINAL PAGE
BLACK AND WHITE PHOTOGRAPH

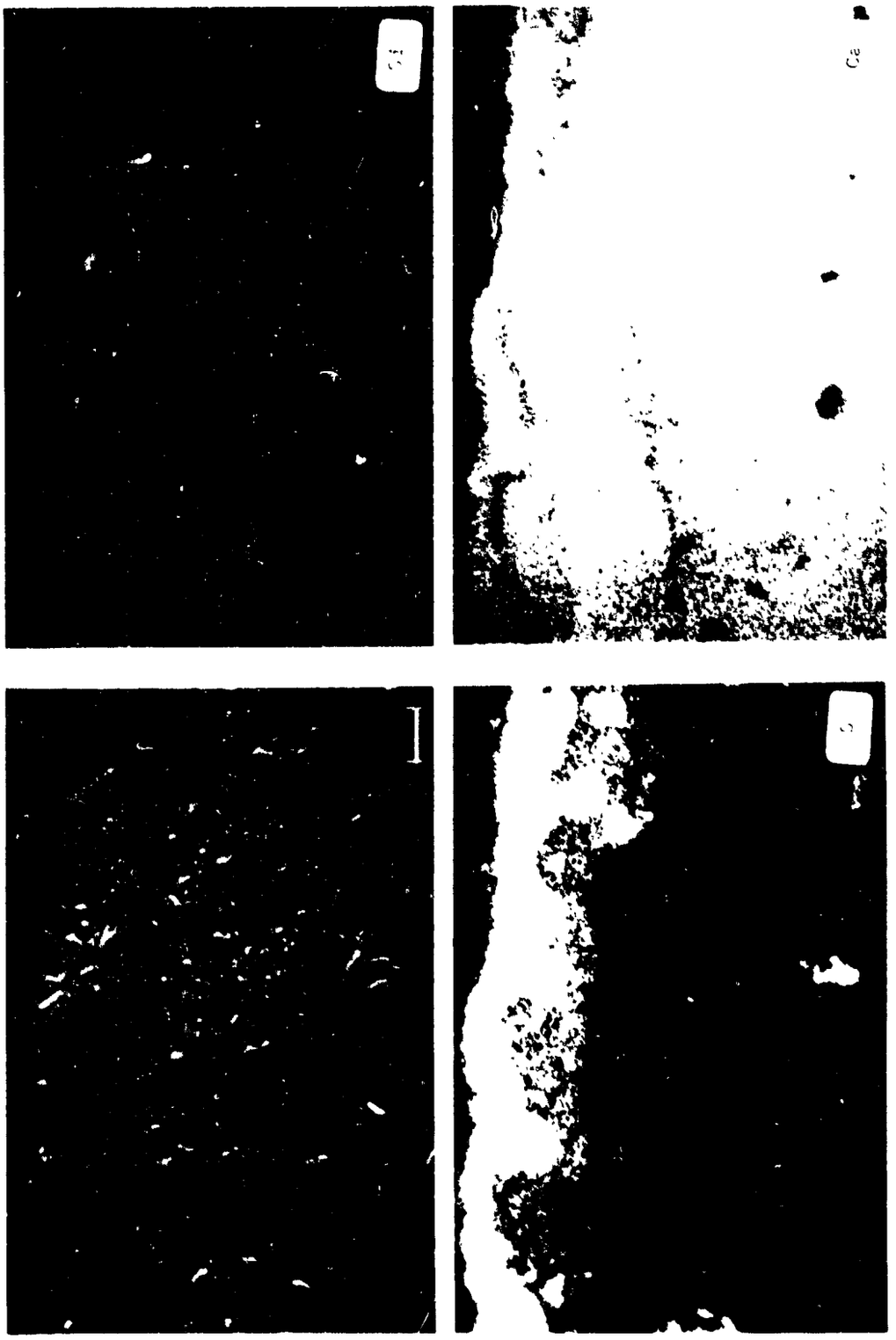

Fig. 77 - EMP scans on Specimen S-1* (D-$CaSiO_4$), 4000 cycle, endurance test

*subjected to accidental temperature excursion

ORIGINAL PAGE
BLACK AND WHITE PHOTOGRAPH

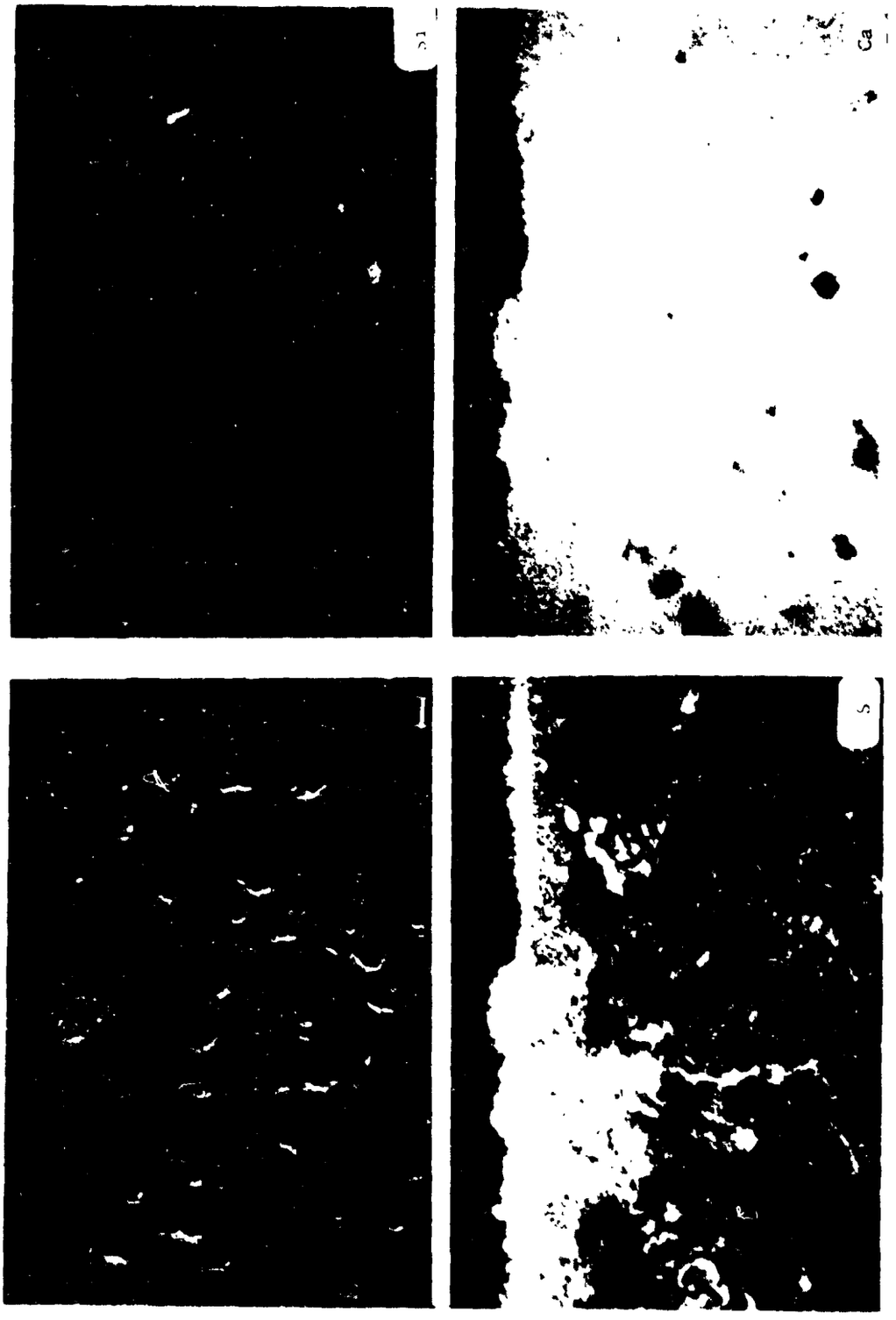

Fig. 76 - EMP scans on specimen S2 ($D\text{-}Ca_2SiO_4$), 3228 cycles, endurance test
Was not subjected to accidental temperature excursion

The NiCrAlY coated specimens were also examined. Besides being slightly oxidized, void formation was evident on both specimens N1 and N2 (Fig. 79). This is especially pronounced on specimen N2 that was subjected accidentally to a higher metal temperature.

3. COATING DEGRADATION MECHANISMS

3.1 Clean Fuel Conditions

The burner rig test results (Task I) and discussion given in previous sections showed clearly that with a few exceptions, the present day thermal barrier coatings selected for this study perform very well in relatively clean burning combustion atmospheres such as represented by GT No. 2 fuel. A major constraint for these coatings in clean fuel operation was the oxidation temperature limitation of the NiCrAlY used for the bond coat and grading of the oxide coatings. This temperature limitation appears to be less than 850°C for graded coatings but greater than 900°C for duplex coatings. The NiCrAlY particles in the graded coatings are more susceptible to oxidation because of the large surface area available for reaction. The NiCrAlY base coats, on the other hand, used for both the duplex and graded coatings sustain much higher temperatures providing that they are dense. High density plasma sprayed bond coats can be achieved either by post-spray heat treatment as is done by the Linde Co. or by modifying the plasma spray process itself, e.g., low pressure plasma spray. Recent work at NASA Lewis has shown the effects of plasma spray parameters on two layer thermal barrier coating system life (Ref. 33).

The Task III endurance test served to confirm the findings discussed above. In this test the graded coatings were subjected to extensive NiCrAlY oxidation within the graded zone after extended periods even at the 1150°C gas/800°C metal test condition. The graded zone of course is somewhat higher in temperature than the 800°C substrate temperature. The dense NiCrAlY bond coats that were nearly as cool as the alloy substrates (800°C) showed only a slightly oxidized surface layer. This thin oxide layer (primarily Al_2O_3) was not detrimental to the duplex coating system life at least within the 3228 hours of cyclic test exposures.

Although limited in scope, the clean fuel pressurized passage tests (Task II) provided very encouraging results. The ability of both the duplex and graded coatings to survive not only many cycles of simulated normal shutdown operation but also many cycles of the very severe conditions of emergency shutdown, i.e., instantaneous shutdown from the operating temperature, was indeed a very positive result. The heat fluxes, which determine thermal stress, generated in the pressurized passage tests were comparable to or greater than those known to develop in actual commercial industrial turbines.

ORIGINAL PAGE
BLACK AND WHITE PHOTOGRAPH

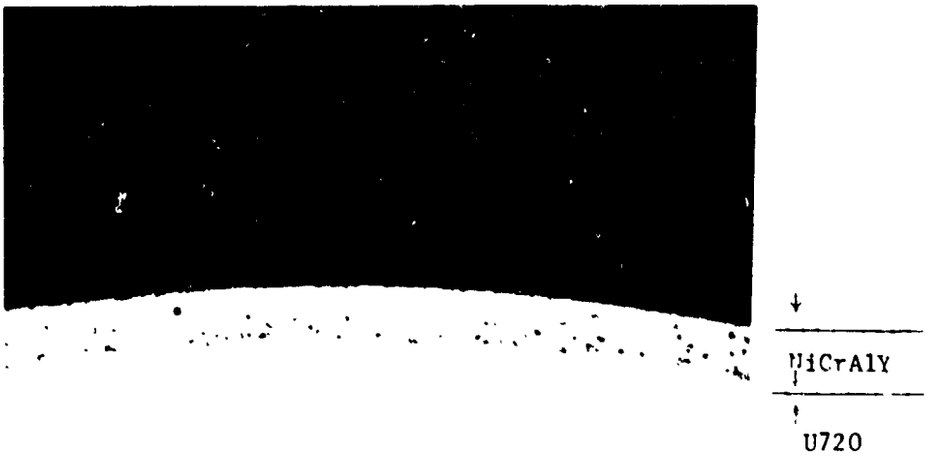

N-1 (3228 cycles)

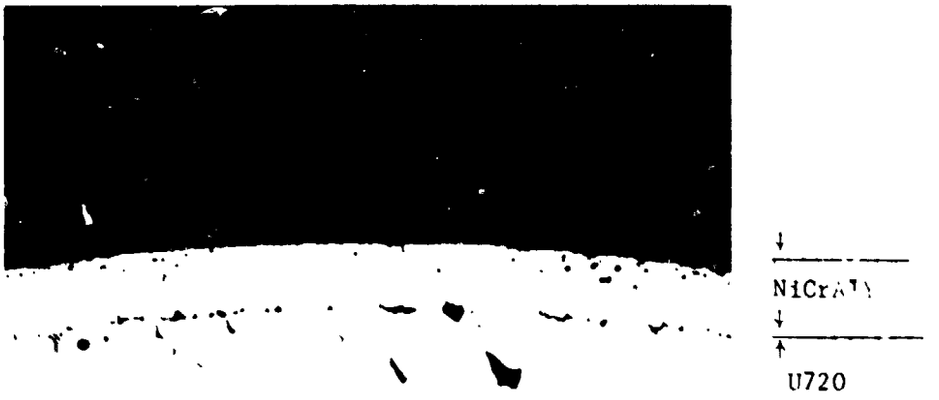

N-2* (4000 cycles)

Fig. 79 - Cross-sections of NiCrAlY coated specimens endurance test (50X)

*subjected to accidental temperature excursion

3.2 Contaminated Fuel Conditions

In contrast to the excellent performance of the thermal barrier coating systems in clean fuel, their performance in contaminated fuels was clearly inadequate. The vanadium impurity which is present in residual fuels was particularly detrimental to the oxide coatings. Accelerated failures occurred with increasing vanadium content even when the other contaminants including the Mg/V ratio remained constant as in tests 1B4, 1B5 and 1C2. The relationship between fuel vanadium content and coating failure time for the duplex $ZrO_2 \cdot 8Y_2O_3$/NiCrAlY coating system is clearly illustrated in Fig. 80.

The mechanism of vanadium attack that leads to coating failures, $ZrO_2(Y_2O_3)$ coatings in particular, was examined. Previous work (Ref. 34-36) has suggested that molten vanadates such as V_2O_5 and $Na_2V_2O_6$ caused the leaching of Y_2O_3 stabilizer from the tetragonal/cubic $ZrO_2(Y_2O_3)$ to form monoclinic $ZrO_2(Y_2O_3)$ according to equations such as:

$$ZrO_2 \cdot a\ Y_2O_3 + x\ V_2O_5\ (\ell) \rightarrow ZrO_2\ (a-x)\ Y_2O_3 + 2xYVO_4$$

(Tetragonal/cubic) (monoclinic)

The postulated effect of this attack is a disruptive volume change of about 5% when the martensitic tetragonal monoclinic transformation occurs, and hence eventual coating failure. However, in the present burner rig tests, the possibility of the vanadium existing as vanadium oxide can be ruled out from Lay's $MgO-V_2O_5-SO_3$ phase study (Ref. 37) which showed that the condensation of V_2O_5 in the presence of MgO and SO_3 is favored only by low temperature and high SO_3 partial pressures. For example the P_{SO_3} required for the condensation of V_2O_5 and temperatures >760°C is 1×10^{-3} atm. This is at least two orders of magnitude higher than the P_{SO_3} developed in the burner rig used for testing.

The formation of the $Na_2V_2O_6$ phase has been determined to be thermodynamically possible. Since $Na_2V_2O_6$ is very soluble in water, a chemical analysis for vanadium was conducted on a selected specimen by first dissolving the soluble constituents of the deposits in water. The insignificant amount of vanadium found suggested that $Na_2V_2O_6$ formation was unlikely.

EMP scans for this same specimen (Fig. 81) confirmed that there was no deep penetrating liquid vanadium salt. In fact all the vanadium concentrations were found close to the coating surface; yet destabilization of tetragonal/cubic $ZrO_2(Y_2O_3)$ was still observed. Based on this information, the authors postulate that the destabilization process is basically induced by the reaction of $ZrO_2(Y_2O_3)$ with solid vanadate condensates or gaseous vanadium oxides such as V_2O_5 (gas). It is also

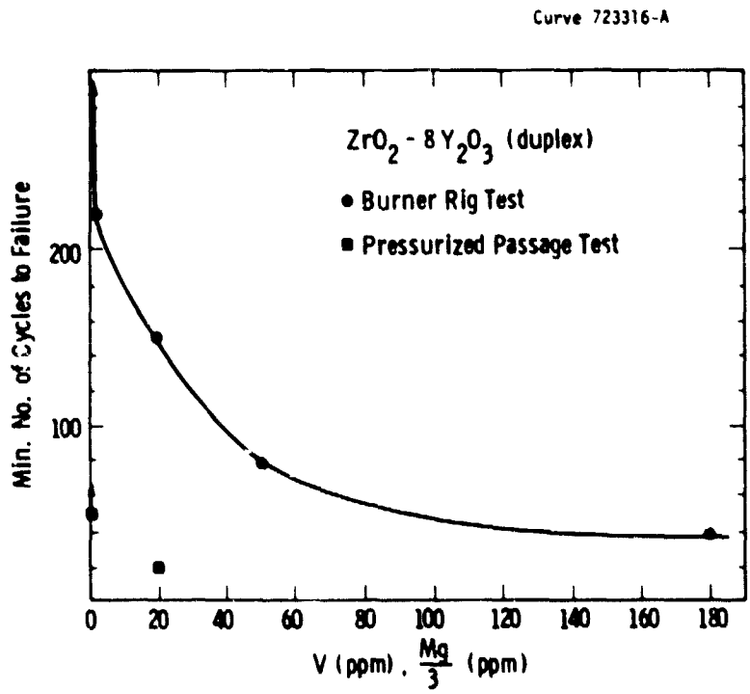

Figure 80 - Coating failure as a function of fuel vanadium content

ORIGINAL PAGE
BLACK AND WHITE PHOTOGRAPH

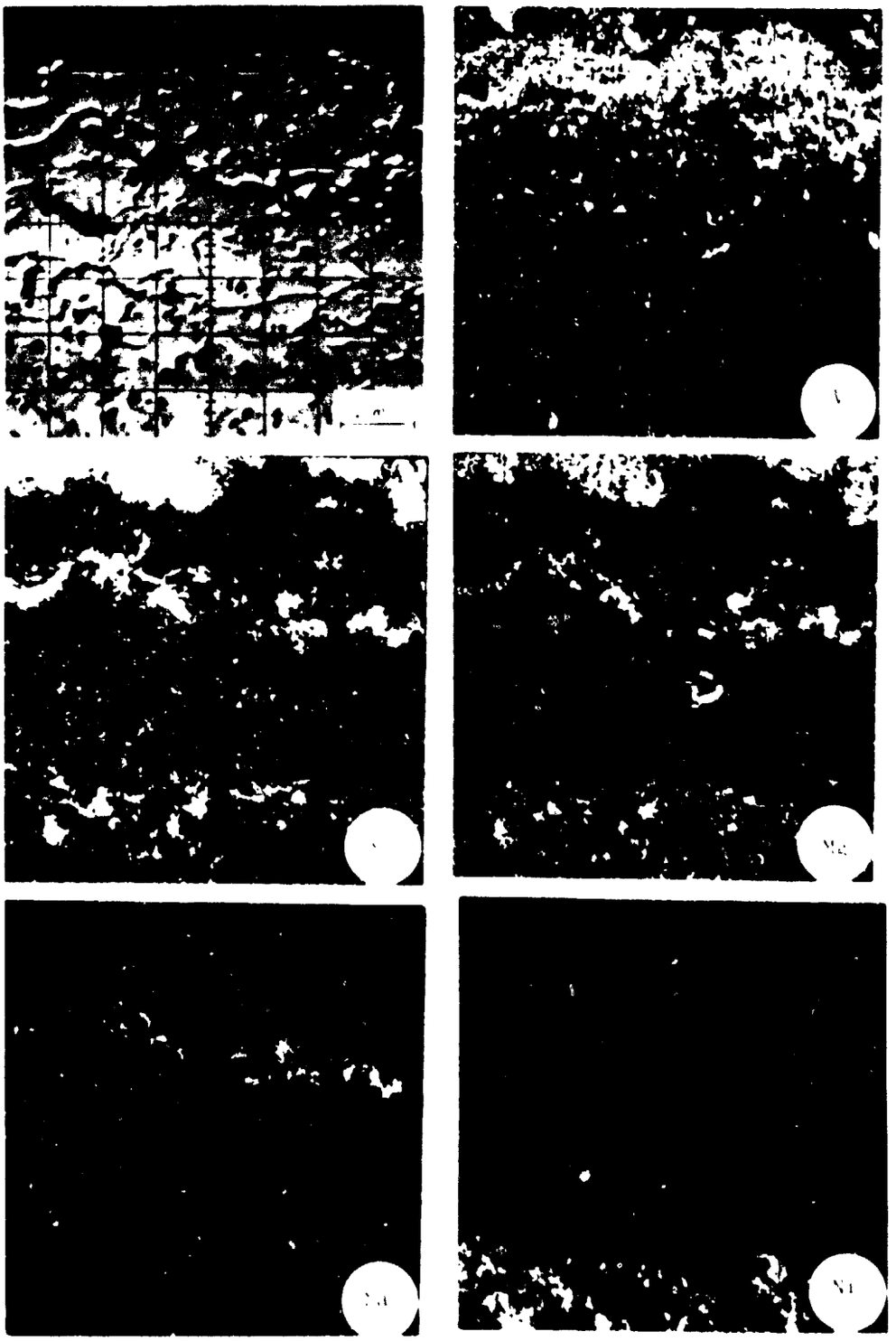

Fig. 81 - Electron microprobe scans on specimen BB4 (G - ZrO_2•8Y_2O_3), 500 cycles, Test IB5

interesting to note from Fig. 81 that the major concentration of vanadium is not associated with magnesium. Instead, it is located rather evenly inside the bulk of the $ZrO_2(Y_2O_3)$ top layer. Since the V, Y, Zr concentrations seem to overlap with one another, it is possible that besides YVO_4, a ternar ZrO_2-Y_2O_3-V_2O_5 solid solution has also been formed. Further experiments are needed to confirm these reaction details.

Since X-ray analysis results indicated that most of the destabilization occurred at regions near the surface of the coatings, the likely degradation mechanism of $ZrO_2(Y_2O_3)$ coatings in vanadium contaminated environments can be described in the following steps: (1) gaseous or solid vanadium compounds react with the $ZrO_2(Y_2O_3)$ coating to leach out Y_2O_3 stabilizer and lead to monoclinic $ZrO_2(Y_2O_3)$ formation at the coating surface; (2) with sufficient monoclinic $ZrO_2(Y_2O_3)$ formed, cracks are initiated at the coating surface when the monoclinic $ZrO_2(Y_2O_3)$ undergoes phase transformation on thermal cycling; (3) these surface cracks propagate and branch into the coating interior and eventually lead to coating spalling.

The deep penetration of Na_2SO_4-$MgSO_4$ molten salts into the porous oxide coating has also been shown to be very detrimental to coating performance. Molten Na_2SO_4 condensate can lead to coating failure through several possible mechanisms.

Palko (Ref. 35) et.al. showed from atmospheric burner rig tests that molten sodium sulfate can penetrate the porous oxide and react with the underlying bond coat at 870°C to cause spalling. Barkalow and Pettit (Ref. 38) suggested from furnace corrosion tests that hot corrosion occurs by acidic dissolution of Y_2O_3 from stabilized $ZrO_2 \cdot Y_2O_3$ according to a reaction of the form:

$$Y_2O_3 \text{ (in } ZrO_2) + 3SO_3 \text{ (in } Na_2SO_4) \rightarrow 2Y^{3+} \text{ (in } Na_2SO_4) + 3SO_4^{2-} \text{(in } Na_2SO_4)$$

The solidified salt on cooling in this case is a hydrated sodium-yttrium sulfate $[Na_2Y_2(SO_4)_4 \cdot 2H_2O]$. This reaction was significant at the relatively low temperature of 700°C and high P_{SO_3} pressure of 7×10^{-4} atm. As shown in this work and earlier by Bratton and Singhal, (Ref. 5) the salt reactions lead to destabilization of the stabilized $ZrO_2 \cdot Y_2O_3$ coating -- an affect that seems important in the failure mode.

However, in the present study, it is clear from the EMP scans shown in Figures 25-27 that the Na_2SO_4-$MgSO_4$ phases are located in the pores and crevices of the oxide coating with no correspondence found between Na and Y or Zr indicating that there is no significant chemical reaction between the molten salt and the coating. Also, since hot corrosion of the bond coat is not always observed when coatings fail, it seems that the failure mode is mechanical in nature. A very possible mechanism is that on thermal cycling the stress generated by the thermal expansion

mismatch between the $ZrO_2(Y_2O_3)$ coating and the entrapped solidified salt condensate causes the coating to crack and spall. Indeed simplified stress calculations based on thermal expansion differences between the condensed melt and oxide coating have indicated that the stress developed during thermal cycling can easily be an order of magnitude higher than the tensile strength of the ceramic coating.

Another possible mechanism is coating densification, at least locally, in the presence of molten Na_2SO_4 that would result in the reduction of coating thermal stress resistance.

Since solid deposits usually accumulate on the coating surface and cannot penetrate deep into the coating interim, it is clear that Na_2SO_4 can induce coating failure only when it is condensed in the molten form. This conclusion is also consistent with experimental observations at NASA Lewis. Using thermochemical calculations of condensate dew points and melting points combined with temperature profiles of test specimens, Miller (Ref. 39) was able to qualitatively explain observed coating failures at NASA.

Figure 82 illustrates several relationships between thermodynamic properties of the salts and the nature of the salt deposit. Thus depending on the relative magnitudes of the salt dew point, melting point and the coating temperature, the physical form of the condensates may vary. While solid or no condensation is preferred, the most severe condition for a porous plasma sprayed ceramic coating is when the dew point of the condensate is above the surface temperature of the ceramic and the melting point of the condensate is below the bond coat temperature.

Reactions with SO_2/SO_3 gas may also adversely affect the integrity of certain coatings. It was demonstrated that both $ZrO_2 \cdot 24.65$ MgO and Ca_2SiO_4 coatings are susceptible to SO_2/SO_3 gas attack. In fact thermodynamic calculations show that at 900°C (the coating surface temperature), the reaction:

$$Ca_2SiO_4 + 2SO_3\ (g) \rightarrow 2CaSO_4 + SiO_2$$

is thermodynamically possible at $P_{SO_3} > 6 \times 10^{-6}$ atm. This is one to two orders of magnitude lower than the P_{SO_3} levels normally found in utility gas turbines (10^{-5} to 10^{-4} atm) burning fuels containing 0.1 to 1 wt % sulfur. Thus, even when relatively clean fuels such as GT No. 2 fuel (typically contains 0.25 wt % S) are used, reaction between SO_3 gas and a Ca_2SiO_4 coating may still occur. This as well as the observations that Ca_2SiO_4 may also be reactive to combustion condensates such as $MgSO_4$ and $Mg_3V_2O_8$, indicates that Ca_2SiO_4 coating may not process adequate chemical stability for long term exposure.

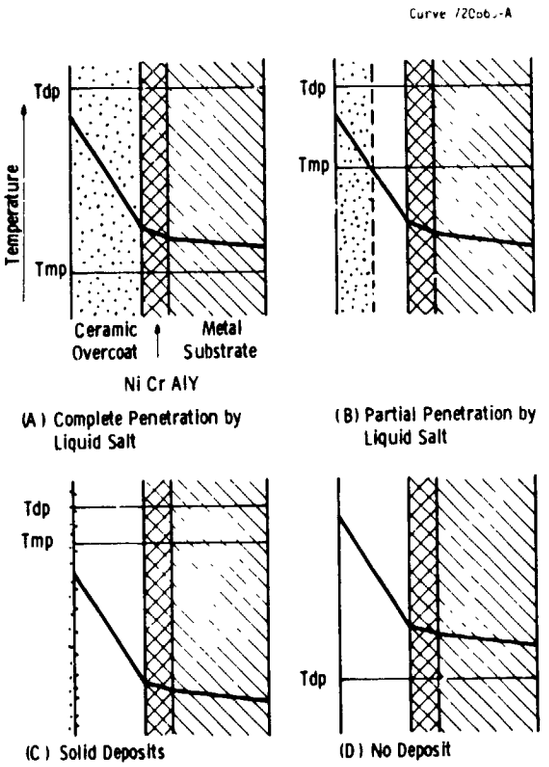

Figure 82 - Schematic representation of relationship between dew point (Tdp), melting point (Tmp) and nature of deposit

3.3 Coal Derived Fuel Conditions

The SRC-2 fuel test was conducted for too short a time to determine conclusively if a chemical reactivity problem exists. However, since the coatings survived a pressurized test with this fuel throughout a test period when chemical induced failures usually occurred, the thermal barrier coatings are considered excellent candidates for further study in terms of turbines burning coal derived liquid fuels.

IV. CONCLUSIONS

1. Present-day thermal barrier coatings are viable candidates for utility turbines burning relatively clean fuel such as GT No. 2, (ASTM-2D) but coating improvements are needed for turbines burning lower grade fuel such as residual oil.

2. The duplex $ZrO_2 \cdot 8Y_2O_3$/NiCrAlY coating is ranked highest for clean fuel turbine operation with the duplex Ca_2SiO_4/NiCrAlY ranked second. The present graded $ZrO_2 \cdot 8Y_2O_3$/NiCrAlY type coating can be operated at temperatures below the oxidation temperature limit of the MCrAlY used for grading from metal to ceramic.

3. Turbine simulation tests in the pressurized passage, and burner rig endurance test support the selection of the duplex $ZrO_2 \cdot 8Y_2O_3$/NiCrAlY coating as the primary coating for near-term field testing. The duplex Ca_2SiO_4/NiCrAlY coating should also be tested to determine its durability under actual turbine operation.

4. Graded coatings such as $ZrO_2 \cdot 8Y_2O_3$-MCrAlY show potential for corrosive turbine operating conditions and therefore warrant further development.

5. In fuels contaminated with vanadium, the present-day zirconia-based coatings are subject to destabilization which may lead to failure. The origin of destabilization is reaction of the coating with solid vanadate condensates or gaseous vanadium oxides.

6. In fuels contaminated with sodium and magnesium sulfate impurities, the present day zirconia-based coatings are subject to failure due to the large mismatch in thermal expansion coefficients between the condensed Na_2SO_4 or Na_2SO_4-$MgSO_4$ phases that deposit in the porous coatings.

7. While $ZrO_2 \cdot MgO$ is inherently unstable, the $ZrO_2 \cdot MgO$/NiCrAlY coating is also susceptible to reaction with the SO_2/SO_3 gas produced from fuels containing sulfur. The reaction product is $MgSO_4$. Accelerated destabilization of the $ZrO_2 \cdot MgO$ solid solution occurs as a result of the SO_3 reaction and leads to failure.

8. The Ca_2SiO_4/NiCrAlY coating is susceptible to reaction with the SO_2/SO_3 gas produced from fuels containing sulfur. The reaction produce is $CaSO_4$ that does not cause gross spalling but causes shallow chipping the coating surface. Ca_2SiO_4 is also reactive towards $MgSO_4$ and $Mg_3V_2O_8$ deposits.

V. RECOMMENDATIONS

This program has identified several promising thermal barrier coatings for use in utility turbines burning GT No. 2 fuel (ASTM-2D) or other clean fuels. The program has further identified the deficiencies of present day thermal barrier coatings in their resistance to lower grade fuels. The following recommendations are made:

1. A field testing program should be initiated using the most promising thermal barrier coating candidates determined from the present study. The coatings should be applied to row 1 turbine blading and the blading installed in a utility turbine engine for long time durability tests. It is recommended that the engine be a W501D in combined cycle, base load operating on a clean fuel.

2. A test program for selected present-day thermal barrier coatings should be extended to gas temperatures above 1150°C and at least to 1260°C which is a near term (5 year) turbine inlet temperature objective for utility turbines.

3. A more extensive fuel sensitivity evaluation program should be conducted using available coal derived liquid fuels, and especially those believed to be available in the future for utility turbine operation.

4. A more oxidation resistant graded-type thermal barrier coating should be developed and evaluated. The emphasis should be on a broader evaluation of MCrAlY type alloys (M is Ni/Co) for grading purposes. This warrants further effort because of the potential durability of graded coatings for use in turbines burning low grade fuel as well as clean fuel.

5. An effort should be made to develop ceramic coating process specifications for utility turbine components. These include combustors, transition pieces and blading.

6. In the past year, new promising ceramic coatings and processes have been under development by Westinghouse and others. It is recommended that these coatings be continually evaluated for their potential use in utility turbines.

REFERENCES

1. Amos, D. J., "Analytical Investigation of Thermal Barrier Coatings on Advanced Power Generation Gas Turbines," NASA CR-135146, March, 1977.

2. Carlson, N. and Stone, B. L., "Thermal Barrier Coatings on High Temperature Gas Turbine Engines," NASA CR-135147, February, 1977.

3. Clark, J. S., Nainiger, J. J., and Heyland, R. E., "Potential Benefit of a Ceramic Thermal Barrier Coating on Large Power Generation Gas Turbines," NASA TM 73712, June, 1977.

4. Levine, S. R. and Clark, J. S., "Thermal Barrier Coatings -- A Near Term High Payoff Technology," NASA TM X-73586, 1977.

5. Bratton, R. J., Singhal, S. C., Lee, S. Y., "Ceramic Gas Turbine Components Research and Development, Part 2 - Evaluation of ZrO_2-Y_2O_3/NiCrAlY Thermal Barrier Coatings Exposed to Simulated Gas Turbine Environments," Final Report, EPRI Contract RP421-1, June 1978.

6. Ingham, H. S. and Shepard, G. P., Flame Sprayed Handbook, Vol. III, Plasma Flame Process, Metco, Inc., 1965.

7. Grisaffe, S. J., "A Simplified Guide to Thermal Spray Coatings," Mach. Des., Vol. 39, No. 17, July 20, 1967, pp. 174-181.

8. Grisaffe, S. J., "Coatings and Protection," in The Superalloys, C. Sims and W. C. Hagel, eds., John Wiley & Sons, Inc., 1972, Chapter 12, pp. 341-370.

9. Chatterji, D., Devries, R. C., and Romeo, G., "Protection of Superalloys for Turbine Application," in Advances in Corrosion Science and Technology, Vol. 6, M. G. Fontana and R. W. Staehle, eds., Plenum Press, 1976, pp. 1-87.

10. Goward, G. W., "Protection Coatings for High Temperature Alloys - State of Technology," Symposium on Properties of High Temperature Alloys, Z. A. Foroulis and F. S. Pettit, eds., The Electrochemical Society, Inc., 1976, pp. 806-823.

11. Schafer, L. J., Jr., "Comparison of Theoretically and Experimentally Determined Effects of Oxide Coatings Supplied by Fuel Additives on Uncooled Turbine-Blade Temperature During Transient Turbojet-Engine Operation," NASA RM E53A19, 1953.

12. Bartoo, E. R., and Clure, J. L., "Experimental Investigation of Air-Cooled Turbine Blades in Turbojet Engine XIII - Endurance Evaluation of Several Protective Coatings Applied to Turbine Blades of Non-strategic Steels," NASA RM E53E18, 1953.

13. Hjelm, L. N., Bornhorst, B. R., "Development of Improved Ceramic Coatings to Increase the Life of XLR 99 Thrust Chamber," Research Airplane-Committee Report on Conference on the Progress of the X-15 Project. NASA TM X-57-72, 1961, pp. 227-253.

14. Curren, A. N., Grisaffe, S. J., and Wycoff, K. C., "Hydrogen Plasma Tests of Some Insulating Coating Systems for the Nuclear Rocket Thrust Chamber," NASA TM X-2461, 1972.

15. Liebert, C. H. and Stecura, S., "Ceramic Thermal Protective Coating Withstands Hostile Environment of Rotating Turbine Blades," NASA Tech. Brief B75-10290, 1975.

16. Stecura, S., "Two-Layer Thermal Barrier Coating for Turbine Airfoils - Furnace and Burner Rig Test Results," NASA TM X-3425, 1976.

17. Stecura, S. and Liebert, C. H., "Thermal Barrier Coating System," U.S. Patent 4,055,705, October 25, 1977.

18. Stecura, S., "Two-Layer Thermal Barrier Coating for High Temperature Components," Am. Ceram. Soc., Bull. Vol. 56, No. 12, Dec. 1977, pp. 1082-1089.

19. Nijpjes, N. M., "ZrO_2 - Coatings on Nimonic Alloys," Sixth Plansee Seminar on High Temperature Materials, F. Benesovsky, ed., Springer-Verlag, 1969, pp. 481-499.

20. Cavanagh, J. R., et.al., "The Graded Thermal Barrier - A New Approach for Turbine Engine Cooling," AIAA Paper 72-361, April 1972.

21. Tucker, R. C., Jr., Taylor, T. A., and Weatherly, M. H., "Plasma Deposited MCrAlY Airfoil and Zirconia/MCrAlY Thermal Barrier Coatings," Proceedings of the 3rd Conference on Gas Turbine Materials in a Marine Environment, (Univ. Bath, Bath, England), September 20-23, 1976.

22. Gaffin, W. O. and Webb, D. E., "JT8D and JT9D Jet Engine Performance Improvement Program - Task 1, Feasibility Analysis," (PWA-5518-38, Pratt and Whitney Aircraft Group; NASA Contract NAS3-20630). NASA CR-159449, 1979.

23. Stecura, S., "Effects of Compositional Changes on the Performance of a Thermal Barrier Coating System," NASA TM-78976, 1978.

24. Stecura, S., "Effects of Yttrium, Aluminum and Chromium Concentrations in Bond Coatings on the Performance of Zirconia-Yttria Thermal Barriers," NASA TM-79206, 1979.

25. Scott, H. G., "Phase Relationships in the Zirconia-Yttria System," J. Mater. Sci., Vol. 10, No. 9, Sept. 1975, pp. 1527-1535.

26. Miller, R. A., Smialek, J. L., Garlick, R., "Phase Stability in Plasma Sprayed, Partially Stabilized Zirconia-Yttria," in Proceedings of First International Conference on the Science and Technology of Zirconia, Cleveland, OH, June 16-18, 1980.

27. Stringer, J., "High Temperature Corrosion of Aerospace Alloys," AGARDograph No. 200, NATO, August 1975.

28. Bratton, R. J., Lau, S. K., Lee, S. Y., and Andersson, C. A., "Ceramic Coating Evaluations and Developments," in Proceedings of the First Conference on Advanced Materials for Alternative Fuel Capable Directly Fired Heat Engines, Castine, Maine, July 31 - August 3, 1979.

29. Bratton, R. J., Lau, S. K., Lee, S. Y., "Evaluation of Present Day Thermal Barrier Coatings for Industrial/Utility Applications," Thin Solid Films, 73 (2) 1980, pp. 427-439.

30. Viechnicki, E., Stubican, V., "Mechanism of Decomposition of the Cubic Solid Solutions in the System ZrO_2-MgO," J. Am. Ceram. Soc. 48, 1965, pp. 292-297.

31. Cook, R. G., Lloyd, D. Z., "Fabrication of Zirconia Bodies and Some Considerations of Their Thermal Shock Properties," in Proceedings of the Fifth Symposium on Special Ceramics, Popper, P., Ed., The British Ceramic Research Assoc., 1972, pp. 125-134.

32. Ginsberg, A. S., "System Na_2SO_4-$MgSO_4$," Phase Diagram for Ceramics, eds. by E. M. Levine, C. R. Robbins and H. F. McMurdie, Amer. Ceram. Soc., Columbus, OH (1964), p. 346.

33. Stecura, S., "Effect of Plasma Spray Parameters on Two Layer Thermal Barrier Coating System Life," NASA Tech. Memo 81724, March 1981.

34. Singhal, S. C., Bratton, R. J., "Stability of a $ZrO_2(Y_2O_3)$ Thermal Barrier Coating in Turbine Fuel With Contaminants," Engineering For Power, Vol. 102, No. 4, October 1980, pp. 770-775.

35. Palko, J. E. and Luthra, K. L. and McKee, D. W., "Evaluation of Performance of Thermal Barrier Coatings Under Simulated Industrial/ Utility Gas Turbine Conditions," Final Report, General Electric Co., 1978.

36. Zaplatynsky, I., "Reactions of Yttria-Stabilized Zirconia with Oxides and Sulfates of Various Elements," DOE/NASA/2593-78/1, NASA TM-78942, 1978.

37. Lay, K. W., "Ash in Gas Turbines Burning Magnesium - Treated Residual Fuel," Paper No. 73-WALCD-3, ASME Winter Annual Meeting, Detroit, MI, November 11-15, 1973.

38. Barkalow, R. and Pettit, F., "Mechanisms of Hot Corrosion Attack on Candidate Ceramic Coating Materials," in Proceedings of the First Conference on Advanced Materials for Alternative Fuel Capable Directly Fired Heat Engines, Castine, Maine, 1979, p. 704.

39. Miller, R. A., "Analysis of the Response of a Thermal Barrier Coating to Sodium-and-Vanadium Doped Combustion Gases," NASA TM-79205, June, 1979.